Lijing Xie

Estimation Of Two-dimension Tool Wear Based On Finite Element Method

Lijing Xie

Estimation Of Two-dimension Tool Wear Based On Finite Element Method

Universität Karlsruhe (TH)

Vorwort des Herausgebers

Der rasche Fortschritt der Produktionstechnik und der weltweite Wettbewerb um technisch-wirtschaftliche Spitzenpositionen machen einen intensiven Austausch von Wissen und Erfahrung zwischen Universitäten und der Industrie erforderlich. In diesem Sinne soll im Rahmen dieser Schriftenreihe in zwangloser Folge über aktuelle Forschungsergebnisse des Instituts für Werkzeugmaschinen und Betriebstechnik der Universität Karlsruhe berichtet werden.

Die Forschungsaktivitäten des Instituts umfassen neben der Untersuchung und Optimierung von Bearbeitungsverfahren, Maschinenkomponenten und Fertigungseinrichtungen insbesondere Aufgabenstellungen, die durch Nutzung informationsverarbeitender Systeme eine Verbesserung der Leistungsfähigkeit fertigungstechnischer Einrichtungen und deren informationstechnisch-organisatorische Einbindung in automatisierte Produktionssysteme ermöglichen.

Prof. Dr.-Ing. Jürgen Fleischer   Prof. Dr.-Ing. Hartmut Weule

Estimation Of Two-dimension Tool Wear Based on Finite Element Method

Zur Erlangung des akademischen Grades eines

Doktors der Ingenieurwissenschaften

von der Fakultät für Maschinenbau
der Universität Karlsruhe (TH)

genehmigte

Dissertation

von

M. Sc. Lijing Xie
aus China

Tag der mündlichen Prüfung: 05. 02. 2004
Hauptreferent: Prof. Dr.-Ing. Jürgen Schmidt
Korreferent: o. Prof. Dr.-Ing. Dieter Spath

Acknowledgement

measuring basic knowledge and helping me to look for the best measuring method, Mr. Thomas Hildenbrand for preparing experimental condition and troubleshooting in the turning experiment. Thanks to Mrs. Margarethe Schüßler for teaching me Deutsch language voluntarily.

At last, I want to thanks my husband, Dan, and my family and Dan's for their love and support. They give me the strength over all the problems in my research.

Karlsruhe, in December 2003   Lijing Xie

Table of Contents

Abbreviation

AI	Artificial Intelligence
ALE	Arbitrary Lagrangian Eulerian
CBN	Cubic Boron Nitride
FDM	Finite Difference Method
FE, FEM	Finite Element Method
HSC	High Speed Cutting
KT	Depth of crater wear
VB	Width of flank wear (mean)
VC	Maximum wear of nose radius
VN	Notch wear

Chapter 1 Introduction

Machining operations comprise a substantial portion of the world's manufacturing infrastructure. They create about 15% of the value of all mechanical components manufactured worldwide [Merc-98]. Because of its great economic and technical importance, a large quantity of research has been carried out in order to optimize cutting process in terms of improving quality, increasing productivity and lowering cost.

Tool wear influences cutting power, machining quality, tool life and machining cost. When tool wear reaches a certain value, increasing cutting force, vibration and cutting temperature cause surface integrity deteriorated and dimension error greater than tolerance. The life of the cutting tool comes to an end. Then the cutting tool must be replaced or ground and the cutting process is interrupted. The cost and time for tool replacement and adjusting machine tool increase cost and decrease productivity. Hence tool wear relates to the economic of machining and prediction of tool wear is of great significance for the optimization of cutting process.

At present, the prediction of tool wear is performed by calculating tool life according to experiment and empirical tool life equations such as Taylor's equation or its extension versions. Although Taylor's equation gives the simple relationship between tool life and a certain cutting parameters, e.g. cutting speed, and is very easy to use, it gives only the information about tool life. For the researcher and tool manufacturer tool wear progress and tool wear profile are also concerned. Tool life equation gives no information about the wear mechanism. But capability of predicting the contributions of various wear mechanism is very helpful for the design of cutting tool material and geometry. In addition, such tool life equations are valid under very limited cutting conditions. For example, when tool geometry is changed, new equation must be established by making experiment.

Some researchers concentrate on the study of wear mechanism and investigate the mathematical relationship between wear due to various wear mechanisms and some cutting process variables such as relative sliding velocity of workpiece material along tool face, cutting temperature of tool face and normal pressure on tool face. Some tool wear equation related to one or several wear mechanisms are developed, such as Usui's tool wear equation.

In the recent decades, with the emergency of more and more powerful computer and the development of numerical technique, numerical methods such as finite element method (FEM), finite difference method (FDM) and artificial Intelligence (AI) are widely used in machining industry. Among them, FEM has become a powerful tool in the simulation of cutting process. Various variables in the cutting process such as cutting force, cutting temperature, strain, strain rate, stress, etc can be predicted by performing chip formation and heat transfer analysis in metal cutting, including those very difficult to detect by experimental method. Therefore a new tool wear prediction method may be developed by integrating FEM simulation of cutting process with tool wear model.

1.1 State Of Art: Finite Element Simulation Of Cutting Process

Chip formation is the essential phenomenon in the cutting process. It is the basic of the research on physical phenomena-cutting force, cutting temperature, tool wear, chatter, burr, built-up-edge, chip curling and chip breakage.

According to a comprehensive survey conducted by the CIRP Working Group on Modelling of Machining Operations during 1996-1997 [Lutt-98], among the 55 major research groups active in modelling, 43% were active in empirical modelling, 32% in analytical modelling and 18% in numerical modelling in which finite element modelling techniques are used as the dominant tool. In recent years, application of finite element in metal cutting develops rapidly because of its advantages and the development of powerful computer [Atha-98][Sand-98].

Compared to empirical and analytical methods, finite element methods used in the analysis of chip formation has advantages in several aspects [Zhan-94]:

- Material properties can be handled as functions of strain, strain rate and temperature;

- The interaction between chip and tool can be modelled as sticking and sliding;

- Non-linear geometric boundaries such as the free surface of the chip can be represented and used;

- In addition to the global variables such as cutting force, feed force and chip geometry, the local stress, temperature distributions, etc can also be obtained.

Finite element method has been used to simulate machining by Klamecki [Klam-73], Okushima [Okus-71], and Tay et al [Tay-74] since the early 1970s. With the development of faster processor with larger memory, model limitations and computational difficulty have been overcome to some extent. In addition, more commercial FE codes are used in chip formation simulation, including: NIKE2^{TM} [Stre-85], ABAQUS/Standard^{TM} [Shi-02], MARC^{TM} [Behr-98a], DEFORM 2D^{TM} [Özel-00b] [Cere-99], FORGE 2D^{TM} [Ng-99] [Mona-99], ALGOR^{TM}, FLUENT^{TM} , ABAQUS/Explicit^{TM} [Baca-00] and LS DYNA^{TM} [McCl-02].

Great progress has been made in this research field: Lagrangian approach is used to simulate the cutting process including incipient chip formation state [Shet-00]; segmental chip formation is modelled to simulate high speed cutting [Bäke-00] [Bäke-02] [West-01], hard-turning [Guo-02] [Usui-84] or large negative rake angle [Ohbu-

03], 3D simulation is performed to analyse oblique cutting [Leop-98] [Klam-73] [Lin-00] [Cere-00] [Guo-02], etc.
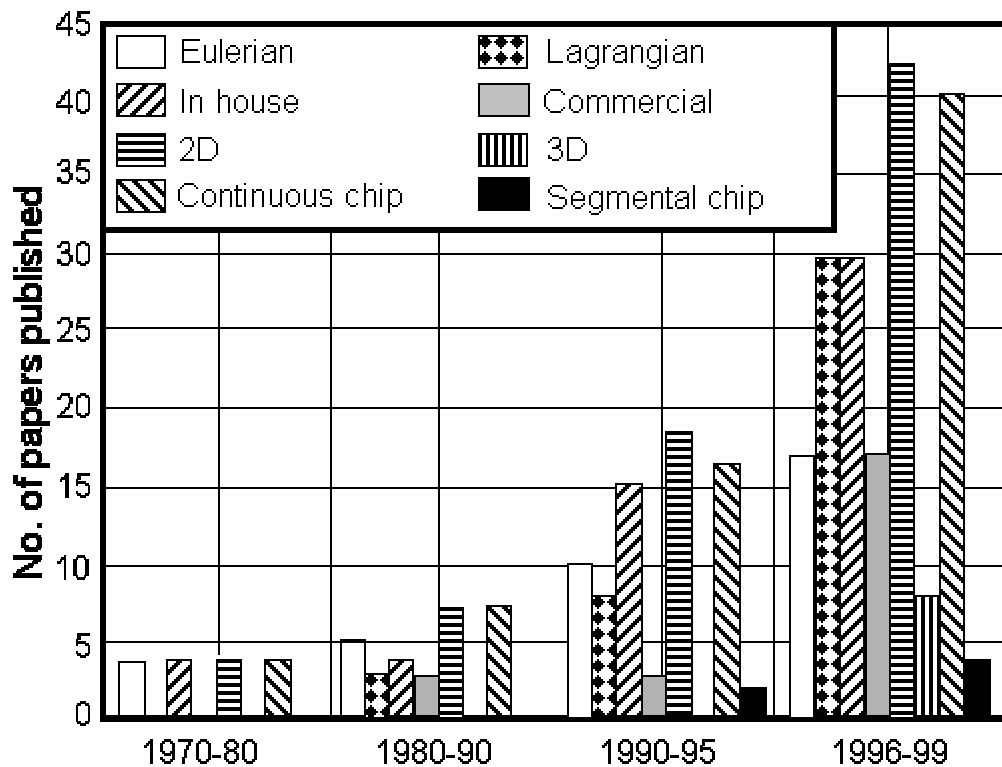
Fig. 1.1 Modelling research trends [Ng-02a]

A diversity of cutting tool and workpiece materials is used in the simulation of cutting process. For example, the modelled cutting tool materials include uncoated carbide [Lin-01b], coated carbide [Mona-99], CBN [Özel-02], cermet, ceramic cutting tool and diamond [Ohbu-03]. The modelled workpiece materials include carbon steel [Behr-98b] [Gu-02], composite [Arol-02], high alloy steel [Ng-02a], cast iron, ductile iron [Chuz-03a] [Chuz-03b], etc.

The effect of tool geometry on the chip formation process is studied, mainly including varing rake angle [Shih-96] and tool geometry. The studied tool geometries include sharp, chamfered [Shat-01b] [Mova-02] and round edge [Ozel-02] [Kim-99], chip breaker [Dill-00], and worn cutting tool [Li-02] [Shih-93].

The mainly simulated cutting types include tuning [Behr-99], milling [Özel-00a], drilling, microscopic cutting of single abrasive grain in grinding [Ohbu-03]. Orthogonal cutting is the most frequently simulated cutting type [Stre-93].

In addition, the influences of sequential cutting [Liu-00] and microstructure of workpiece material [Chuz-03a] [Chuz.03b] on chip formation are studied.

Except the normally discussed variables cutting force, cutting temperature and stress, residual stress [Yang-02] [Shih-93], tool wear [Söhn-01b] [Yen-02], tool performance [Ahma-89], burr formation [Guo-00], chip breakage [Maru-02], chip flow angle [Stre-02], etc are investigated as well.

1.1.1 Numerical Aspects

The implementation of cutting process simulation is based on numerical theory and technique. Their development is helpful to improve the capability of the simulation.

1.1.1.1 Approach

Several approaches are supplied for numerical modelling: Lagrangian, Eulerian and Arbitrary Lagrangian Eulerian (ALE).

Eulerian Approach

In Eulerian approach, the mesh is fixed spatially and the material flows through the mesh. Eulerian approach is suitable to analyse the steady state of cutting process, not including the transition from initial to steady state cutting process, varying cutting thickness in milling operation or serrated chip in high-speed-cutting because it is unable to simulate free surface conditions. Cutting process analysis with Eulerian approach requires less calculation time because the workpiece model consists of fewer elements. That is the reason why before 1995 the applications of Eulerian approach in chip formation analysis overrun those of Lagrangian approach. But experimental work is often necessary in order to determine the chip geometry and shear angle, which is an unavoidable part of geometry modelling.

Lagrangian Approach

In Lagrangian approach, the mesh follows the material. Because the deformation of the free surface of the chip can be automatically treated by elastic-plastic material deformation, Lagrangian approach can be used to simulate from initial to steady state of cutting process. But in order to extend the cutting time until steady state, a long

workpiece is needed in geometry modelling, which increases the calculation time. In order to perform chip separation, chip separation criteria and realization method are necessary.

Arbitrary Lagrangian Eulerian Approach (ALE)

ALE approach combines the features of pure Lagrangian and Eulerian approach, in which the mesh is allowed to move independently of the material. It is an effective tool for improving mesh quality in the analysis of large deformation problem. Many commercial FE codes introduce ALE approach by adjusting mesh based on different mesh adaptivity.

The adaptive meshing technique in ABAQUS/Explicit belongs to ALE approach. It can be used to analyse not only Lagrangian problem but also Eulerian problem. By giving suitable mesh control parameters, the whole process from initial to steady state can be simulated without the need of chip separation criterion or any chip geometry data from experiment. Furthermore, it is not necessary to extend the size of workpiece model. Hence the calculation time is not increased.

1.1.1.2 Mesh Adaptivity

Three types of mesh adaptivity are designed to create a new spatial discretisation and improve mesh quality: h-adaptivity, p-adaptivity and r-adaptivity [Kalh-01].

- H-adaptivity changes the size of the mesh. The new mesh has different number of elements and the connectivity of the nodes is changed.
- In p-adaptivity the degree of the interpolating polynomial is changed.
- R-adaptivity is based on relocation of the nodes, without altering the topology (elements and connectivity) of the mesh.

For example, adaptive meshing technique in ABAQUS/Explicit is accomplished by using R-adaptivity. During meshing nodes are moved to more favourable positions to improve mesh distortion. In addition, solution-dependent meshing is supplied to concentrate mesh towards the developing boundary concave, e.g., chip separation area in the vicinity of the cutting edge, and produce local mesh refinement in this area.

But it is found that only the application of r-adaptivity is not sufficient to maintain the mesh quality. Therefore some FE codes, e.g. Deform-2D and AdvantEdge employ

the combination of r- and h-adaptivity. Mesh is refined where great difference in the gradients of a certain solution is detected between elements. For example, Marusich et al propose to refine mesh according to plastic work rate in each element [Maru-95]; Owen et al use an error estimator based on the rate of fracture indicator to produce a fine mesh in high plastic deformation area and the regions where material failure is going to take place [Owen-99].

Chip separation is produced during meshing and mesh refining. In addition, the contact at tool-chip interface can be improved as well.

1.1.2 Mechanical Aspects

The development of metal cutting theory helps people get more and more correct understanding in mechanical aspects of cutting process including contact and friction, material property, chip separation, etc. The modelling of these aspects influences the accuracy of cutting process simulation.

1.1.2.1 Contact And Friction

Friction behaviour on the tool face determines the cutting power, machining quality and tool wear. It plays an important role in metal cutting.

Development Of Friction Model In Metal Cutting

The nature of friction between two dry sliding surfaces was described by Amontoms in 1699 [Amon-99]. He put forward that the coefficient of friction μ is independent of apparent area of contact A and applied normal load F_n. In 1785, Coulomb [Coul-85] approved and developed these laws by proposing that the coefficient of friction is substantially independent of the sliding velocity. Accordingly a constant coefficient of friction is expected on the tool face in metal cutting process.

$$\mu = \frac{F_f}{F_n} = const \tag{1.1}$$

where F_f is the friction force.

However in metal cutting process, it is generally observed that the mean coefficient of friction on the tool face varies considerably with the change in cutting speed, rake angle and so on. This results from the extreme conditions of metal cutting area where the normal pressure at tool-chip interface is very high.

According to Eq. 1.2 proposed by Finne and Shaw [Finn-56], the ratio of the real area of contact A_r to the apparent area of contact A approaches or reaches 1 under cutting conditions, which is different from the application conditions of Coulomb's assumption.

$$\frac{A_r}{A} = 1 - e^{-BN} \tag{1.2}$$

where N is normal force.

Based on the assumption of shearing action within the workpiece material, Zorev proposed the distribution of shear and normal stress on the rake face as shown in Fig.1.2 [Zore-63]. The chip-tool interface is divided into sticking and sliding regions. In sticking region, adjacent to the cutting edge, $\frac{A_r}{A}$ approaches unity under very high normal stress, and shear stress is believed equal to shear strength of the workpiece material. In sliding region, $\frac{A_r}{A}$ is less than unity, and the coefficient of friction is believed constant.
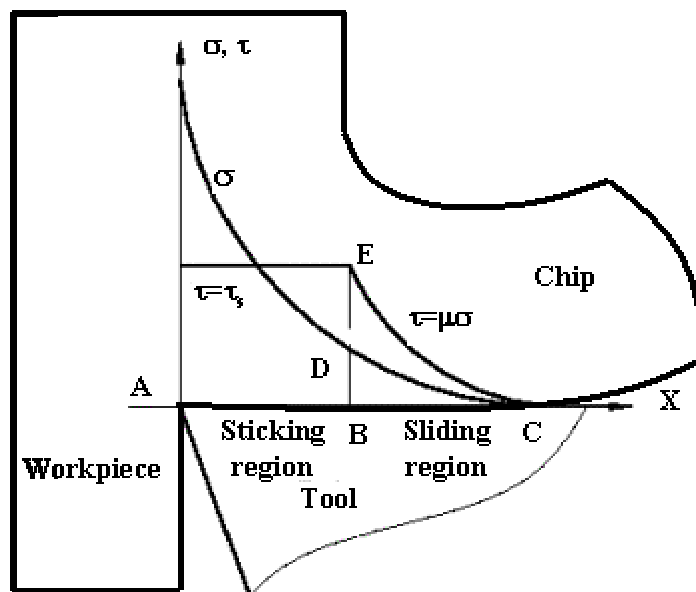
Fig. 1.2 Stress distribution on tool-chip interface

Plenty of evidence from worn tools, from quick-stop sections and from chips showed the coexistence of sticking and sliding at tool/chip interface under many cutting conditions [Tren-77].

Some advanced testing technologies, e.g. photoelastic measurements [Rice-60] or split tool dynamometers [Kato-72] [Chil-98], are used in experiments to discover the form of stress distribution on the rake face. But these techniques are limited when the stresses very close to the cutting edge are determined.

Applied Friction Models In Cutting Process Simulation

In the finite element analyses of metal cutting, various approaches are used in the modelling of friction. Constant coefficient of friction based on Coulomb's friction law is used in most cases. Normally the coefficient of friction μ is calculated by using Eq.1.3 according to the cutting force F_c, thrust force F_t, and rake angle α.

$$\mu = \frac{F_t + F_C \tan\alpha}{F_C - F_t \tan\alpha} \tag{1.3}$$

Ng and his co-operators performed orthogonal cutting tests under different cutting conditions to establish a linear relation between the coefficient of friction μ, cutting speed v_c, rake angle α, and feed f, given by Eq. 1.4, by using Regression analysis [Ng-02b].

$$\mu = 1.034 - 0.00446\alpha - 3.888f - 0.0002v_c \tag{1.4}$$

Liu et al [Liu-00] determined the coefficient of friction by performing simulation using different values and carrying out the sensitivity study on the coefficient of friction.

When Zorev's sliding-sticking friction model is employed in the simulation, the division of the two regions is determined by two methods: one is to prescribe the length of each region [Shih-95] [Wu-96] [Shat-00], the other is to determine the sliding and sticking region automatically by program according to a criterion [Zhan-94] [Guo-00], given by Eq. 1.5.

$$\tau = \min(\mu\sigma, \tau_s) \tag{1.5}$$

where

τ_s is the shear flow stress of the chip material;

τ is friction stress;

σ is normal stress.

Iwata et al [Iwat-84] proposed the relationship given by Eq. 1.6 after put forward a method to test friction between newly created surfaces and tool material.

$$\tau = \left(\frac{H_V}{0.07}\right) \tanh\left(\frac{0.07\mu p}{H_V}\right) \text{ Mpa} \qquad (1.6)$$

where

H_V is the Vickers hardness of the workpiece material;

p is contact pressure in MPa.

A frictional shear factor is introduced into the relationship in order to make the calculated results agree with those of experiment.

Yang and Liu [Yang-02] proposed a stress-based polynomial model of friction, given by Eq. 1.7.

$$\tau = \sum_{n=0}^{n=4} a_n \sigma^n \qquad (1.7)$$

a_0, a_1, a_2, a_3 and a_4 are determined by fitting experimental stress curve on rake face.

1.1.2.2 Material Constitutive Model

The accuracy of the finite element analysis is severely dependent on the accuracy of the material mechanical properties.

Influence Factors Of Material Property

Experiments shows that material properties, e.g. stress-strain relationship, are affected by the strain rate and temperature during material forming process with plastic deformation. For the same value of strain, the stress is higher at higher strain rate due to the viscous effect during plastic deformation and lower at higher temperature due to material softening, as shown in Fig. 1.3. This overstress effect by strain rate is more pronounced as the temperature increases [Shih-91]. In metal cutting process, temperature, strain and strain rate are very high. Thermal-

viscoplastic material constitutive model is necessary for the finite element analysis of metal cutting.
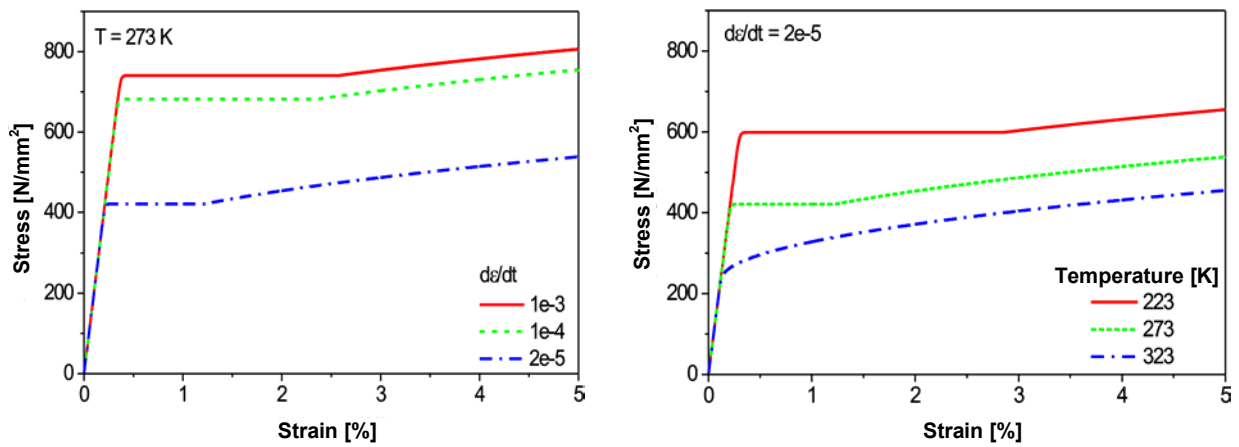
Fig. 1.3 Material property curve

Many researchers are making efforts to establish such material constitutive models for different workpiece materials through experimental [Kopp-01], analytical or simulation methods [Shat-01a] [Özel-00b] [Batz-02]. Based on their supports, a material model database has been developed by Söhner et al [Söhn-01a].

Material Constitutive Model For Mild Carbon Steel

The main workpiece materials used in the following research are mild carbon steel CK45 and AISI1045.

- For CK45

The material constitutive model developed by O. Vöringer is used, which is described by Eq. 1.8 and Eq. 1.9.

$$\sigma_v^*(T, \dot{\varepsilon}) = \sigma_0^* \left(1 - \left(\frac{T}{T_0} \right)^n \right)^m \tag{1.8}$$

$$\text{with } T_0 = \frac{\Delta G_0}{kIn \dfrac{\dot{\varepsilon}_0}{\dot{\varepsilon}^{(pl)}}} \tag{1.9}$$

where the constants for CK45 are: m=1.78, n=0.53, $\Delta G_0 = 0.58 ev$, $\dot{\varepsilon}_0 = 7.29 \times 10^5 s^{-1}$, and $\sigma_0^* = 1352 MPa$. *k* is Boltzmann constant and T is temperature in Kelvin [Schu-00].

In the simulation of cutting process, a user material subroutine based on this material constitutive model is employed.

- For AISI1045

To describe the material property of AISI1045, the Johnson-cook constitutive equation is used.

$$\sigma = \left(B \varepsilon^n \right) \left(1 + C \ln \left(\frac{\dot{\varepsilon}}{1000} \right) \right) \left(\left(\frac{T_{melt} - T}{T_{melt} - T_{room}} \right) + ae^{-0.00005(T-700)^2} \right) \tag{1.10}$$

where *B=996.1, C=0.097, n=0.168, a=0.275, T_{melt}=1480℃* [Kopp-01], σ is the effective stress in MPa, and *T* is temperature in °C.

1.1.2.3 Chip Separation

In the cutting process, with the cutting tool advancing into the workpiece, the workpiece material is separated into two parts. The unwanted part forms the chip. By chip separation, a new workpiece surface is formed on the created part.

The realization of chip separation is one of the main problems in the simulation of chip formation process. Normally it includes two aspects of consideration: chip separation criterion and model realization.

Chip Separation Criterion

The chip separation criteria used by researchers can be categorized as two types: geometrical and physical.

Geometrical criteria define geometric parameters, e.g. a distance value. When the distance between the nearest workpiece node on the moving path of the cutting edge

and the cutting edge is equal to or smaller than this given distance value, chip separation takes place [Shih-95].

Physical criteria is related to some physical meaning of chip separation. They are based on physical parameters such as stress [Iwat-84], strain energy density [Lin-99] or effective plastic strain [Shir-93]. When such physical parameter reaches a critical value, material failure takes place. The most reliable critical value is obtained by performing experiments, although sometimes it is defined at random. A critical value considering multi-influencing factors, for example, temperature- and strain rate-dependent strain at failure will provide a better simulation result.

According to the investigation on both types of criteria made by Huang and Black [Huan-96], neither had a substantial effect on chip geometry, distribution of shear stress, effective stress or effective plastic strain in the chip and in the machined surface. However, the magnitude designated for these criteria did have a major effect on mesh distortion together with the value of maximum shear stress, and the effective stress in the machined surface [Ng-02a].

Model Realization

There are several methods to model chip separation in finite element mesh. They are related with the applied software.

- Element removal [Cere-96]

When chip separation criterion, normally physical criterion, is reached, material failure happens and the element carries no stress any more as if they do not exist. Such element can be removed and does not display.
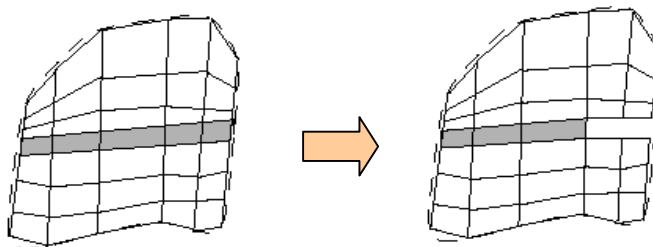
Fig. 1.4 Element removal [Behr-98b]

- Node debond [Shi-02] [Shet-00] [Shet-03]

The chip and the workpiece are two separated parts. They are perfectly bonded together through some pair of nodes along the prospective parting line. The chip separation can be geometrical, physical or their combination. When chip separation criterion is reached, debond of the node pair takes place and the two nodes move in different direction.
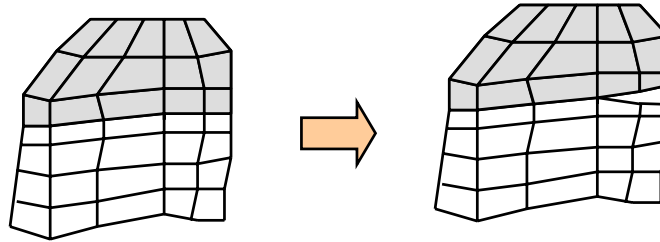
Fig. 1.5 Node debond

- Node splitting [Shih-95]

Chip separation is realized by element separation in front of cutting edge. The two neighbouring elements have common node before separation. When the separation criterion is met, for example, a node is very close to the cutting edge. Element separation takes place and a new node is created at the same position; two nodes overlap together and connect to two different elements. Through the further movement of the cutting tool, the two elements move in different direction and lose contact.
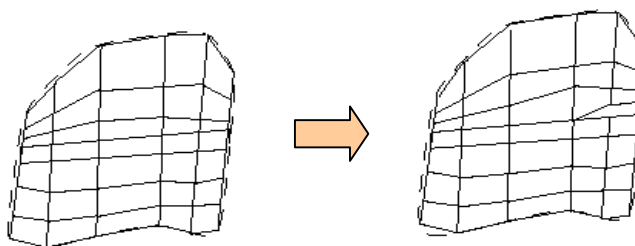
Fig. 1.6 Node splitting [Behr-98b]

- Mesh adaptivity [Arra-02]

Chip separation is performed by mesh refinement in the separation zone by increasing the number of elements or relocation of the nodes.

1.2 Technical Background About Tool Wear

Prediction of tool wear is complex because of the complexity of machining system. Tool wear in cutting process is produced by the contact and relative sliding between the cutting tool and the workpiece and between the cutting tool and the chip under the extreme conditions of cutting area; temperature at the cutting edge can exceed 1800°F and pressure is greater than 2,000psi [John-01]. Any element changing contact conditions in cutting area affects tool wear. These elements come from the whole machining system comprising workpiece, tool, interface and machine tool:
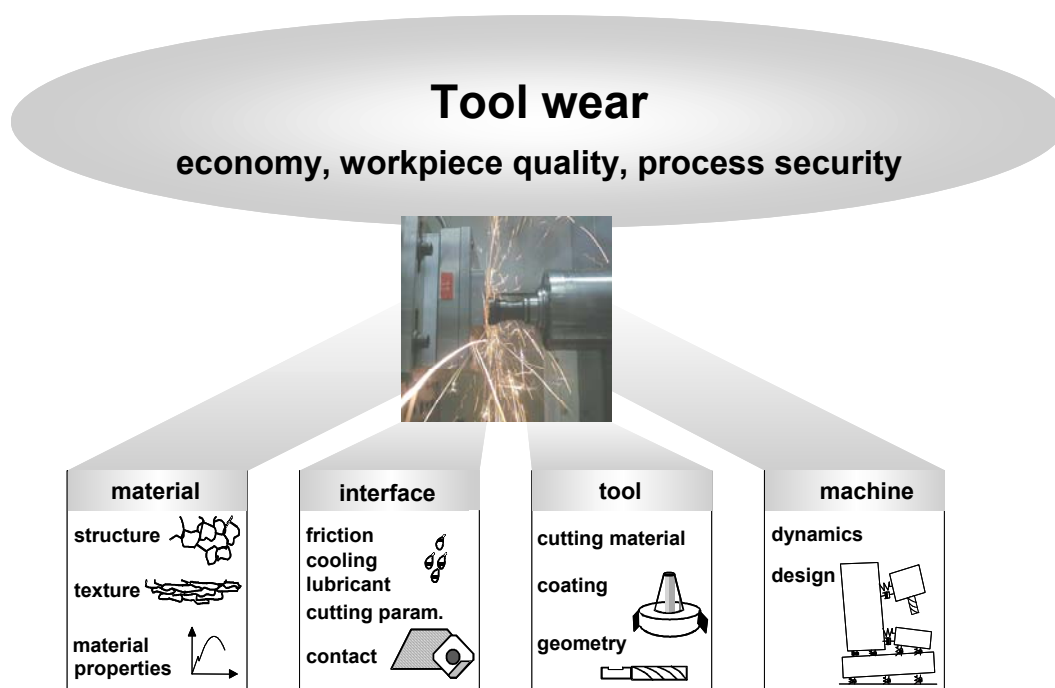
Fig. 1.7 Influencing elements of tool wear [Söhn-01b]

- Workpiece: It includes the workpiece material and its physical properties (mechanical and thermal properties, microstructure, hardness, etc), which determine cutting force and energy for the applied cutting conditions.
- Tool: Tool material, tool coatings and tool geometric design (edge preparation, rake angle, etc) need to be appropriately chosen for different operations (roughing, semi-roughing, or finishing). The optimal performance of a cutting tool requires a right combination of the above tool parameters and cutting conditions (cutting speed, feed rate, depth of cut, etc)
- Interface: It involves the interface conditions. In 80% of the industrial cutting applications, coolants are used to decrease cutting temperatures and likely

reduce tool wear. Increasingly new technologies, such as the minimum liquid lubrication, have been developed to reduce the cost of coolant that makes up to 16% of the total machining costs [Walt-98].

- Dynamic: The dynamic characteristic of the machine tool, affected by the machine tool structure and all the components taking part in the cutting process, plays an important role for a successful cutting. Instable cutting processes with large vibrations (chatters) result in a fluctuating overload on the cutting tool and often lead to the premature failure of the cutting edge by tool chipping and excessive tool wear.

1.2.1 Wear Types In Metal Cutting

Under high temperature, high pressure, high sliding velocity and mechanical or thermal shock in cutting area, cutting tool has normally complex wear appearance, which consists of some basic wear types such as crater wear, flank wear, thermal crack, brittle crack, fatigue crack, insert breakage, plastic deformation and build-up edge. The dominating basic wear types vary with the change of cutting conditions. Crater wear and flank wear shown in Fig. 1.8 are the most common wear types.
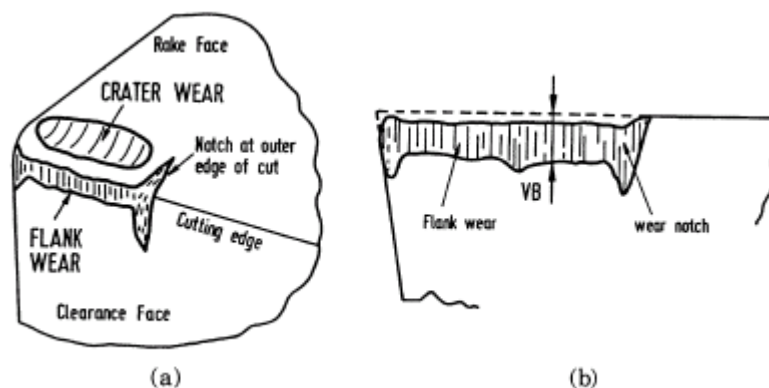
Fig. 1.8 Wear types [Lim-01]

- Crater wear: In continuous cutting, e.g. turning operation, crater wear normally forms on rake face. It conforms to the shape of the chip underside and reaches the maximum depth at a distance away from the cutting edge where highest temperature occurs. At high cutting speed, crater wear is often the factor that determines the life of the cutting tool: the tool edge is weakened by the severe cratering and eventually fractures. Crater wear is improved by

selecting suitable cutting parameters and using coated tool or ultra-hard material tool.

- Flank wear: Flank wear is caused by the friction between the newly machined workpiece surface and the tool flank face. It is responsible for a poor surface finish, a decrease in the dimension accuracy of the tool and an increase in cutting force, temperature and vibration. Hence the width of the flank wear land VB is usually taken as a measure of the amount of wear and a threshold value of the width is defined as tool reshape criterion.

1.2.2 Wear Mechanism

In order to find out suitable way to slow down the wear process, many research works are carried out to analyze the wear mechanism in metal cutting. It is found that tool wear is not formed by a unique tool wear mechanism but a combination of several tool wear mechanisms.

Tool wear mechanisms in metal cutting include abrasive wear, adhesive wear, delamination wear, solution wear, diffusion wear, oxidation wear, electrochemical wear, etc. Among them, abrasive wear, adhesive wear, diffusion wear and oxidation wear are very important.

- Abrasive wear: Tool material is removed away by the mechanical action of hard particles in the contact interface passing over the tool face. These hard particles may be hard constituents in the work material, fragments of the hard tool material removed in some way or highly strain-hardened fragments of an unstable built-up edge [Boot-89].

- Adhesive wear: Adhesive wear is caused by the formation and fracture of welded asperity junctions between the cutting tool and the workpiece.

- Diffusion wear: Diffusion wear takes place when atoms move from the tool material to the workpiece material because of the concentration difference. The rate of diffusion increases exponentially with the increase of temperature.

- Oxidation wear: A slight oxidation of tool face is helpful to reduce the tool wear. It reduces adhesion, diffusion and current by isolating the tool and the workpiece. But at high temperature soft oxide layers, e.g. Co_3O_4, CoO, WO_3, TiO_2, etc are formed rapidly, then taken away by the chip and the workpiece. This results in a rapid tool material loss, i.e., oxidation wear.

Under different cutting conditions dominating wear mechanisms are different. For a certain combination of cutting tool and workpiece, the dominating wear mechanisms vary with cutting temperature, as shown in Fig.1.9. According to the temperature distribution on the tool face, it is assumed that crater wear is mainly caused by abrasive wear, diffusion wear and oxidation wear, but flank wear mainly dominated by abrasive wear due to hard second phase in the workpiece material.
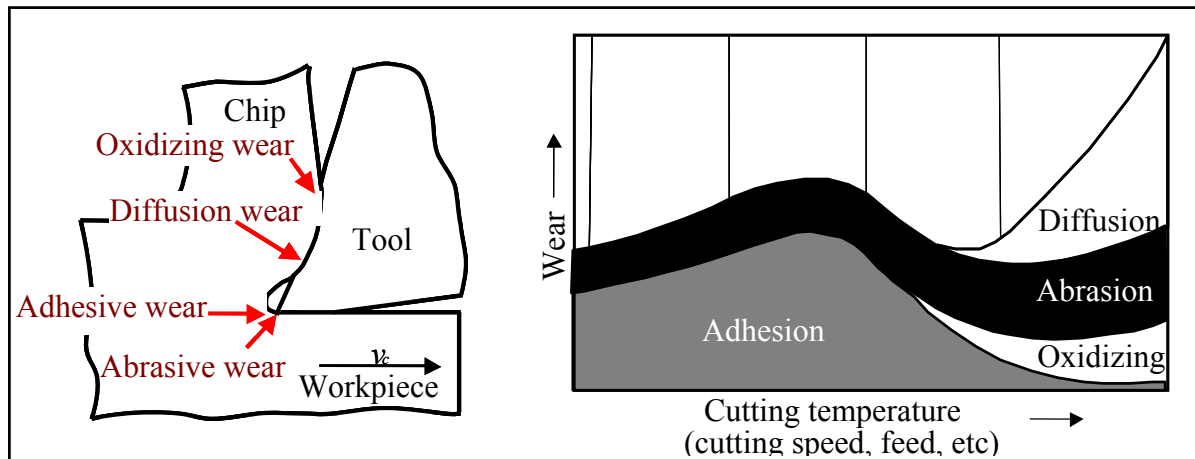
Fig. 1.9 Wear mechanism [Köni-84]

1.2.3 Tool Wear Model

Many mathematical models are developed to describe tool wear in quantity. They can be categorized into two types: tool life models and tool wear rate models.

- Tool life models: This type of wear models gives the relationship between tool life and cutting parameters or variables. For example, Taylor's tool life equation [Tayl-07], reveals the exponential relationship between tool life and cutting speed, and Hastings tool life equation describes the great effect of cutting temperature on tool life [Hast-79], see Table 1.1. The constants n, C_T, A and B are defined by doing a lot of experiments with cutting speed changing and fitting the experimental data with the equation. It is very convenient to predict tool life by using this equation. In various sizes of cutting database, Taylor's tool life equation and its extension versions under different cutting conditions appear most frequently.

  Tool life equations are suitable to very limited range of cutting conditions. As the new machining technologies, e.g. high-speed-cutting or dry cutting, are getting spread in manufacturing industry, the existing tool life equations need

to be updated with new constants and a lot of experimental work has to be done. In addition, except that tool life can be predicted by these equations, it is difficult to get further information about the tool wear progress, tool wear profile or tool wear mechanisms that are sometimes important for tool designers.

- Tool wear rate models: These models are derived from one or several wear mechanisms. They provide the information about wear growth rate due to some wear mechanisms. In these modes, the wear growth rate, i.e. the rate of volume loss at the tool face (rake or flank) per unit contact area per unit time (mm/min), are related to several cutting process variables that have to be decided by experiment or using some methods [Kwon-00].

Table 1.1 Tool wear models

Empirical Tool Life Models	*"Differential" Tool Wear Rate Models*
Taylor's tool life equation: $$v_c \cdot T^n = C_T$$ *(n, C_T = constants)*	***Takeyama & Murata's model, considering abrasive wear and diffusive wear (1963):*** $$dW/dt = G(v_c, f) + D \cdot \exp(-E/R\theta)$$ *(G, D = constants)*
Hastings tool life equation (Hastings et al, 1979): $$\theta^B \cdot T = A$$ *(A, B = constants)* v_c = Cutting speed R = Universal gas constant T = Tool life θ = Cutting temperature E = Process activation f = Feed energy $v_{s\cdot}$ = Sliding velocity	***Usui's model, which was derived from equation of adhesive wear [Usui et al., 1978]:*** $$dW/dt = C\sigma_t v_s \exp(-\lambda/\theta)$$ *- (C, λ = constants)* *- dW/dt = rate of volume loss per unit contact area per unit time (mm/min)* *- σ_t, θ = normal stress and temperature* *- C, λ = wear characteristic constants*

In Table 1.1, the right column shows two tool wear rate models, which are obtained from literatures.

Takeyama & Murata's model is developed by considering the combination action of abrasive wear and diffusive wear. Therefore the equation sums two parts up. One part shows that abrasive wear is influenced by the cutting speed and feed. Another part including universal gas constant and tool temperature describes diffusive wear.

Usui's model is derived from Shaw's equation of adhesive wear [Usui-78c]. Except the constants A and B, Usui's equation includes three variables: sliding velocity between the chip and the cutting tool, tool temperature and normal

pressure on tool face. These variables can be predicted by FEM simulation of cutting process or combining analytical method and FDM. Therefore Usui's equation is very practical for the implementation of tool wear estimation by using FEM or by using the combination of FDM and analytical method.

When tungsten carbide tools are used to machine carbon steels, crater wear on rake face was assumed mainly caused by adhesive wear. According to cutting experiment, Usui determined the constants for such cutting conditions and validated this model by the prediction of crater wear.

The latter study showed that this equation is able to describe flank wear as well, which mainly results from abrasive wear [Kita-88]. All the points for flank wear and crater wear defined by experiment distribute along two characteristic lines with different gradients, which intersect at the critical temperature of around 1,150K. The experimental points for crater wear usually lie on the line in the higher temperature range, whereas those for flank wear are usually distributed around the line in the lower temperature range.

The constants in tool wear rate models are depending on the combination of workpiece and cutting tool material. Table 1.2 shows the charateristic constants in Usui's equation for the combination of carbon steel and carbide tool that obtained from literature [Kita-89]. They are introduced in the later tool wear estimation models.

Table 1.2 : Characteristic constants for carbon steels [Kita-89]

C [m^2/MN]		λ [K]	
$\theta_f \geq 1150K$	$\theta_f < 1150K$	$\theta_f \geq 1150K$	$\theta_f < 1150K$
1.198×10^{-2}	7.8×10^{-9}	2.195×10^{4}	5.302×10^{3}

1.3 Research Of Tool Wear With Finite Element Methods

1.3.1 Comparison Between FEM Method And Empirical Method

Based on tool wear rate models, the estimation of tool wear profile progress with the cutting process can be implemented by predicting cutting process variables using finite element method. Its advantages and disadvantages are shown by the comparison with the empirical method in Table 1.3.

Table 1.3 Comparison of FEM method and empirical method

Compared aspects	Empirical method	FEM method
Environment requirement	Special machine, tool, workpiece, personnel for cutting tests	Powerful computer, tool wear rate model and FEM code
The procedure of calculating tool wear	Cutting tests and regressive analysis	Obtaining tool wear rate model by experiment or from literature, running the program with tool wear rate models under new cutting conditions
Application under new cutting conditions	New experiments have to be carried out to update the constants of tool life models	If only tool wear rate model is updated according to new cutting conditions, the program can be used again
Time	The development of new tool life models is time consuming; Whereas the prediction of tool wear with the tool life model is very efficient	The time for developing the entire program is relative long. The time for calculating the tool wear with the program depends on the performance of computer
Wear mechanism	Wear mechanism is not	Yes, even the contributions

	considered	of the main mechanisms can be calculated
Workpiece material	Uneven material distribution result from impurity, heat treatment, work hardening	Homogeneous material model, thermal visco-plastic material
Tool material	Uneven material properties result from impurity, heat treatment, etc	Homogeneous material model, ideal elastic material
Medium	Sensitive to the cooling method, coolant type, cooling effect, etc	The types of heat emission through tool face and workpiece surface under various cooling conditions and their FEM implementation have to be considered
Vibration of machine-tool-workpiece system	The constants are sensitive to the vibration of the system	Not considered at present
Predicted wear parameters	Very limited information can be obtained, for example only tool life is predicted with Taylor's tool life equation	Comprehensive information about tool wear including crater wear profile, flank wear profile, VB, KT, VC (for 3D), VN (for 3D), etc can be predicted
Cutting type	Tool life models under various cutting type can be developed	At present, only tool wear prediction in turning and milling operations are studied. For different cutting types, the tool wear program may need adjusting according to the characteristic of relative

		motion of cutting tool and workpiece
Requirement on the user	No special requirement	At present, except basic knowledge about metal cutting theory, user needs the basic knowledge about FEM chip formation, heat transfer analysis
Application at present	Used in the real production	For research and education
Quality of the prediction	Quantitative	Qualitative

1.3.2 State Of Art: Numerical Implementation Of Tool Wear Estimation

Tool wear estimation with Finite Element Method is developed from tool wear estimation with the combination of analytical method and Finite Difference Method (FDM).

1.3.2.1 Tool Wear Estimation With The Combination Of Analytical Method And FDM

Usui's Research-Prediction Of Crater Wear

The earliest reported research work on tool wear estimation with the combination of analytical energy method and FDM was performed by E. Usui et al in 1978. He first derived a characteristic equation of crater wear theoretically by combining M.C.Shaw's adhesive wear, temperature-dependent material asperity hardness and temperature-dependent Holm's probability, given by

$$\frac{dw}{dt} = C\sigma_t v_s \exp(-\lambda/\theta) \qquad\qquad (1.11)$$

Then he verified the equation experimentally.

a.) Implementation Procedure

The chip formation, sliding velocity of the chip and cutting force are predicted through energy method proposed in previous papers [Usui-78a] [Usui-78b] [Usui-78c].

By using the predicted cutting force and tool-chip contact length together with an assumption of an exponential normal stress distribution and a triangle or trapezoidal frictional stress distribution on the tool face, the frictional stress is calculated.

The temperature distribution within the chip and the tool at steady state is obtained with FDM by considering the heat source on the shear plane and on rake face.

The characteristic constants of the equation for the combination of carbon steel and P20 are determined with the aid of the predicted temperature, stress on tool face and the measured wear by curve fitting.

Then computer calculation of crater wear is carried out by using the characteristic equation, and the predicted distribution of the stress and the temperature.

b.) Result

The predicted crater wear was reported in good agreement with the measured in experiment in depth and contour except some discrepancy in the location of the deepest portion.

c.) Limitations

- When using the energy method to predict the chip formation and cutting force, orthogonal cutting data about shear stress on shear plane, friction angle and shear angle are needed, the prediction of crater wear cannot be carried out without making experiment in advance.
- The energy method is developed based on single shear plane for the cutting tool with sharp cutting edge. The effect of cutting edge preparation, such as round cutting edge, or rounded cutting edge due to wear on the tool wear cannot be considered.

Kitagawa's Research-Prediction Of Flank Wear

By analysing the flank wear characteristics of tungsten carbide tools in turning plain carbon steels at steady-state cutting without a built-up edge experimentally, Kitagawa finds that flank wear can be described by the same characteristic equation, Eq. 1.11, for crater wear. Tool wear consists of two characteristic lines with different gradient, which intersect at the critical temperature of around 1,150K. The experimental points for crater wear usually lie on the line in the higher temperature range, whereas those for flank wear are usually distributed around the line in the lower temperature range.

a.) Implementation Procedure

In the prediction, the sliding velocity of workpiece material on the flank wear land is assumed equal to the cutting speed.

The values of cutting force, thrust force and chip contact length obtained from orthogonal experiment must be given beforehand. By prescribing a triangle distribution of frictional stress along the tool-chip contact length with maximum value at the cutting edge and neglecting the contribution of stress on flank face to the cutting force and thrust force, the frictional stress is calculated.

On the flank wear, the frictional stress at the cutting edge is set equal to the maximum value on rake face, and frictional stress on the other sites is arbitrary set. Normal stress on flank wear is set equal to frictional stress.

Then the temperature on flank wear land is predicted by considering the heat generated on the flank wear, rake face and in the shear plane using FDM.

The wear rate on the flank wear is calculated according to the predicted temperature, arbitrary set normal stress and sliding velocity. Normal stress on flank wear is adjusted continuously until a uniformly distributed wear rate is achieved everywhere on the flank wear land.

b.) Result

It was reported that the predicted tool life, temperature and mean stresses on the flank wear land are in reasonable agreement with experiment even with changing cutting speed, feed and workpiece material.

c.) Limitations

- The prediction method is developed under the assumption of no crater wear formed on the rake face. This limits its application to low cutting speed range.
- The assumption of uniform wear rate on flank wear excludes the formation of rounded edge due to wear that is often observed in experiments.
- The prediction method is not applicable to the cutting tool with any edge preparation because of the assumption of stress distribution on rake face
- The prediction is based on cutting force, thrust force and chip contact length obtained from orthogonal experiment. These values vary with the development of flank wear. Whether the predicted crater wear is sensitive to the frequency of measuring these values during the development of flank wear is very important for its application perspective.

1.3.2.2 Tool Wear Estimation With FEM

Yen And Söhner's Research (FEM)

Although in a paper in 1999, J. Monaghan and T. MacGinley claimed that they performed tool wear analysis based on a wear function related to normal stress and sliding velocity by predicting stress distribution within coated and uncoated carbide tool with and without chip breaker using commercial FEM code-FORGE2 [Mona-99], no implementation procedure, clear predicted tool wear profile and wear value are described or provided. It is suspected that only the tendency and possibility of tool wear distribution were analysed qualitatively.

Hence the earliest reported research of tool wear estimation in quantity with FEM was done by Y. C. Yen and J. Söhner et al since 2001.

According to the paper in 2002 [Yen-02] and the dissertation of Söhner [Söhn-03], the numerical implementation of the integration of tool wear rate models with FEM calculations to predict the evolution of the tool wear was performed by using commercial FE code DEFORM-2D.

a.) Implementation Procedure

Usui's wear model is used to calculate the wear rate of the uncoated carbide tool in cutting carbon steel.

The complete procedure includes four phases. In the first phase, a coupled thermal-viscoplastic Lagrangian cutting simulation combined with an introduced special simulation module, 'Konti-cut', which can prolong the cutting simulation to a sufficient long cutting time, is used to perform chip formation analysis until mechanical steady state is reached. In the second phase, pure heat transfer analysis for the tool is performed to attain thermal steady state in the tool. Both the chip formation and heat transfer analyses are performed with commercial FE code DEFORM-2D. With the values of nodal temperature, normal stress and sliding velocity under steady-state cutting condition provided by the first two phases, the nodal wear rate is calculated in the third phase. Then new tool geometry accounting for tool wear is calculated based on the user input for a cutting time increment. In the last phase, the tool geometry model is updated by moving nodes.

b.) Result

Simulation study was made with worn tool initially including a pre-defined wear land of 0.06mm on the flank face. The wear rates of flank wear and crater wear are of the same order, the location of the maximum wear rate and the low wear rate close to tool radius are consistent with the experimental result.

When a sharp tool is used, the predicted wear rate on the flank face is one order of magnitude smaller than that on the rake face, while crater wear and flank wear occur simultaneously at a similar wear rate in the experiment. This problem was improved by using a new tool wear model especially developed for the simulated cutting condition [Fran-02].

c.) Limitations

- The tool geometry was updated manually, instead of being performed automatically according to a certain algorithm.
- The selection of a suitable cutting time increment is very difficult to perform for a user without doing experiment in advance.

1.3.2.3 Summary Of Literature

According to the above literature analysis, some conclusions can be obtained:

- The advantages of tool wear estimation with FEM over tool wear estimation with the combination of analytical method and FDM are considered in several aspects, as shown in Table 1.4.

- Because of the short history of the research on tool wear estimation with FEM, only 2D tool wear of uncoated carbide tool cutting carbon steel workpiece AISI1045 was studied. The cutting type is limited turning operation and orthogonal cutting.

- Only the commercial FE code DEFORM-2D is used in tool wear estimation. However, the simulation of cutting process is assumed more suitable to be performed with explicit method because of the large deformation, impact and complex contact problem. The study should be carried out with some FE code using explicit method and providing good development platform as well, for example, ABAQUS.

- At present, numerical implementation of tool wear estimation is only developed for the cutting process with steady state. The end of tool life in intermittent cutting, for example, milling operation, is mainly caused by progressive tool wear. Tool wear estimation in intermittent cutting, is different from turning operation because of the lack of steady state. Therefore the estimation of tool wear should be studied by developing new simulation procedure.

Table 1.4 Comparisons between tool wear estimation with FEM and tool wear estimation with the combination of analytical method and FDM

Compared aspects	With the combination of analytical method and FDM	With FEM
Realization	Analytical method, e.g. energy method; Assumption and simplification of the cutting condition; Tool wear rate model	FEM chip formation analysis; FEM heat transfer analysis; Tool wear rate model
Predicted wear value	Only crater wear or only flank wear	Crater wear and flank wear simultaneously
Tool	For crater wear estimation, tool without flank wear, For flank wear estimation, tool without crater wear. Edge preparations are not considered	Crater wear, flank wear and edge preparation can be included in tool geometry model
Experimental data	Yes, cutting force, tool-chip contact length, etc	No
Applicable conditions	Conventional cutting speed	Conventional cutting and HSC
Prospective	Limited	A necessary supplement to the empirical method

Chapter 2 Objective And Approach

2.1 Objectives

The objective of this research is to develop methodology to predict tool wear and tool life in cutting process using finite element simulations. The study is not limited to turning operation, the prediction of tool wear in milling operation is considered as well.

Because of the complexity of tool wear mechanisms and forms in real cutting process, the study at present will be concentrated on two-dimension tool wear estimation of uncoated carbide tool in dry cutting mild carbon steel.

This tool wear estimation method is performed by predicting tool temperature, sliding velocity of chip and normal stress on tool face with FEM simulation of cutting process. Therefore to achieve the objective, FEM simulation of turning and milling process are studied at first, including chip formation analysis and pure heat transfer analysis. Several modeling tools are used in order to accomplish the entire research project.
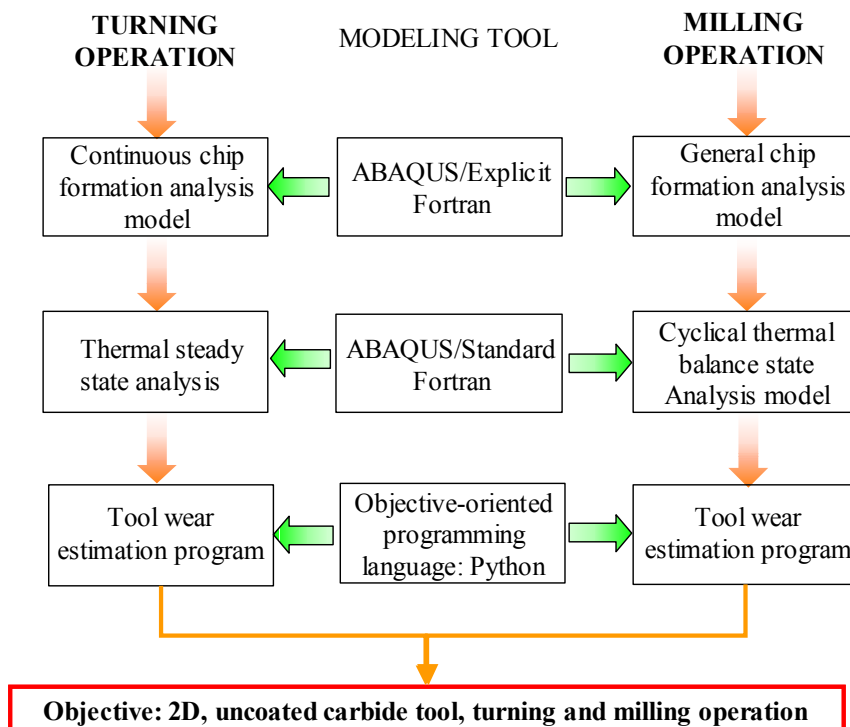
Fig. 2.1 Objective and modeling tool

Turning operation is a steady-state process when continuous chip is formed. The implementation of tool wear estimation is relatively easier and studied first. Based on

the obtained experience in turning operation, the methodology of tool wear estimation in milling operation is discussed by analyzing the feature of milling operation. Two different tool wear estimation models are developed, one is for turning operation, another for milling operation.

2.2 Approach

Although the tool wear estimation models for turning and milling operations are different, the calculation procedure are similar and mainly composed of chip formation analysis, heat transfer analysis, wear calculation and tool geometry updating, as shown in Fig. 2.2.
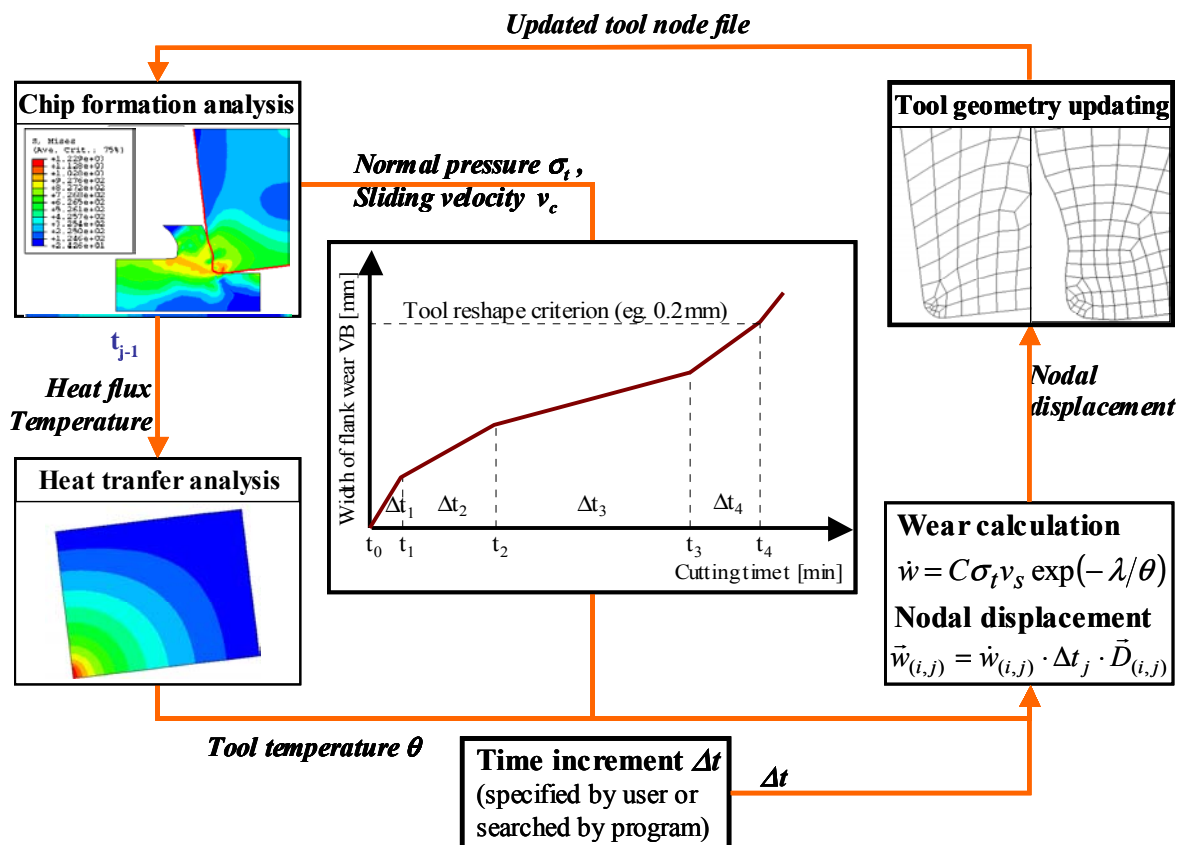
Fig. 2.2 Approach and procedure of tool wear estimation

The study process for turning operation includes:

Stage 1: chip formation analysis

A new chip formation modeling method for continuous steady state chip formation is developed. It can simulate the entire chip formation process from initial chip

formation, chip growth to steady state by making use of Arbitrary Lagrangian Eulerian technique in ABAQUS/Explicit.

Stage 2: heat transfer analysis

In order to save the calculation time, the temperature distribution in the cutting tool at thermal steady state is studied by performing pure heat transfer analysis. The concerned modeling problem is discussed.

Stage 3: tool wear estimation modeling

Through the previous stages, normal stress, sliding velocity and tool temperature at steady state can be obtained. Then the tool wear estimation modeling is studied. It includes the calculation of wear rate at steady state, the searching method of a suitable cutting time increment, the calculation of nodal displacement due to wear and tool geometry updating.

The study process for milling operation includes:

Stage 1: chip formation analysis

The chip formation modeling method in milling operation is studied. It simulates the chip formation process in the first milling cycle.

Stage 2: heat transfer analysis

In order to analyze the variation of tool temperature in the further milling cycles, the cooling of the workpiece is studied, then pure heat transfer analysis of the tool is performed for several milling cycles.

Stage 3: tool wear estimation modeling

Through the previous two stages, normal stress, sliding velocity, and tool temperature can be obtained. Then the tool wear estimation modeling is studied. It includes the calculation of average wear rate in one selected milling cycle, the searching method of a suitable cutting time increment, the calculation of nodal displacement due to wear and tool geometry updating.

Chapter 3 Chip Formation Simulation Technology

3.1 Introduction

Optimisation of the cutting process requires comprehensive knowledge about the relation between cutting process and the combination of cutting parameters, cutting tool and workpiece. In this chapter, chip formation process is simulated using commercial FEM code, ABAQUS/Explicit.

3.1.1 Explicit Algorithm In Chip Formation Simulation

The chip formation simulation is performed using explicit method. In the simulation the entire cutting process is discretized into many small time increments. In every small time increment, dynamic and thermal analysis procedures are based on the implementation of an explicit integration rule.

3.1.1.1 Dynamic Analysis Procedure

Dynamic analysis procedure is performed with the following algorithm.
- Nodal calculation

Accelerations are calculated by satisfying the dynamic equilibrium at the beginning of the increment:

$$\ddot{u}_{(i)} = M^{-1}(P_{(i)} - I_{(i)})$$
(3.1)

where $\ddot{u}_{(i)}$ is the acceleration at the beginning of the increment i,

M is the diagonal or lump mass matrix,

$P_{(i)}$ is externally applied load,

and $I_{(i)}$ is internal load.

Then the accelerations are integrated through time using the central differential rule.

$$\dot{u}_{(i+\frac{1}{2})} = \dot{u}_{(i-\frac{1}{2})} + \frac{(\Delta t_{(i+1)} + \Delta t_{(i)})}{2}\ddot{u}_{(i)}$$
(3.2)

The velocities are integrated through time.

$$u_{(i+1)} = u_{(i)} + \Delta t_{(i+1)} \dot{u}_{(i+\frac{1}{2})} \tag{3.3}$$

- Element calculations

Element strain increment, $d\varepsilon$, is computed from the strain rate, $\dot{\varepsilon}$, which is decided according to the velocity of nodes.

Then stress, σ, is computed from the material constitutive equation.

$$\sigma = f(\varepsilon, \dot{\varepsilon}, \theta) \tag{3.4}$$

3.1.1.2 Thermal Analysis Procedure

In the chip formation analysis, the stress analysis is dependent on the temperature distribution and the temperature distribution depends on the stress solution. Fully coupled thermal-stress analysis is employed.

In the analysis, heat transfer equations are integrated using the explicit forward difference time integration rule.

$$\theta^N_{(i+1)} = \theta^N_{(i)} + \Delta t_{(i+1)} \dot{\theta}^N_{(i)} \tag{3.5}$$

where θ^N is the temperature at node N.

The values of $\dot{\theta}^N_{(i)}$ are computed at the beginning of the increment by

$$\dot{\theta}^N_{(i)} = (C^{NJ})^{-1}(P^J_{(i)} - F^J_{(i)}), \tag{3.6}$$

where

C^{NJ} is the lumped capacitance matrix;

P^J is the applied nodal source vector;

F^J is the internal flux vector.

The explicit integration rules are realized in both dynamic and thermal analysis procedures by using lumped mass matrix and capacitance matrix. The heat transfer

and mechanical solutions are obtained simultaneously by an explicit coupling. Therefore no iterations or tangent stiffness matrices are required.

3.1.2 Stability Limit

The central difference and forward difference integrate constant accelerations, velocities and temperature increments per unit time. In order to produce accurate result, the time increment must be quite small so that the integrated variables are nearly constant during an increment. The time increment must be smaller than a stability limit otherwise the solution becomes numerically unstable. For coupled thermal-stress analysis, the stability limit can be calculated by

$$\Delta t \leq \min(\frac{2}{w_{\max}}, \frac{2}{\lambda_{\max}}) \tag{3.7}$$

where $w_{\max}$ is the highest frequency in the system of equations of the mechanical solution response and $\lambda_{\max}$ is the largest eigenvalue in the system of equations of the thermal solution response.

The ABAQUS/Explicit solver supplies the default time incrementation scheme, which is fully automatic and requires no user intervention.

3.2 Continuous Chip Formation Simulation

Continuous chip is very common when most ductile materials, such as wrought iron, mild steel, copper, and aluminium, are machined. Cutting under these conditions is steady-state process with steady chip shape, cutting force and temperature. Many chip formation models were developed for these cutting conditions with different FE codes. They are based on different approaches: Lagrangian or Eulerian.

3.2.1 Limitation Of The Existing Chip Formation Models

This continuous chip formation process cannot obtain very satisfactory simulation result because of the limitations of the existing models using ABAQUS FE code:

- Most models take chip formation as a Lagrangian problem. Under the consideration of reducing calculation time, the length of the workpiece is often very small, only enough to produce a steady chip shape. If analysis of the further cutting process is required, a longer workpiece has to be used in the simulation, which increases calculation time direct proportionally.

- In most chip formation models, chip separation is realized by element removal or node debond. A small crack is always created before tool edge, as shown in Fig. 3.1. But evidences from cutting experiments show that for the quasi-continuous chip formation that takes place in machining ductile materials under favourable cutting conditions, crack occurs along the shear direction [Didj-97]. Only for discontinuous chip formation and chip formation with build-up edge, crack is found ahead of the cutting edge.

(a) Node debond [McCl-02]   (b) Element removal [Ng-02a]
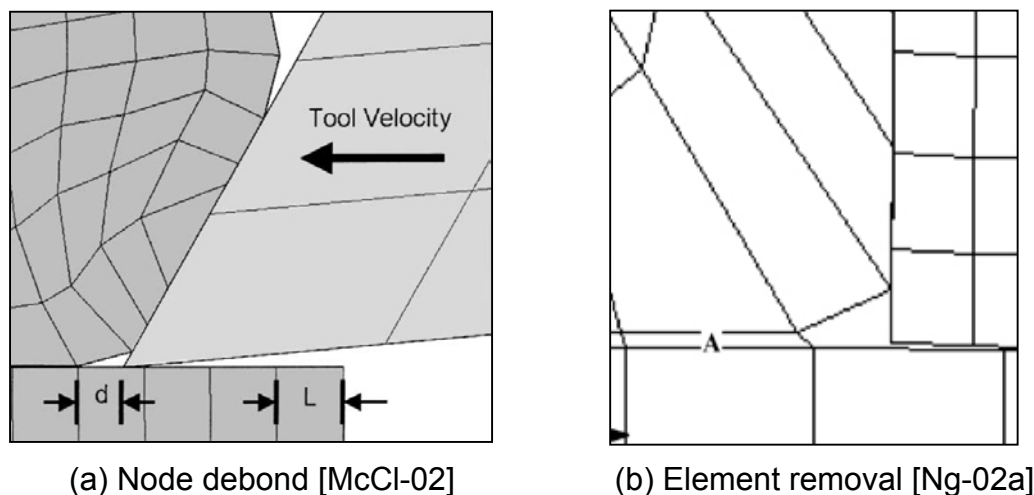
Fig. 3.1 Cracks formed before tool edge in the simulations

- The chip separation path is often predetermined instead of formed automatically by the deformation of workpiece material under the cutting action. When round edge cutting tools are used, the position of the predetermined chip separation path has influence on the volume of material to be cut away. Whether the cutting force components, residual stress, etc change with the position of the separation path or not needs analysing as well.

- A chip separation criterion is necessary. In ABAQUS, chip separation criterion is given by defining material failure criterion. The failure parameters are material dependent and different parameters are required for Johnson-cook and other material models. Although many material constitutive models are provided for the commonly used material by literatures, the failure parameters are seldom given as well. Failure parameters relate to the successful implementation of chip formation simulation. They should be determined experimentally instead of being given at random. This limits the usage of many material constitutive models.

- When the steady-state chip formation process is modelled as a Eulerian problem with ABAQUS/Explicit, as reported by Arrazola et al [Arra-02], the conflict between the cutting time to reach steady state and the length of the workpiece model limited by calculation time is solved. Steady-state analysis is performed by prolonging the cutting time without increasing the length of the workpiece. In addition no shear failure criterion is required. But an initial chip geometry must be given according to experiment or experience in machining. When the given initial chip geometry is not suitable, chip geometry cannot adapt itself when the chip tends to swell up or to shrink too much from the given initial geometry, as shown in Fig. 3.2.
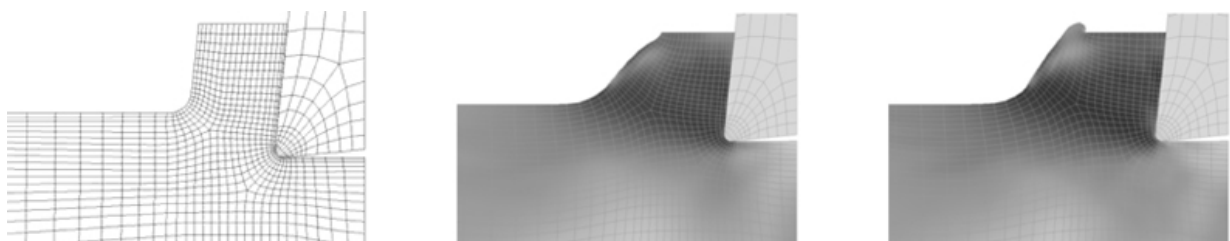
(a) When the given initial chip is thinner than in experiment, the chip swells up from the initial geometry
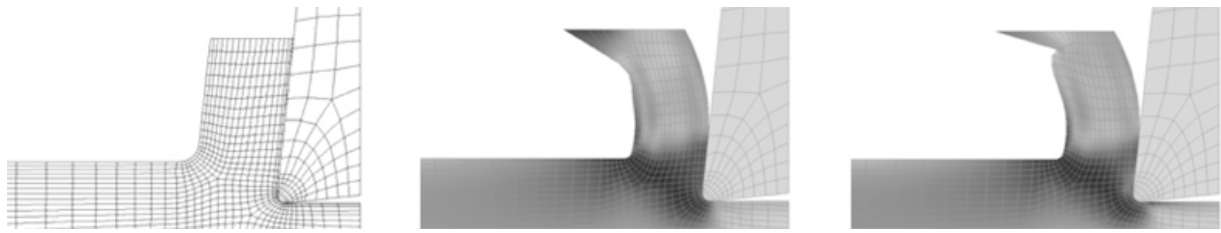
(b) When the given initial chip is thicker than in experiment, the chip shrinks from the initial geometry

Fig. 3.2 Problems in the chip formation analysis with an unsuitable initial chip geometry [Arra-02]

3.2.2 Advantages Of The New-developed Chip Formation Model

Due to the limitations mentioned above, a new continuous chip formation model is developed with ABAQUS/Eplicit. This model has the following advantages:

- Workpiece geometry in the model only stands for a control area. Workpiece material is unlimited and flowing through this control area continuously. User can prolong the cutting time without changing the size of the control area.

- Chip separation is realized with adaptive meshing technique supplied by ABAQUS/Explicit; no shear failure criterion or material failure parameters are required. Most of the material constitutive models can be used in this model.

- Chip separation is performed by the deformation of the workpiece material, instead of forming crack along a predetermined path.

- Good contact is maintained in the cutting tool edge area. No obvious crack is formed.

- This model is especially suitable to simulate the cutting process with round edge tool or chamfered tool.

- No initial chip geometry is required. Chip formation simulation includes the entire process from initial chip formation, chip growth, to steady state.

3.2.3 Adaptive Meshing Technique In ABAQUS/Explicit

This model is developed based on adaptive meshing technique in ABAQUS/Explicit. It combines the features of pure Lagrangian and Eurerian analysis and can be used

to both Langrangian, e.g. initial chip formation, and Eulerian problems, e.g. steady-state chip formation.

3.2.3.1 Boundary Region Types

Adaptive meshing is performed in adaptive meshing domains, which can be either Lagrangian or Eulerian.
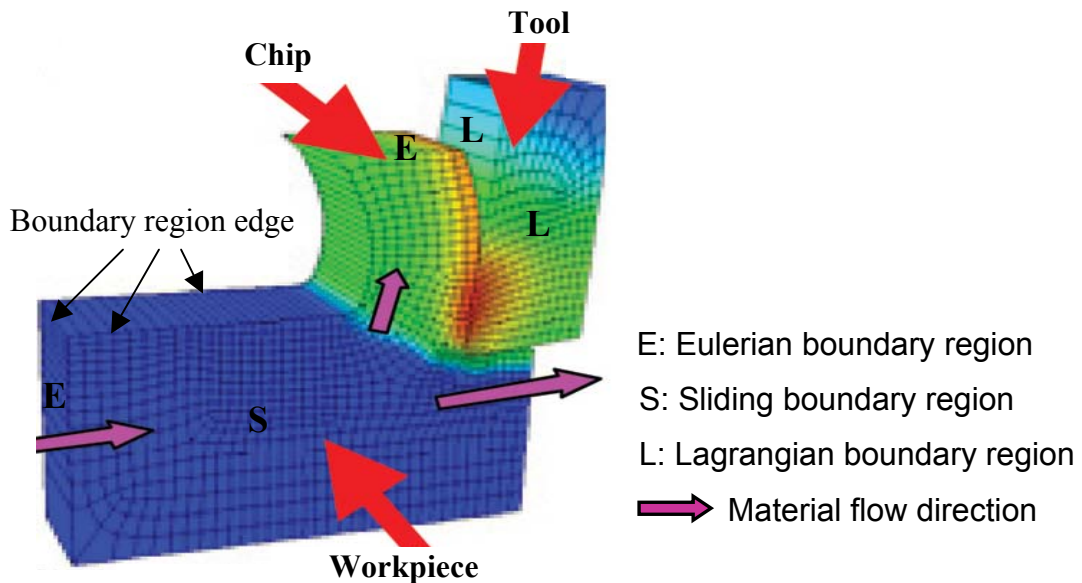
Fig. 3.3 Boundary regions in chip formation model

The boundary regions of the adaptive meshing domain can be either Lagrangian, sliding or Eulerian. In Lagrangian boundary region, the mesh is constrained to move with the material in the direction normal to the surface of the boundary region and in the directions perpendicular to the boundary region edge. In sliding boundary region, the material is constrained to move with the material in the directions normal to the boundary region, but it is completely unconstrained in the directions tangential to the boundary region. Eulerian boundary regions can be defined only on the exterior of a geometry model and the material flows across the boundary, as in a fluid flow problem. Mesh on the Eulerian boundary regions are fixed in space using spatial mesh constrains, and material flow velocity across the boundary is defined by boundary conditions. When the adaptive meshing domain is Eulerian type, only sliding and Eulerian boundary regions can be defined, for example the workpiece in Fig. 3.3.

3.2.3.2 Geometry Features

On boundary regions where the angle θ between the normals on adjacent element faces is greater than an initial geometric feature angle θ_I given by the user, geometry features are detected initially. Adaptive meshing cannot be performed well across such geometry features because the nodes cannot move across the geometry features unless they flatten. Therefore it is sometimes necessary to deactivate the geometry features by defining a greater initial geometry angle.

(a)   (b)
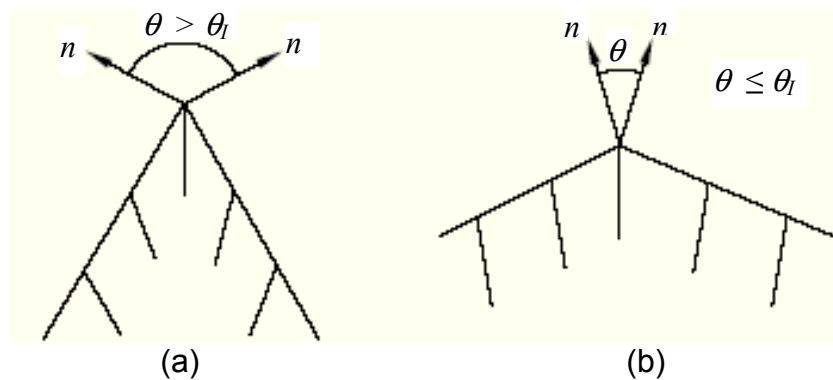
Fig. 3.4 Geometry Features (a) Geometry feature is detected, no mesh flow is permitted past the corner (b) No geometry feature is detected, mesh flow is permitted

3.2.3.3 Curvature Refinement

During adaptive meshing, mesh-smoothing algorithms based on minimizing element distortion tend to reduce the mesh refinement in area of concave curvature, especially as the curvature evolves. Having sufficient mesh refinement near highly curved boundaries is very important to model the detail of the chip shape near the chip separation area. To prevent the natural reduction in mesh refinement of areas near evolving concave curvature, solution-dependent meshing is used to focus mesh gradation toward these areas automatically by defining the curvature refinement weight α_c a high value, for example, $\alpha_c = 1$.

(a) α_c=0   (b) α_c=1
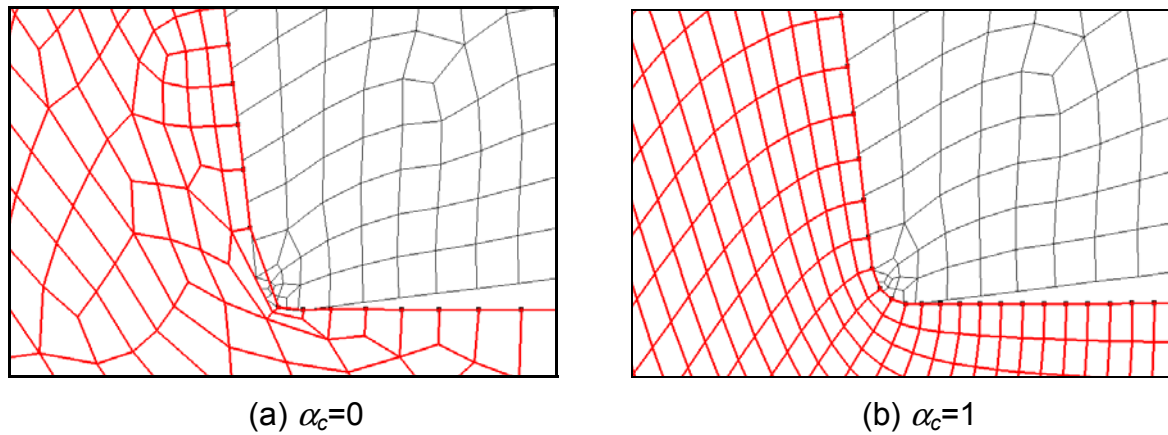
Fig. 3.5 Effect of curvature refinement

3.2.4 Analysis Steps

The entire continuous chip formation process is performed with a complete modeling procedure from initial chip formation to the realization of steady state, which consists of three analysis steps, including initial chip formation, chip growth, and steady-state chip formation as described in detail in the following parts. The first two analysis steps supply steady chip geometry for the steady-state chip formation analysis step. During all the chip formation steps, coupled thermo-stress analyses are performed. The simulated cutting condition is given in Table 3.1.

Table 3.1: Cutting condition

Cutting type	Orthogonal cutting, turning operation, dry cutting
Work material	Mild carbon steel AISI1045
Tool material	Uncoated carbide WC-Co
Tool geometry	$\gamma_o = -7°$, $\alpha_o = 7°$, $r_\varepsilon = 0.0245mm$
Cutting parameters	$v_c = 300m/\min$, $a_p = 2mm$, $f = 0.145mm/r$

In the finite element model, the workpiece has a size of 0.6×3.2mm, which is meshed with 4-node bilinear coupled temperature-displacement plain strain elements CPE4RT. In order to save calculation time, only the part of the cutting tool near the cutting edge is included in the chip formation modelling. Moreover in the first two steps, the cutting tool is defined as a rigid body, whereas in the last analysis step the cutting tool is modelled as a deformable body in order to obtain better analysis result and more comprehensive analysis data.

3.2.4.1 Initial Chip Formation

This analysis step aims to form initial chip geometry. This chip formation process is modelled as a Lagrangian problem.

(a) Initial geometry and mesh   (b) Initial chip geometry formed at t=0.18ms
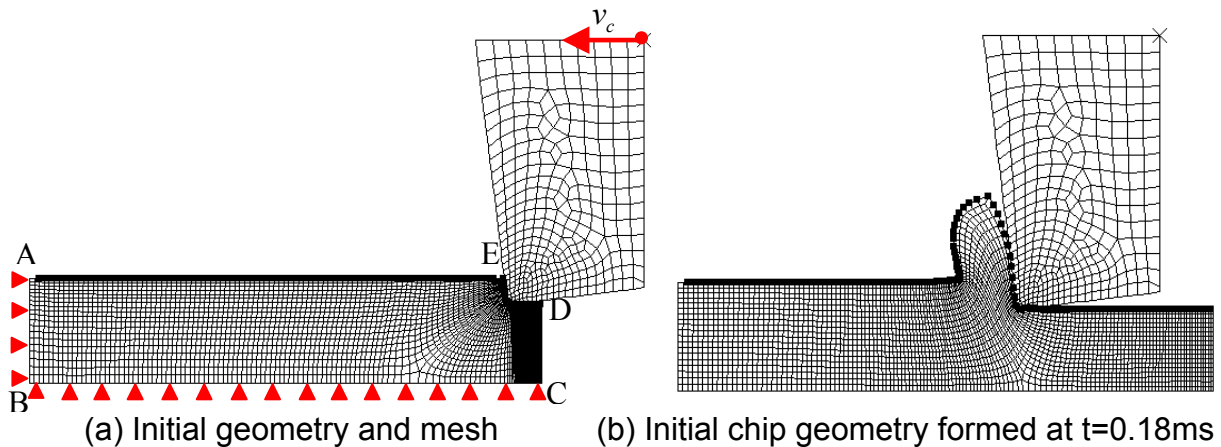
Fig. 3.6 Initial chip formation analysis

The initial workpiece geometry is designed to have a concave at the top-right corner under the consideration of seeding more nodes along the concave surface (see Fig. 3.6(a)). The boundary of the workpiece consists of only Lagrangian boundary regions. During the initial chip formation process, the Lagrangian boundary region on the top surface of the workpiece traces the chip material continuously and forms the shape of the chip.

At the cutting edge, chip material separates with workpiece material. Only very fine mesh can show exactly the shape of this area. In order to maintain the mesh refinement in this area while the chip formation process continues, the initial geometry feature angle should be given a suitable value. According to this value, the four corner points A, B, C and D in Fig. 3.6(a) can be detected as geometry features but corner point E and the workpiece nodes on the surface ED should not be taken as geometry features. The value is defined by calculating the angle θ^i between the normals on adjacent element faces in chip separation area, as shown in Fig. 3.7, finding out the maximum angle value, then taking an angle value between this maximum angle value and 90 deg (because the angles at point A, B, C and D are about 90 deg). Adaptive meshing can be performed on any boundary regions except point A, B, C and D.
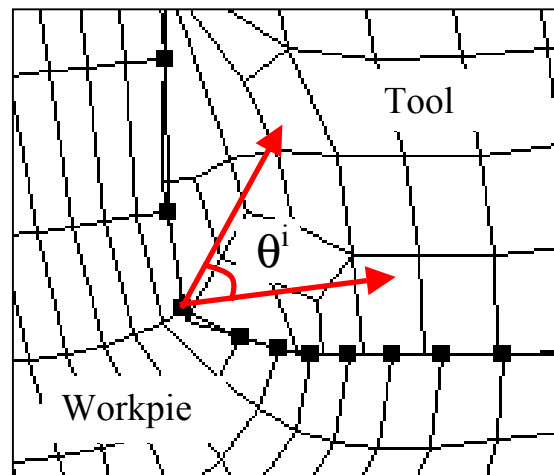
Fig. 3.7 Determination of initial geometry feature angle

In addition solution-dependent meshing is used to focus mesh toward the chip separation areas automatically by setting the curvature refinement weight α_c to unity. At the beginning the cutting tool is at the right side of the workpiece. The workpiece is fixed and the cutting tool is moving in the negative x-direction[1]. With the cutting tool advancing into the workpiece, elements along the concave surface extend and compose the outside surface of the chip. After 0.18ms an initial chip is formed. Fig. 3.6(b) shows the mesh after the initial chip is formed.

3.2.4.2 Chip Growth

After the initial chip is formed, chip growth analysis step is performed. This analysis step aims at forming steady chip geometry. In this step the chip formation process is treated as a Eulerian problem.

A user program is developed with Python language. It reads the variables about nodal coordinate, nodal temperature, etc of the workpiece and the cutting tool from the selected time point of the initial chip formation analysis step, when a desirable initial chip shape is produced. Then it writes them into the model files of the chip growth analysis step, including node input file, initial temperature input file, etc. Therefore the initial state of the workpiece and the cutting tool in this step remains the state at the selected time point of the former analysis step. For example, in this simulation the initial state information is read from the former analysis step at 0.18ms.

---

[1] In all figures of this paper, x-direction is pointed to the right side and y-direction to the top of the page.

In this step, the relative movement between the cutting tool and the workpiece is performed by the movement of workpiece material. The cutting tool is fixed in space. The workpiece mesh in Fig. 3.8 represents only a control area. The left and right boundary of the control area are defined as Eulerian boundary regions, whose mesh is fixed in x-direction by using mesh constrain definition, but material flows into the control area continuously from the left boundary at the cutting speed and flows out of from the right boundary, as indicated with the small arrows in Fig. 3.8(a). The top and bottom boundary are sliding boundary regions. The movement of the mesh on the bottom boundary is constrained in y-direction, indicated with small triangle in Fig. 3.8(a). But the movement of the mesh on the top boundary is not constrained; the mesh will adjust itself to fit in with the developing chip geometry.

Initial geometry feature angle is defined in the same way as explained above. The curvature refinement weight α_c is set to unity.

Fig. 3.8(b) shows that the chip is growing with the material flowing into the control area.

(a) Initial geometry and mesh   (b) Chip growth at t= 0.09ms
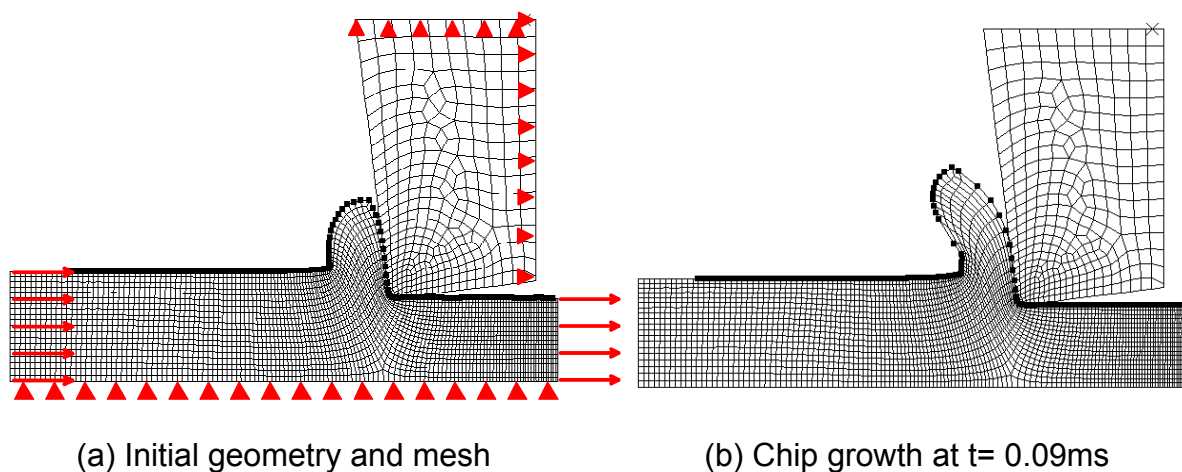
Fig. 3.8 Chip growth analysis

3.2.4.3 Continuous Steady-state Chip Formation

In the second analysis step, with the chip growing to a certain extent, the mesh of the chip extends too much in the direction of chip growth so that adaptive meshing cannot solve mesh distortion problem any more. The steady-state chip formation analysis step is designed for simulating the further cutting process. In this step, the cutting process is treated as a Eulerian problem as well. According to the definition of

the workpiece mesh, two methods can be used in the continuous steady-state chip formation step: mesh modification and model regenerating.

Method 1: Mesh Modification

During the growth of the chip in the second analysis step, the chip geometry near the chip root becomes steady since a certain time point. The state of the workpiece and the cutting tool at this time point is written into the model files of steady-state cutting analysis step. For example, the mesh in Fig. 3.9(a) is read from chip growth analysis step at t=0.09ms, see Fig. 3.8(b).

In order to allow the chip to flow out of the mesh and grow unlimitedly instead of grow visually with the mesh, the mesh at the top boundary of the chip is defined as a Eulerian boundary region. The coordinates of the nodes on this boundary are adjusted to locate these nodes along a vertical line in order to facilitate the definition of mesh movement constrain in x-direction, as shown in Fig. 3.9(a). The mesh of the boundary is not constrained in y-direction; its position and size can adjust with the chip automatically in y-direction.

The definition of boundary regions and conditions for the other part of the workpiece control area are similar to those in the second analysis step. Initial geometry feature angle and curvature refinement weight α_c are defined in the same way as explained above.

Because the cutting tool is a deformable body, its movement is fixed by defining constraint in x-direction at the right boundary and in y-direction at the top boundary. Fig. 3.9(b) shows the formed mesh at 1ms.

    (a) Initial geometry and mesh   (b) Mesh at t=1ms
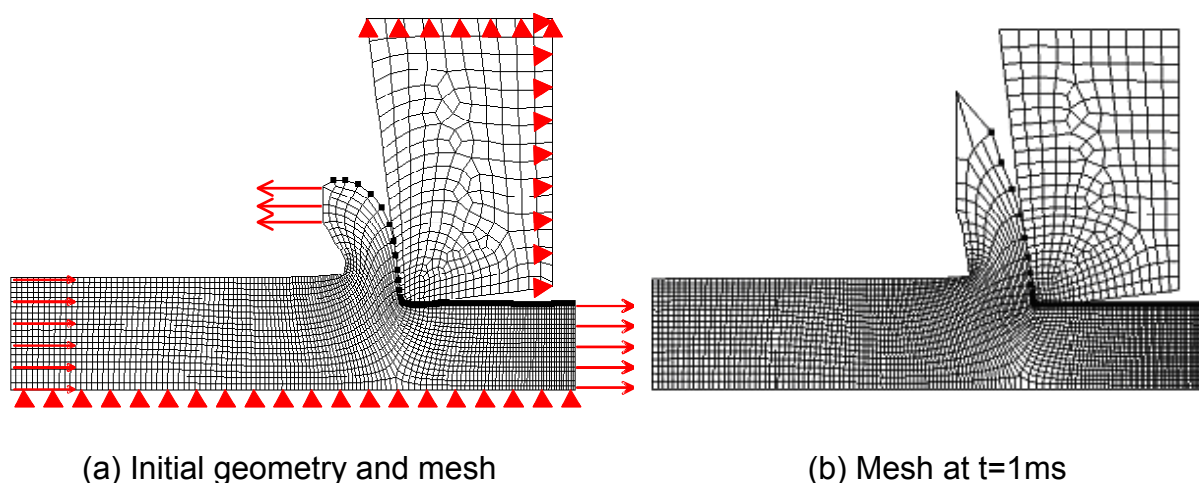
Fig. 3.9 Mesh modification

Method 2: Model Regenerating

This method is especially important when the cutting tool has some special geometry, e.g. crater wear, and good contact between the workpiece and the cutting tool in these areas is desired.

ABAQUS/Explicit supplies only r-adaptivity. When the mesh concentrates in the cutting edge area according to solution-dependent meshing rule, the mesh in other area becomes coarse. But sometimes fine mesh along the whole tool-workpiece and tool-chip interface is required. Model regenerating supplies an approach to improve the contact problem.

The information necessary for model regenerating includes chip thickness and tool-chip contact length. They can be obtained from the former two analysis steps, initial chip formation and chip growth analysis step, in which a steady chip shape is formed. The regenerated workpiece model in Fig. 3.10(a) has a chip connected to the workpiece. The chip is 0.3mm thick, and 0.5mm long. The length of the chip should be determined carefully. It is larger than the tool-chip contact length. But when the chip is too long, it will complicate the definition of mesh constraint.

The mesh at the top boundary of the chip is defined as a Eulerian boundary region. The mesh movement is constrained in y-direction. The mesh position and size in x-direction will be adjusted with the chip automatically.

(a) Initial geometry and mesh   (b) Mesh at t=1ms
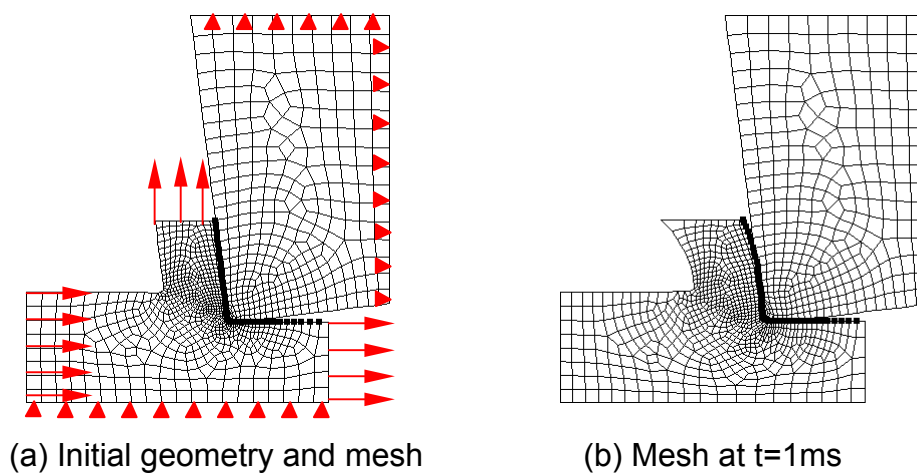
Fig. 3.10 Model regenerating

Very fine mesh is given along the entire tool-chip interface. This ensures good contact between the cutting tool, the workpiece and the chip throughout the entire steady-state analysis process, as shown in Fig. 3.11.
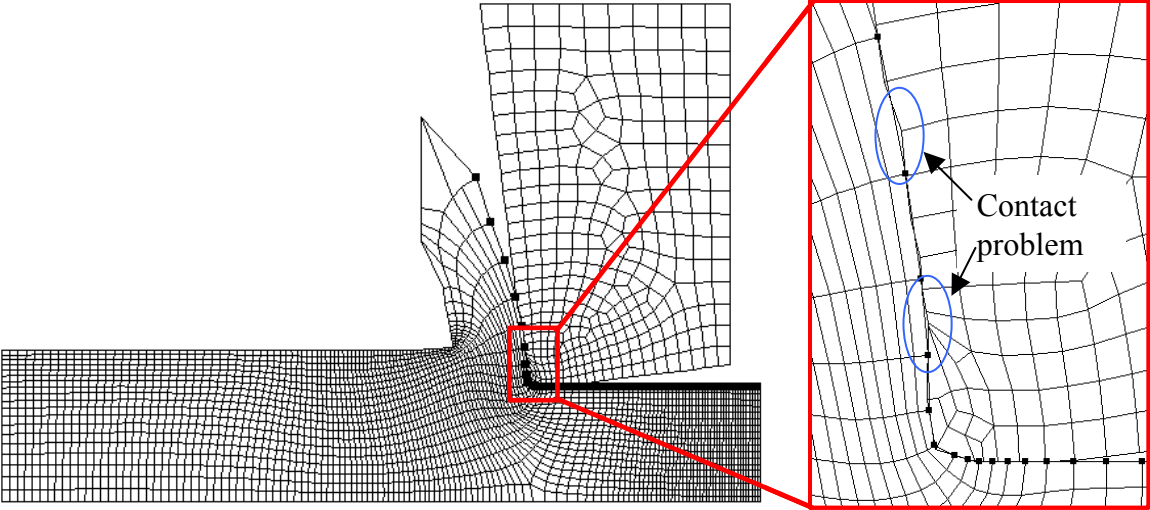
(a) Contact problem is created by using mesh modification
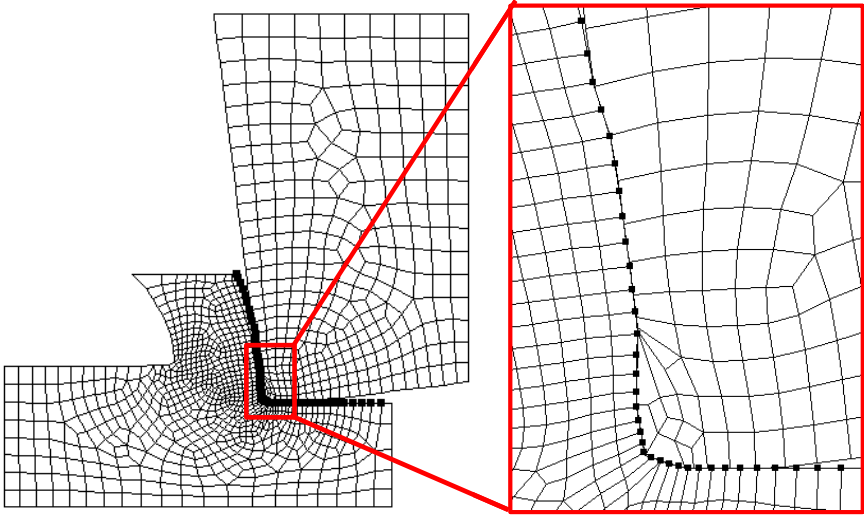
(b) Contact is improved by using model regenerating

Fig.3.11 Contact status along tool-chip interface

3.2.5 Results & Discussion

3.2.5.1 Stress Analysis

Fig. 3.12 shows the stress distribution in the three analysis steps. Maximum stress is located in the primary shear zone; the workpiece material undergoes serious shear plastic deformation in primary shear zone and becomes chip.

Further the underside of the chip undergoes high stress because of the contact and friction with the tool face when sliding away.

The newly formed machined surface has contact and friction with the round edge and sometimes a small part of the flank face. This results in a high stress in the workpiece material beneath the cutting tool edge.

(a) Initial chip formation analysis, t=0.18m   (b) Chip growth analysis, t=0.3ms

(c) Steady state analysis, t=1ms
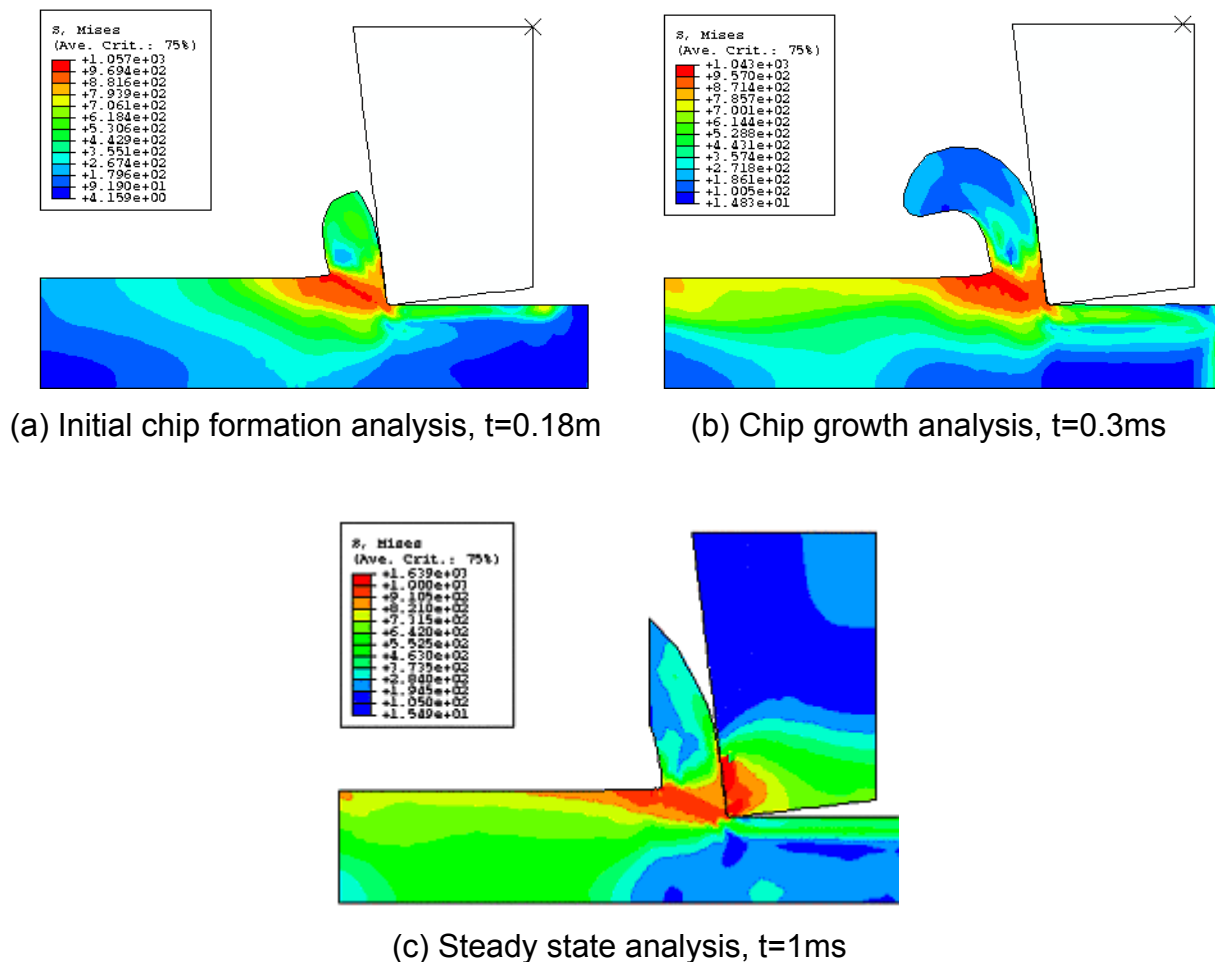
Fig. 3.12 Stress distribution (MPa)

In steady state analysis step, the cutting tool is modelled as a deformable body; very high stress is observed in the small part of the cutting tool directly under the tool-chip contact area.

3.2.5.2 Plastic Strain Analysis

Fig. 3.13 shows that the workpiece material undergoes serious plastic deformation in primary shear zone. The material in the chip underside deforms plastically again

under the pressure and friction of the cutting tool face. This results in higher plastic strain formed in the chip underside than in the other part of the chip.
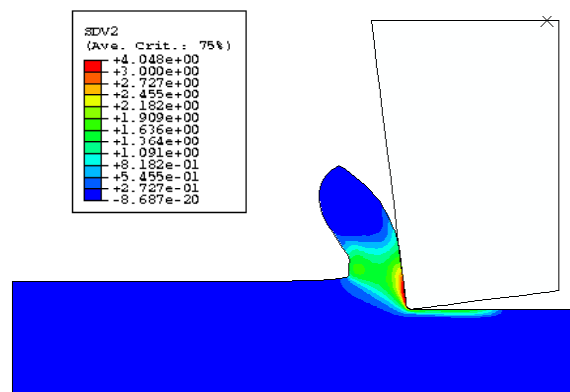
(a) Chip growth analysis step, t=0.09ms
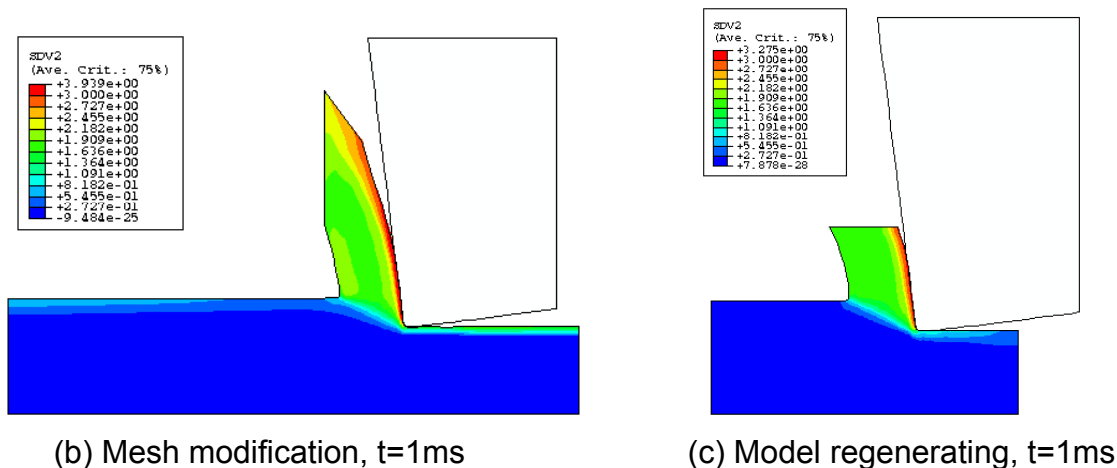
(b) Mesh modification, t=1ms   (c) Model regenerating, t=1ms

Fig. 3.13 Equivalent plastic strain distribution

In Fig. 3.13(a), the top of the chip has no plastic strain because only the geometry of this part is imported from the initial chip formation analysis step, not including the created plastic strain. In the steady-state analysis, the two model methods create similar plastic strain field, and only the maximum values are different which is caused by the different contact condition due to element size in the workpiece model and the difference between deformable cutting tool and rigid body cutting tool.

3.2.5.3 Strain Rate

Fig. 3.14 shows the distribution of strain rate, which is defined as solution SDV9 by material subroutine. Under the example cutting condition, the maximum strain rates

distribute along the primary shear zone, especially in the areas close to the cutting tool edge and the free surface of the workpiece, and reach up to 10^5, which is assumed as typical maximum strain rate in conventional machining [Arnd-73].

(a) Chip growth step, t=0.09ms

(b) Mesh modification, t=1ms   (c) Modal regenerating, t=1ms
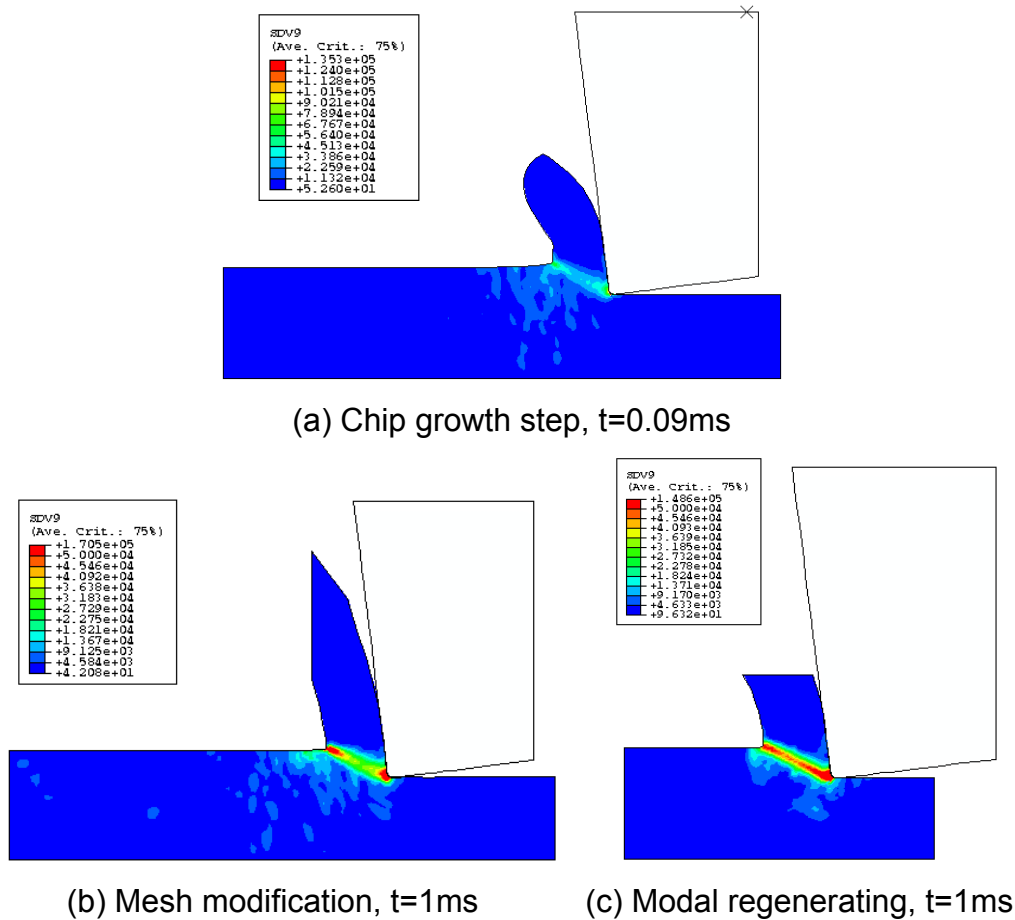
Fig. 3.14 Strain rate distribution

3.2.5.4 Temperature Analysis

In Fig. 3.15(b), within the cutting process of 1ms cutting temperatures at most of the tool face nodes in the tool/chip interface, i.e. the highlighted nodes in Fig. 3.15(a), is reaching steady values, while at the tool face nodes inside the cutting insert, the highlighted nodes in Fig. 3.15(c), the temperature is still climbing, as shown in Fig. 3.15(d). This means that thermal steady state is not realized in the whole cutting tool.
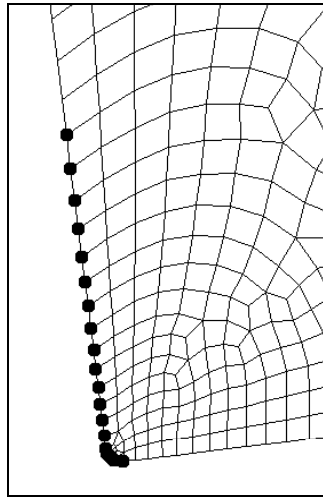
(a) Position of monitored tool face nodes   (b) Temperature progress
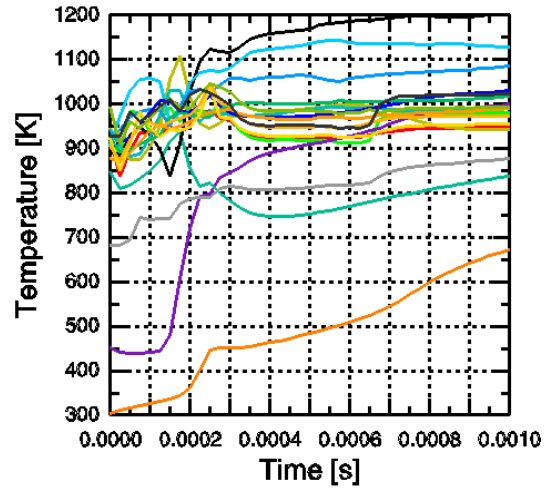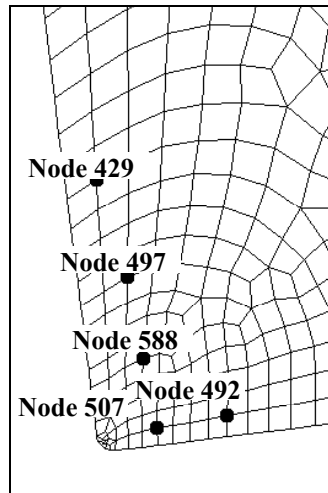
(b) Position of nodes inside the tool   (d) Temperature history
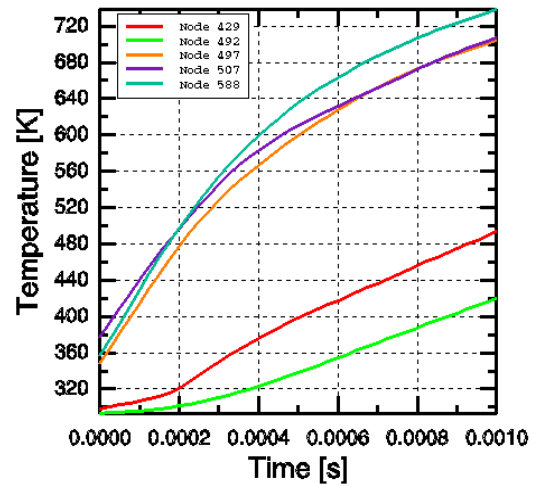
Fig. 3.15 Temperature history of tool nodes at steady-state chip formation analysis step

Fig. 3.16 shows the temperature distribution at 1ms. The highest temperature is at the rake/chip interface and most part of the tool is still at room temperature.
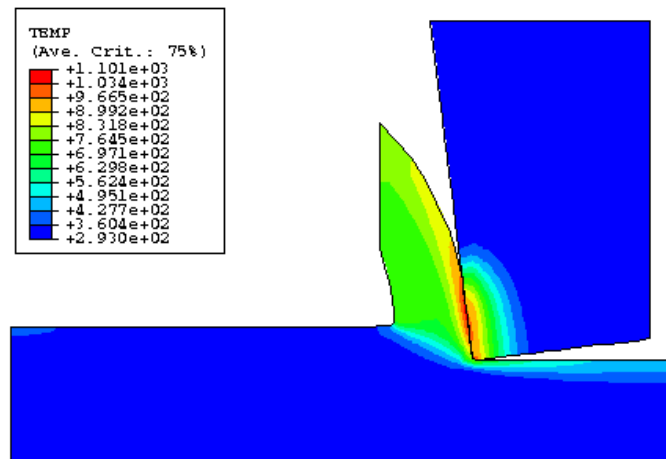
Fig. 3.16 Temperature distribution at t=1ms of steady-state chip formation analysis step

3.2.5.5 Verification With Experimental Data

By adding the reaction force component in the same direction at all constrained nodes of the cutting tool and then taking the negative value, the cutting force components F_c and F_t in the continuous steady-state chip formation step are obtained. Fig. 3.17 shows that the cutting force components change within a very narrow range from 0.7ms, and it is deemed that the mechanical steady state is realized.
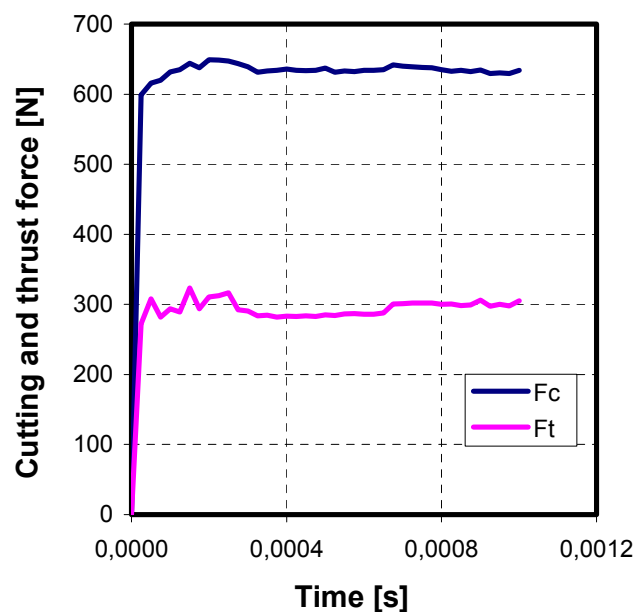
Fig. 3.17 Cutting force progress (under cutting condition: v_c=300m/min, a_p=2mm, f=0.145mm/r)

In Fig. 3.18, the cutting force values obtained from the simulation with ABAQUS/Explicit code are compared with the experiment data [Feve-01] and the result from other software including Third Wave, Deform2D and Oxcut-F [Söhn-03].

The results from ABAQUS include ABQ-f030I, ABQ-f030S, ABQ-f048I and ABQ-f048S. I means the result is obtained from initial chip formation step, while S from continuous steady state chip formation step. Two different frictional coefficient values are used. One is 0.30, another is calculated according to Eq. 1.3, and the value is 0.48.

Fig. 3.18 shows that the cutting force components obtained from initial chip formation step and continuous steady state chip formation step have no great difference. The cutting force components created in the chip formation analysis with the frictional coefficient of 0.48 gives the better result than other FEM code, the prediction error of cutting force F_c is about 2%, and the error of thrust force F_c is about 5%.
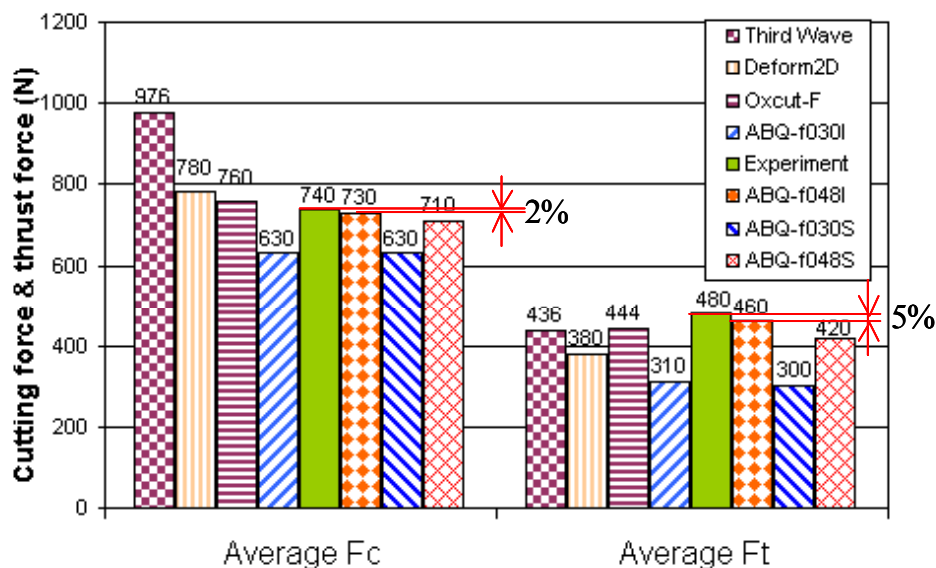
Fig. 3.18 Comparison of cutting force (under cutting condition: v_c=300m/min, a_p=2mm, f=0.145mm/r)

3.3 Chip Formation Simulation For Milling Operation

In milling operation, cutting action is discontinuous and the chip produced is discontinuous. The modelling method developed for the continuous chip formation is not suitable to simulate chip formation process in milling operation. Therefore a different modelling method is introduced in the following part.

3.3.1 Chip Separation

In every milling cycle, the produced chip will separate with the newly produced workpiece surface without any connection when the cutting tool disengages from the workpiece. Hence the adaptive meshing technique in ABAQUS/Explicit cannot be used as a chip separation tool any more. In this method, chip separation is realized by defining shear failure criterion.

3.3.1.1 Shear Failure Criterion

The shear failure model is based on the value of the equivalent plastic strain at element integration points; when the equivalent plastic strain reaches the strain at failure $\bar{\varepsilon}_f^{pl}$, then the damage parameter w exceeds 1, material failure takes place. If at all the integration point material failure takes place, the element is removed from the mesh. The damage parameter, w, is defined as

$$w = \sum \left(\frac{\Delta \bar{\varepsilon}^{pl}}{\bar{\varepsilon}_f^{pl}} \right), \tag{3.8}$$

where $\Delta \bar{\varepsilon}^{pl}$ is an increment of the equivalent plastic strain. The summation is performed over all increments in the analysis.

There are two methods to define the strain at failure. For Johnson-cook plasticity model, the stain at failure is given according to Eq. 3.9.

$$\bar{\varepsilon}_f^{pl} = \left[d_1 + d_2 \exp\left(d_3 \frac{p}{q} \right) \right] \left[1 + d_4 In\left(\frac{\dot{\bar{\varepsilon}}^{pl}}{\dot{\varepsilon}_0} \right) \right] \left(1 + d_5 \hat{\theta} \right) \tag{3.9}$$

where strain at failure, $\bar{\varepsilon}_f^{pl}$, is dependent on a nondimensional plastic strain rate, $\dot{\bar{\varepsilon}}^{pl}/\dot{\varepsilon}_0$; a dimensional pressure-stress ratio, p/q (where p is the pressure stress and q is the Mises stress); and a nondimensional temperature, $\hat{\theta}$ (defined as 0, $(\theta - \theta_{transition})/(\theta_{melt} - \theta_{transition})$, or 1 depending on the temperature range). Stain at failure is defined by giving the failure parameters $d_1 - d_5$.

For Mises plasticity model, strain at failure or the dependencies of strain at failure on strain rate, pressure/stress ratio and temperature are given directly in tabular form in the data line.

3.3.1.2 A Numerical Method To Determine Strain At Failure

Normally, equivalent plastic strain at failure, $\bar{\varepsilon}_f^{pl}$, is obtained by using experimental methods. For example, Bacaria et al determined failure parameters $d_1 - d_5$ by performing tensile and torsion tests [Baca-00]. Ng et al integrated orthogonal tests with some analytical equations in metal cutting theory to define the dependency of the equivalent plastic strain at failure $\bar{\varepsilon}_f^{pl}$ on the plastic strain rate $\dot{\bar{\varepsilon}}^{pl}$; the hydrostatic stress p and temperature [Ng-02b].

By employing the continuous chip formation analysing methods, it is possible to determine stain at failure without making any experiment.

Observing the movement of material points on the chip underside and the machined workpiece surface in steady-state chip formation process, we can find a separation area of the workpiece material. For example, in Fig. 3.19, the separation area is between Node 13 and Node 16. The material above the separation area moves upwards into the chip and the material below the separation area moves downwards to join in the machined surface.
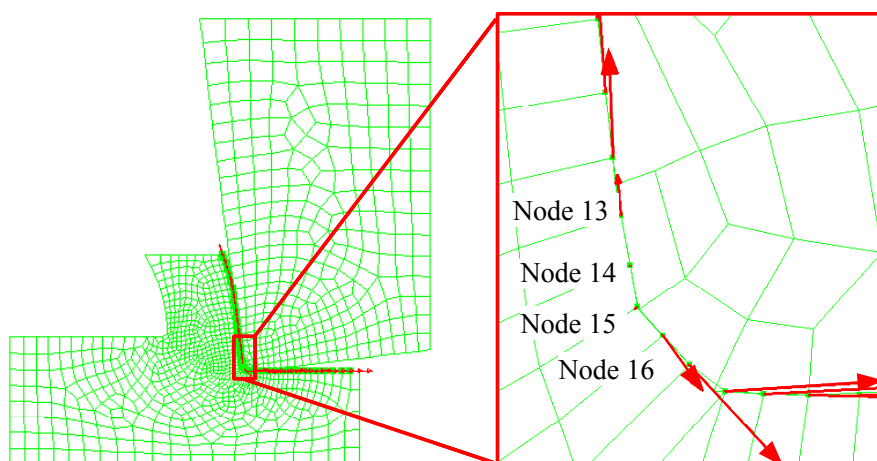
Fig. 3.19 Velocity of material points at workpiece nodes on the chip underside and the machined surface (the arrows shows the velocity vectors)

According to the sliding velocities of the workpiece material points along tool-chip interface, a more exact position of the separation area can be defined in Fig. 3.20. The directions of sliding velocities of the material points in the area between Node 15 and Node 16 change. It can be assumed that material failure is taking place in this area. The equivalent plastic strain between Node 15 and Node 16 gives a value range from 2.25 to 2.7 to strain at failure.
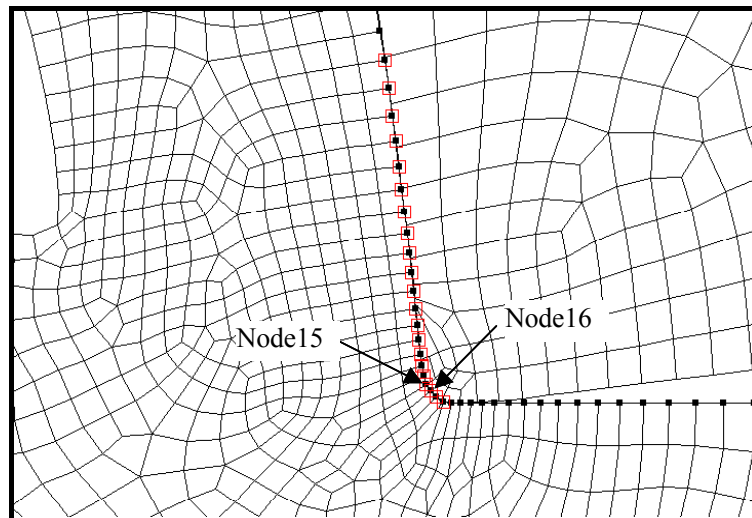
(a) Monitored points
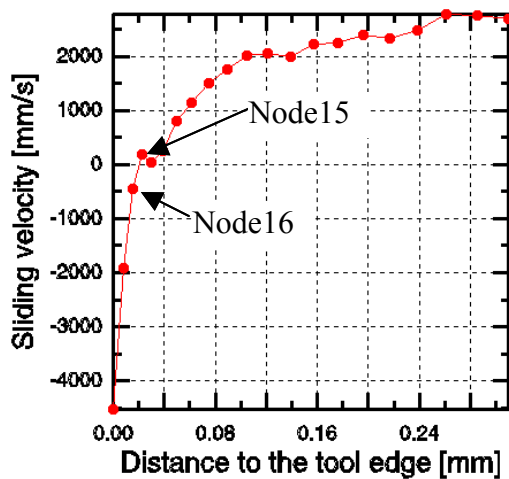
(b) Sliding velocity of monitored points   (c) Equivalent plastic strain of monitored points
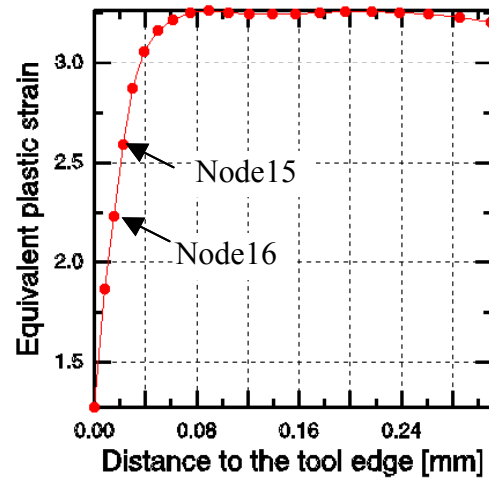
Fig. 3.20 Determination of strain at failure

By varying cutting parameters or tool geometry, the dependency of strain at failure on temperature, strain rate, pressure, etc can be studied.

In the following part of this chapter, strain at failure for mild carbon steel is set to 2.5.

3.3.2 Chip Formation Modeling

This chip formation modeling method is explained by taking a milling case as an example in which an uncoated carbide tool is used to machine mild steel CK45. The cutting condition is given in Table 3.2.

Table 3.2 Cutting condition

Cutting type	Orthogonal cutting, milling operation, dry cutting
Work material	Mild carbon steel CK45
Tool material	Uncoated carbide WC-Co
Tool geometry	$\gamma_o = 7°$, $\alpha_o = 7°$
Cutting parameters	$v_c = 600 m/\min$, $a_e = 2mm$, $a_p = 1mm$, $f_z = 0.2mm/r$

The diameter of the milling tool is 125mm. In order to reduce the calculation time, only a small part of the workpiece and the cutting insert is included in the model. Fig. 3.21 shows the initial geometry, mesh and assembly of the workpiece and the cutting insert.
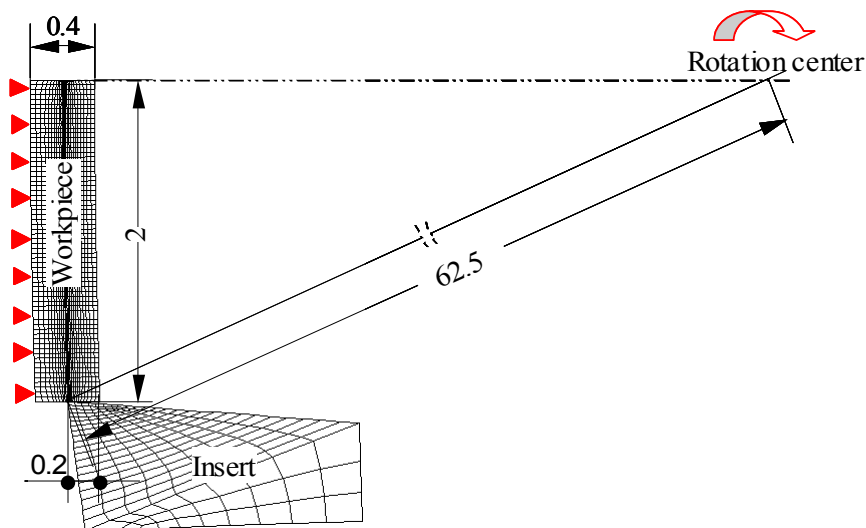
Fig. 3.21 Initial geometry, mesh and assembly of the tool and the workpiece in chip formation analysis

The workpiece is simplified as a small segment of a ring; whose outside radius is 62.7mm and inside radius 62.3mm. The centre of the ring is positioned at the rotation centre of the cutting insert. The workpiece is 2mm high. The extension of its upper

surface passes through the center of the ring and the lower surface is parallel to the upper surface. The workpiece is discretized with a mesh composed of CPE4RT elements, and local fine mesh is given along the moving path of the cutting edge because of very high gradients of solutions in this area, such as temperature, stress, etc.

The cutting insert in the model includes only the part near the cutting edge, which is discretized with CPE4RT elements. The cutting insert is modelled as a deformable body in order to obtain all the necessary cutting process variables for the latter study on tool wear.

The chip formation process is treated as a Lagrangian problem. Every boundary segment of workpiece is defined as a Lagrangian boundary region.

There are different ways to assign shear failure criterion to form different shape of chips. Ng et al designed two different kinds of shear failure criteria, one criterion is assigned to a line of element along the moving path of the cutting edge to separate the chip from the workpiece; another criterion is assigned to part of the chip material to generate cracks in order to simulate serrated chips [Ng-02b]. Bacaria defined only one material shear failure model for the whole workpiece material [Baca-00]. In the model the shear failure criterion is integrated with a material model designed specially for the workpiece material CK45 and assigned to the whole workpiece.

One milling cycle takes 39.27ms. In each milling cycle, cutting phase takes 0.2ms and cooling phase takes 39.07ms. The chip formation analysis is performed for 0.5ms, covering the whole cutting phase and 0.3ms of the later cooling phase.

3.3.3 Result & Discussion

3.3.3.1 Stress Analysis

At the beginning, the cutting insert is at the bottom of the workpiece, and there is no contact with the workpiece. With the tool rotating in clock-wise direction, the cutting insert engages in the fixed workpiece. A small chip is formed, and the contact between the chip and the cutting insert concentrates in a small area near the cutting edge, which results in a high stress in this area, as shown in Fig. 3.22(a).

Fig. 3.22(b) shows that the primary deformation zone has the maximum stress in the workpiece.

In Fig. 3.22(c), the cutting insert is disengaging the workpiece. The workpiece material to be cut away deforms seriously under the pressure of the cutting insert and protrudes from the original top surface, which provides a possibility for burr formation. But after crack generates, it propagates along the direction of maximum stress deeper and deeper into the workpiece material, instead of along the moving path of the cutting edge.

During the entire cutting phase, the cutting edge is bearing higher stress than other part of the insert because of positive rake angle and very sharp tool edge.

(a) t= 0.025ms   (b) t= 0.100ms

(c) t=0.175ms   (d) t=0.200ms
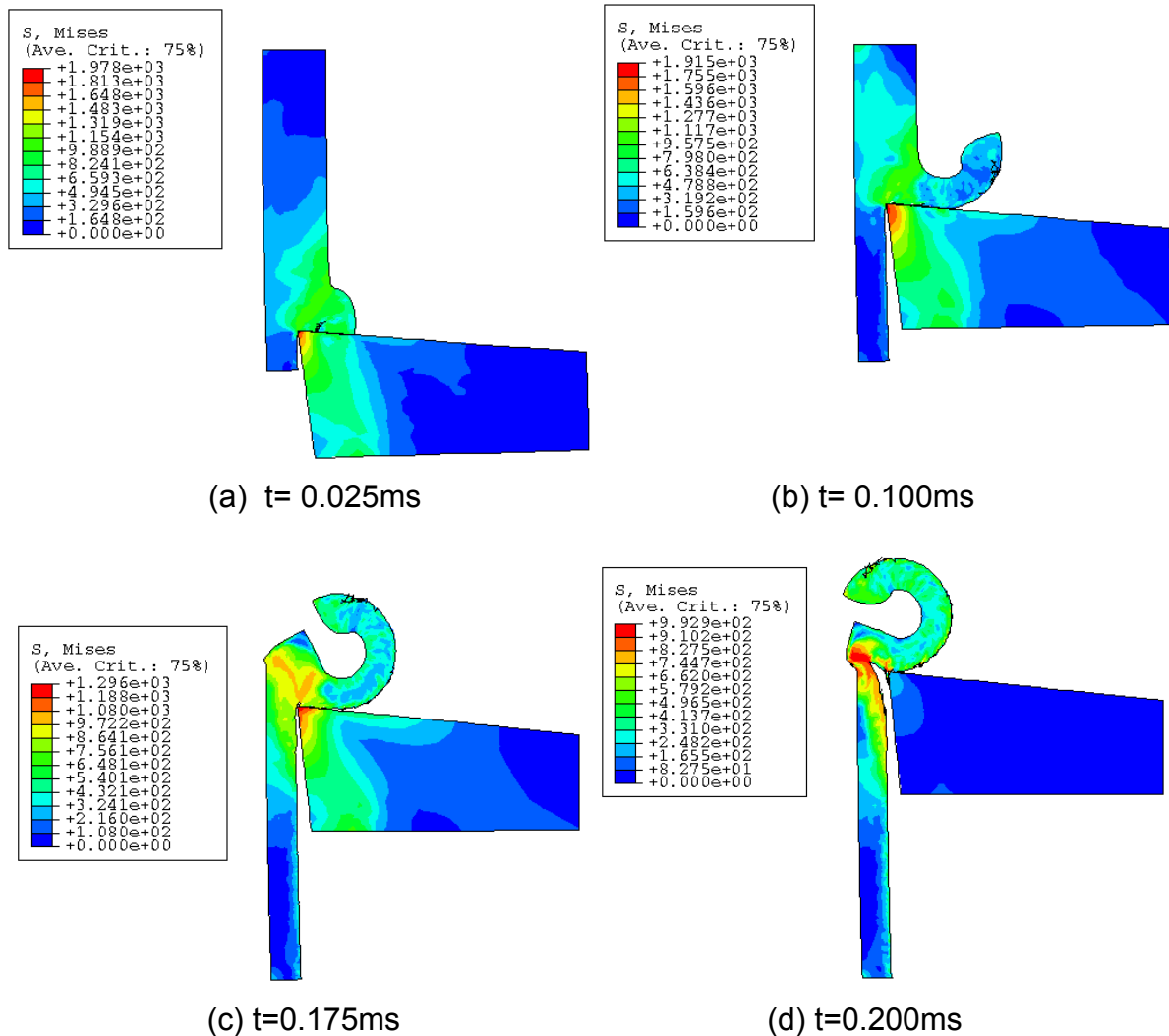
Fig. 3.22 Stress field (Mpa) in the chip formation analysis

3.3.3.2 Cutting Temperature

The predicted temperatures generated during chip formation process are shown in Fig. 3.23. The heat is generated mainly in two zones, the shear zone and the chip underside sliding along the tool face. The obvious temperature increment take place in shear zone, then the chip underside is heated again to a higher temperature by the friction with the tool face, as shown in Fig. 3.23(b), 3.23(c) and 3.23(d). In addition, when chip breakage takes place in Fig. 3.23(a), local high temperature is formed.

(a) t= 0.025ms   (b) t= 0.100ms

(c) t=0.175ms   (d) t=0.200ms
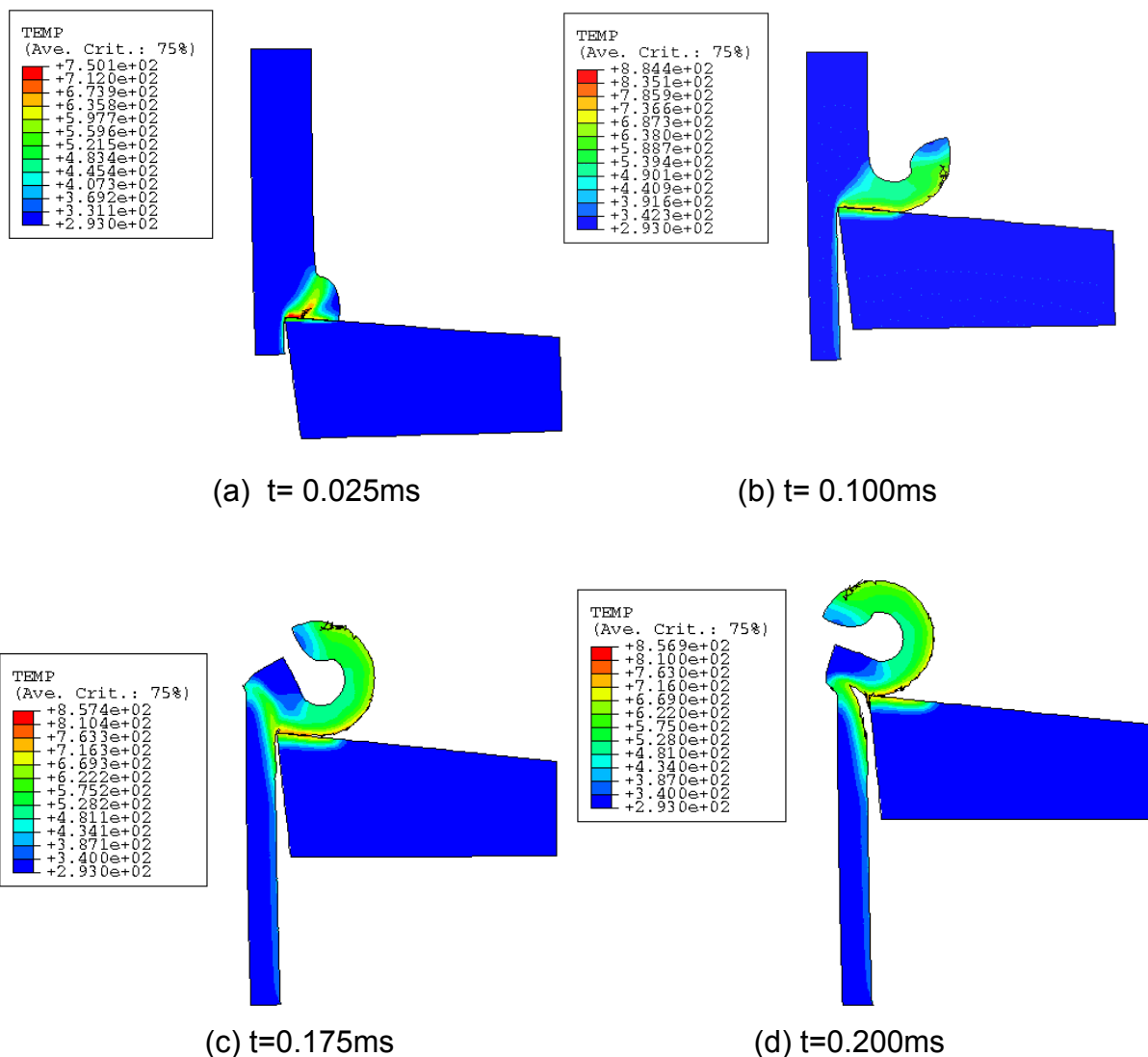
Fig. 3.23 Temperature distribution (in Kelvin) in the chip formation analysis

3.3.3.3 Cutting Force Analysis

In order to make the cutting insert rotate as a deformable body, its bottom is pinned on and rotates with the rotation center point. Therefore cutting force is exerted on the rotation center point. Fig. 3.24 shows the cutting force progress during the cutting process. Because the cutting insert has exited from the workpiece and no contact with the workpiece any more after 0.2ms, cutting force components in x-direction and y-direction are reducing to zero. The 'noise' of the cutting force signal is caused by the removal of the elements; they reach the shear failure criterion and then stresses in these elements are set to zero, which result in the fluctuation of cutting force. This is different from 'noise' observed in continuous chip formation analysis, which always appear when the element of workpiece is coarser than tool element, and contact problem results in 'noise' of cutting force signal.
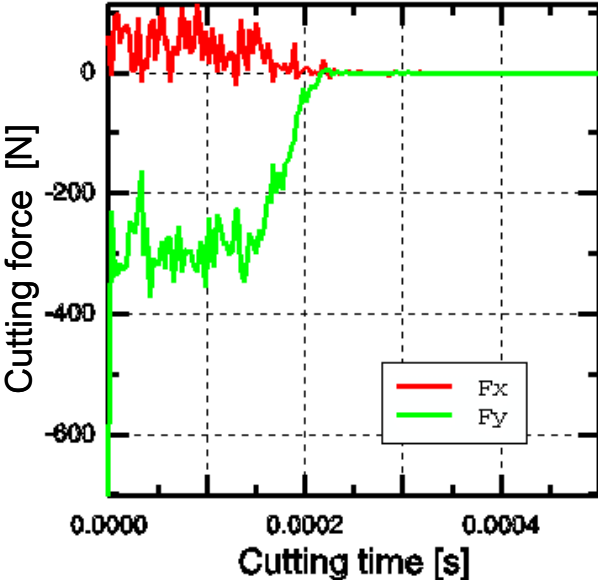
Fig. 3.24 Cutting force progress during the cutting process

3.4 Summaries & Conclusion

Two different chip formation modeling methods are designed to simulate the chip formation process in milling operation and turning operation.

Chip formation model for turning operation is designed to simulate the whole cutting process including initial chip formation, chip growth and steady state. No experiment is required to get material failure parameters or steady chip geometry. Chip separation is formed automatically by using ALE technique supplied by ABAQUS/Explicit. In order to get good contact between the chip and the tool face even when a serious crater wear is formed on rake face, model regeneration method is suggested to update and refine the mesh of the workpiece, especially at the tool-chip interface.

With this complete model, the normal tool geometry such as blunted, chamfered and worn cutting tool can be used in the chip formation model.

The calculation time to reach steady state is relative short comparing with the chip formation model in which the chip formation is taken as a pure Lagrangian problem. Especially when it is used in tool wear estimation, the total calculation time to reach tool reshape criterion is reduced sharply because except the initial chip formation and chip growth are run only one time and then with the tool wear increasing, only steady state analysis step is necessary.

Chip formation in milling operation is modeled by introducing the shear failure criterion because of the intermittent cutting process. The shear failure criterion is used to the entire workpiece. This model is expected to have a wider application because it can model various chip type, such as serrated chip, when the suitable material constitutive and material failure model are provided.

Chapter 4 Heat Transfer Analysis In Metal Cutting

4.1 Introduction

When the cutting process is simulated using chip formation analysis, the cutting time is normally limited to a short time, because coupled thermal mechanical analysis is too expensive. For example, in the former chapter, at the end of the chip formation analysis in turning operation, temperatures at nodes inside the cutting tool are still climbing while those at tool-chip interface nodes approach steady state. It is concerned how the temperature distributes in the cutting tool finally. For milling operation, the chip formation analysis is only carried out in the first milling cycle. It is important for the correct calculation of tool wear how the tool temperature changes in the further milling cycles.

Therefore pure heat transfer analysis is performed after chip formation analysis for the further cutting process in order to get such knowledge at a low calculation cost.

4.2 General Considerations

4.2.1 Geometry And Mesh

In the heat transfer analysis, only a single object is considered, for example only the cutting tool or the workpiece. Otherwise, the simulation will become complex because of the interaction between the cutting tool and the workpiece.

ABAQUS uses some Eulerian elements, diffusive elements, which have only temperature degrees of freedom, to model convective heat transfer. Diffusive elements are provided in one, two or three dimension. Interpolation can be first-order and second-order [ABA-01b]. Two-dimensional first-order four node diffusive element, DC2D4, is chosen to discretize the geometry of the studied object in the heat transfer analysis because quantities of DC2D4 are integrated at nodes and this simplifies the design of heat flux subroutine by importing heat flux at nodes of chip formation model directly into integration points of heat transfer model as basic data for the calculation of the current heat flux. In addition, the error caused by the conversion from nodal value to integration point value is avoided during the importation of temperature data. These advantages are based on the conservation of

the node label, element label and element connectivity of the chip formation analysis model.

4.2.2 Heat Flux

In the cutting phase the cutting tool is heated by the heat flux acted on the tool-chip and tool-workpiece interface. The total heat flux is composed of frictional heat flux q^f and conductive heat flux q^c. Frictional heat flux is created due to the sliding friction between the workpiece material and the tool face. The amount of frictional heat flux into the cutting tool is calculated by Eq. 4.1.

$$q^r = (1 - f)\eta\tau \cdot v_s \tag{4.1}$$

where

τ is the frictional stress;

v_s is the sliding velocity;

η specifies the fraction of mechanical energy converted into thermal energy;

f gives the fraction of the generated heat flowing into the workpiece.

Therefore frictional heat flux is influenced by chip form, sliding condition and contact with the tool face.

Conductive heat flux is caused by the temperature difference of tool-chip and tool-workpiece at the interface. It is governed by Eq. 4.2.

$$q^c = k(\theta_A - \theta_B) \tag{4.2}$$

where

q^c is the conductive heat flux crossing the interface from point A on the workpiece to point B on the cutting tool;

k is the gap conductance;

θ is the nodal temperature on the surface.

Therefore conductive heat flux is temperature dependent.

Both heat flux components are varying from node to node and the basic nodal heat flux data can be obtained from the chip formation analysis.

4.3 In Turning Operation

4.3.1 Modeling

In order to study on the temperature distribution of the cutting tool at steady state, heat transfer analysis is performed after the chip formation analysis finishes.

Because in the orthogonal cutting experiment [Schm-02], the part of the cutting edge engaged in the cutting is located in the center part circled in Fig. 4.1, the geometry model of the cutting tool used in the two-dimensional heat transfer analysis is the section created by intersecting the center area with a surface perpendicular to the edge. It includes the part, which is surrounded by the rake face, flank face, bottom face, and the surface of the central hole. The part of the tool used in the former chip formation analysis steps is only the highlighted part, and the element label, node label and element connectivity of this part in chip formation analysis steps remain unchanged.
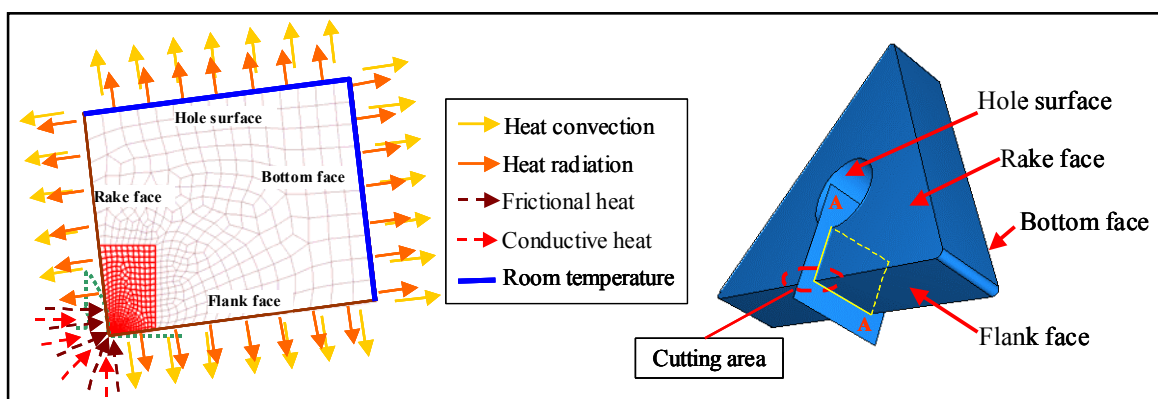
Fig. 4.1 Geometry and mesh of the cutting tool used in heat transfer analysis, the circled part is the part of the edge engaged in the cutting

Temperature data at the end of the steady-state chip formation analysis step is imported and used as the initial temperature definition of the nodes in the highlighted part. At other nodes the initial temperature is set to room temperature.

At the nodes on tool/chip interface heat flux is defined. In steady-state chip formation analysis step, it is found that the total heat flux (heat passing through the tool-chip and tool-workpiece interface per second) is changing as the cutting process continues, as shown in Fig. 4.2. One component of the total heat flux, the total

frictional heat flux, reaches steady state in a short time once the chip gets into contact with the tool face and restores to the steady sliding velocity, while another component, the total conductive heat flux, is always decreasing within the entire analysis period. At the end of analysis, as the temperature of cutting tool and workpiece become steady, the decreasing rate is becoming lower and lower and approaching a steady value.
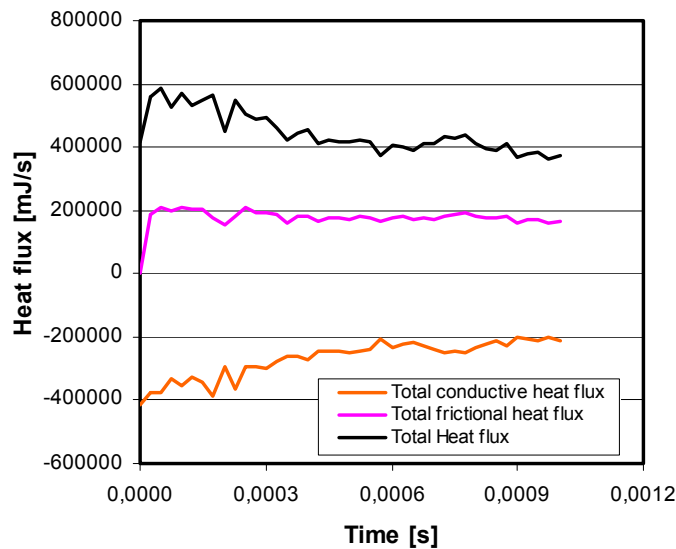
Fig. 4.2 Heat flux at tool-chip and tool-workpiece interface in steady-state chip formation analysis step

Observation of nodal temperature of workpiece nodes at tool-chip interface shows that the variation of nodal temperature at the end of the analysis is very small, as shown in Fig. 4.3. Therefore thermal steady state is assumed in workpiece material at the interface. Then the nodal conductive heat flux can be converted from Eq. 4.1 into Eq. 4.3

$$q^c = k\left(\theta_{(A,t_s)} - \theta_{(B,t_s)}\right) + k\left(\theta_{(B,t_s)} - \theta_B\right) \tag{4.3}$$

where

t_s is the time point at the end of steady-state chip formation analysis. Because of the above assumption about steady nodal temperature of workpiece node at interface, $\theta_{(A,t_s)}$ is equal to and replaces θ_A. The first part $k\left(\theta_{(A,t_s)} - \theta_{(B,t_s)}\right)$ is nodal conductive heat flux, which can be obtained from the end of steady-state chip formation analysis. The second part is the variation of nodal conductive heat flux and it is dependent on

the difference in temperature between current nodal temperature and the temperature at the end of steady-state chip formation analysis.
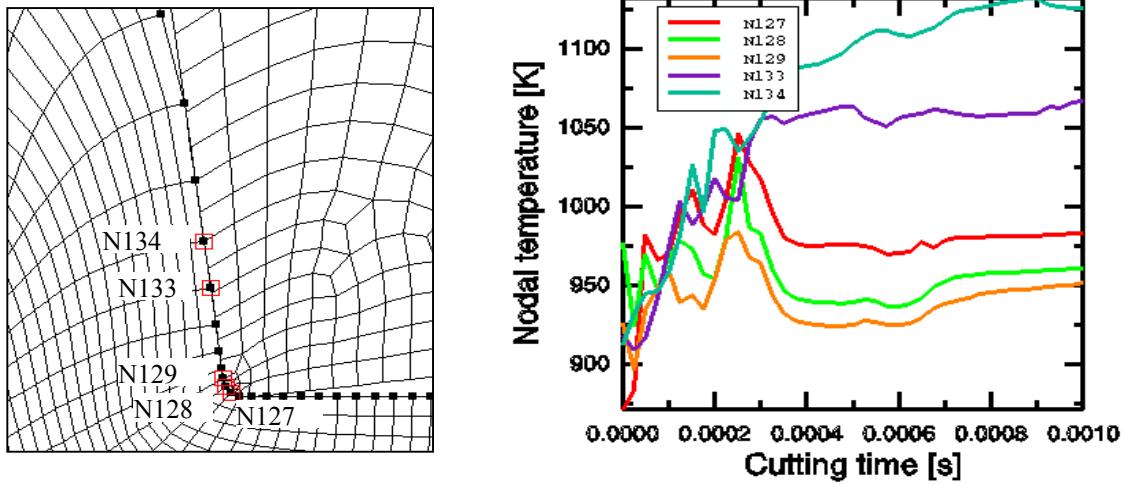
Fig. 4.3 Nodal temperature at selected workpiece nodes

Therefore nodal total heat flux can be expressed by Eq. 4.4.

$$q^t = q^r_{t_s} + q^c_{t_s} + k\left(\theta_{(B,t_s)} - \theta_B\right)$$ (4.4)

where

q^t is the total nodal heat flux;

$q^c_{t_s}$ stands for $k\left(\theta_{(A,t_s)} - \theta_{(B,t_s)}\right)$;

$q^r_{t_s}$ is the nodal frictional heat flux;

$q^c_{t_s}$ and $q^r_{t_s}$ do not change after importation. Based on Eq. 4.4, a temperature-dependent heat flux subroutine is developed for the heat transfer analysis.

In addition, the tool makes heat transfer with the environment through rake face and flank face by heat convection and radiation.

The nodes on bottom face and hole surface always keep room temperature because of their contact with the tool holder and the screw.

4.3.2 Results & Discussion

When maximum temperature change of 10K between two times of incrementation of heat transfer analysis is defined as steady state criterion, steady state is reached in

the whole tool in 2.2s.s Fig. 4.4 shows the progress of temperature at four selected nodes in the tool.
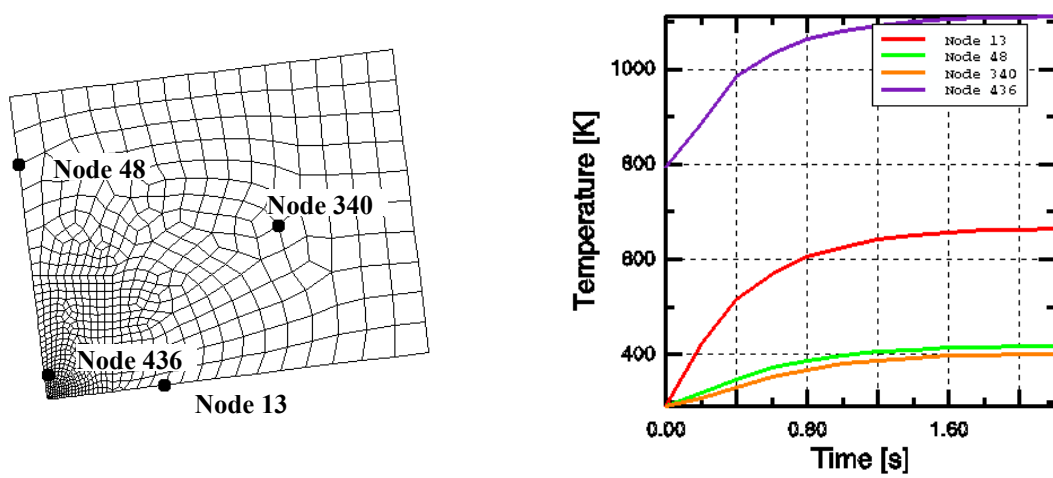
(a) Position of the selected nodes   (b) Temperature history

Fig. 4.4 Temperature history of nodes in the tool
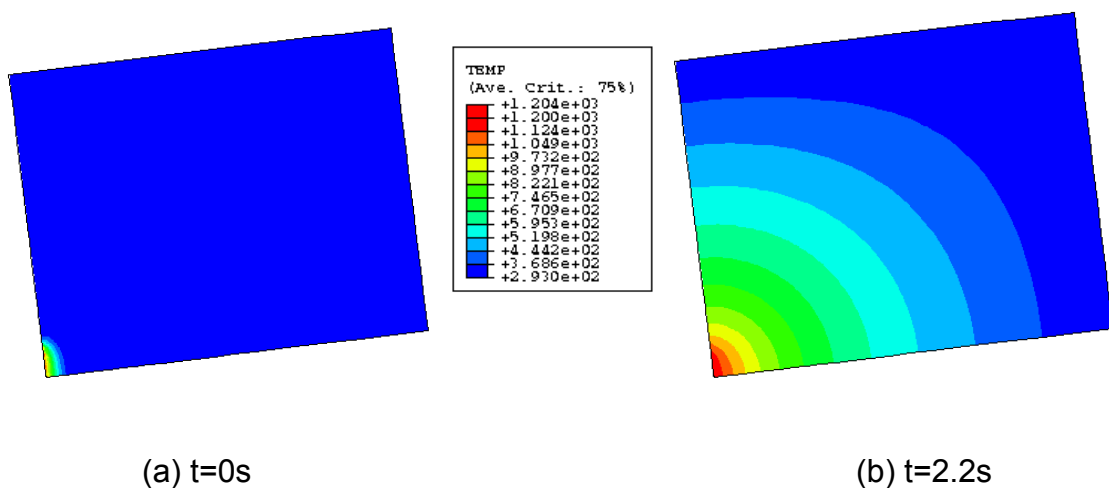
(a) t=0s   (b) t=2.2s

Fig. 4.5 Temperature field (Kelvin) change of the tool in heat transfer analysis

Fig. 4.5 shows that at the beginning of heat transfer analysis the high temperature region concentrates in a small area near the cutting edge, and after 2.2s this region extends to nearly one-third of the tool.

4.4 In Milling Operation

Heat transfer analysis is performed for both the workpiece and the cutting tool. In the cooling phase of the first milling cycle, whether the workpiece can restore to room temperature affects the chip formation, temperature distribution and heat transfer with the cutting tool in the second milling cycle. Study on the development of temperature distribution in the cutting tool in multi milling cycles is important for the implementation of tool wear estimation.

4.4.1 On Workpiece

4.4.1.1 Modelling

Generally, the actual workpiece is very huge comparing with the small part of workpiece used in the chip formation analysis. Therefore the workpiece geometry is extended in the heat transfer analysis. It is composed of two parts, as shown in Fig. 4.6. Part 1 is the remaining workpiece geometry after the chip is cut away in the chip formation analysis. Part 2 is some additional workpiece material; it is attached to the bottom of part 1.

part 1   part 2   workpiece
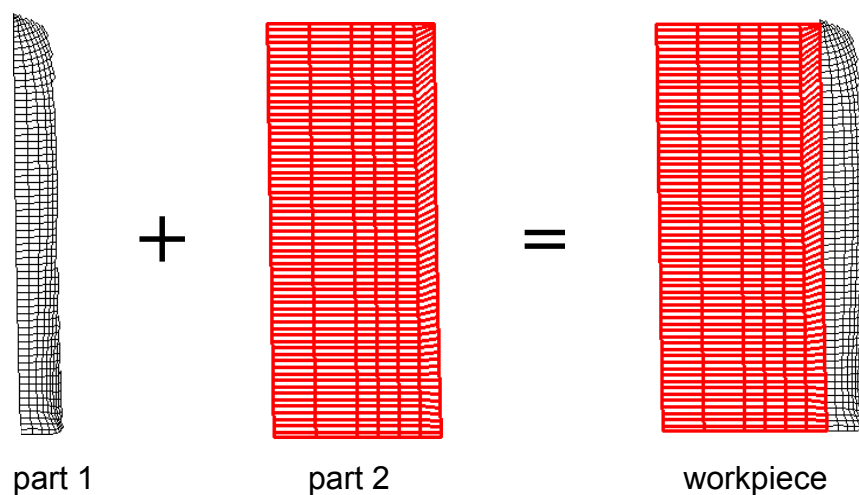
Fig. 4.6 Geometry and mesh of the workpiece in heat transfer analysis

The initial temperature of part 2 is set to room temperature. Nodal temperature at the end of previous chip formation analysis step is imported and defined as initial temperature of part 1. Fig. 4.7(a) shows the temperature distribution at the beginning of heat transfer analysis.

(a) t=0ms   (b) t=38.77ms
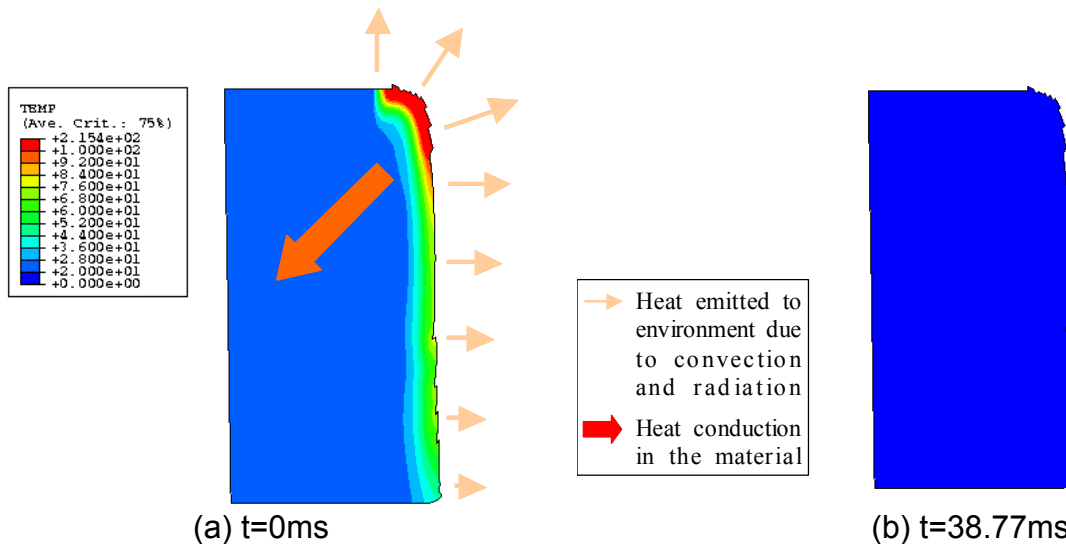
Fig. 4.7 Temperature field (in Celsuis) change of the workpiece in heat transfer

analysis

During the cooling phase, in addition to the heat conduction from cutting area to the whole workpiece bulk, the workpiece cools down due to heat convection and radiation through boundary.

Heat flux due to convection is calculated by

$$q^v = -h\left(\theta - \theta^0\right) ;$$ (4.5)

where

q^v is the heat flux due to convection;

h is a reference film coefficient, unit $J/s.m^2.°C$;

θ is the temperature at a point on the surface;

θ^0 is the sink temperature, i.e. room temperature.

Heat flux due to radiation to the environment is governed by

$$q^r = \varepsilon\sigma\left[\left(\theta - \theta^z\right)^4 - \left(\theta^0 - \theta^z\right)^4\right],$$ (4.6)

where

q^r is the heat flux due to radiation on a surface;

ε is the emissivity of the surface;

σ is the Stefan-Boltzmann constant;

θ is the temperature at a point on the surface;

θ^0 is the ambient temperature;

θ^z is the value of absolute zero on the temperature scale being used.

4.4.1.2 Results & Discussion

The heat transfer analysis covers the rest period of the first milling cycle after the chip formation analysis ends. Fig. 4.7(b) shows that after 38.77ms of cooling, the entire workpiece restores nearly to room temperature. The heat in the workpiece is emitted to the environment.

Observation on the temperature progress at several selected nodes shows that after the first milling cycle the temperature increment is smaller than 10K, as shown in Fig. 4.8. It is assumed that temperature increment of the workpiece in the real cutting experiment is smaller than the predicted because the huge workpiece used in reality supplies a higher heat capacity and a bigger boundary surface to emit the heat.
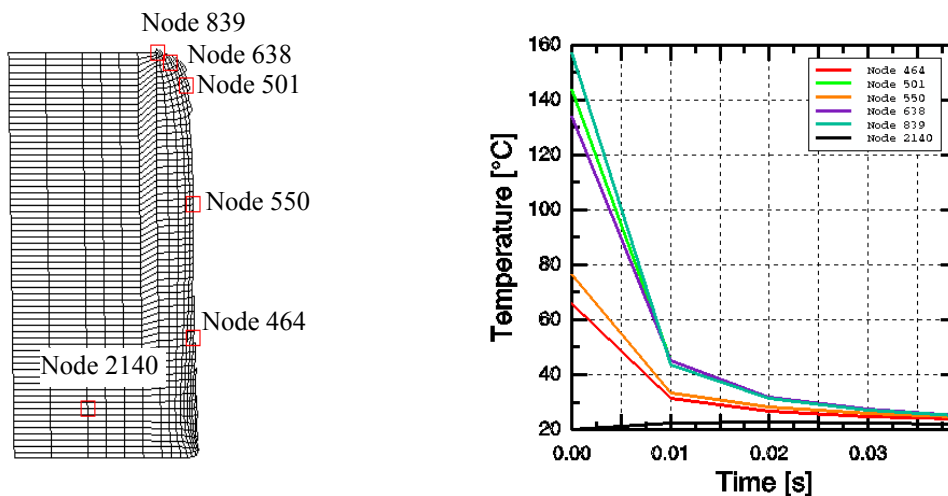
(a) Monitored nodes   (b) Temperature progress at monitored nodes

Fig. 4.8 Temperature history of workpiece nodes in heat transfer analysis step

It is assumed that in the second milling cycle this small temperature variation in the workpiece has no big influence on material deformation, heat generation, temperature distribution in the workpiece and tool-chip and tool-workpiece contact. It is expected that if the influence of the temperature variation of the cutting tool is not considered, chip formation analysis result in the second milling cycle can be assumed similar to that in the first milling cycle. Solutions obtained from the chip

formation analysis in the first milling cycle can be used to the second milling cycle. According to the same reasoning, they are useable in the third, fourth, and further milling cycles. Therefore solutions obtained from the chip formation analysis of the first milling cycle are used in the heat transfer analysis of the cutting tool in multi milling cycles and tool wear estimation.

4.4.2 On Tool

4.4.2.1 Modeling

In the cooling phase of milling operation, if the heat in the tool is not emitted completely to the environment by heat convection and heat radiation, the temperature of the tool will get an increment in the later milling cycle due to the remaining heat. This part will try to analyse the temperature variation of the tool with the accumulation of heat. The heat transfer analysis is performed in 8 milling cycles.

The tool geometry and mesh in chip formation analysis are inherited and used in the heat transfer analysis. Although the real cutting tool moves continuously with the rotation of the shaft, in the simulation it is fixed spatial because the degree of freedom in the heat transfer analysis is limited only to temperature.

Heat transfer analysis starts from the time when the chip formation analysis ends. The temperature distribution at the end of the chip formation analysis is imported into the heat transfer analysis as initial conditions.

In every milling cycle, the tool is heated in the cutting phase by the heat flux at the tool-chip and tool-workpiece interface. The two components of the total heat flux, frictional and conductive heat flux are time-dependent varying. Frictional heat flux changes because of varying shear stress and sliding velocity caused by the change of chip thickness in milling operation. Conductive heat flux changes with the varying of difference in temperature between the tool and the workpiece at contact interface.

Although the nodal total heat flux in the cutting phase is changing continuously from time to time, it is possible to obtain the basic values of nodal frictional heat flux and nodal conductive heat flux from the chip formation analysis of the first milling cycle only at some discrete time points $0, t_1, \ldots, t_j, \ldots, t_n$. These data are written in the heat flux and temperature files. The heat flux value at other time point is obtained by performing interpolation.

In addition, conductive heat flux is temperature dependent. When the nodal temperature of the cutting tool in the later milling cycles is higher than that in the first milling cycle due to the accumulation of heat, the nodal conductive heat flux value will change due to the varying of the difference in temperature between the cutting tool and the chip or the workpiece.

Based on these analyses, a heat flux subroutine DFLUX is designed to create time- and temperature-dependent nodal heat flux data.

Every time when the subroutine DFLUX is called, the time, element number, face number and integration point are entered as input variables. The subroutine first finds out the corresponding nodal label because only nodal label is used in the heat flux and temperature files. Then the basic nodal total heat flux and temperature values at all time points are read from the heat flux and temperature files. By finding out the remainder of the current time divided by the period of one milling cycle and comparing this remainder with the time points, the interval and the two time points at the end of the interval is determined. If the cutting tool is in the cooling phase, the current nodal total heat flux is set to zero. Otherwise when the tool is located between the time point j-1 and j, the nodal total heat flux is calculated by

$$q_i^c = 0.5 \times \left(q_{(i,j)}^t + q_{(i,j-1)}^t\right) - \left(\theta_i - 0.5 \times \left(\theta_{(i,j)}^b + \theta_{(i,j-1)}^b\right)\right) \times k \qquad (4.7)$$

where

q^c is the current nodal total heat flux;

q^t is the basic nodal total heat flux (the sum of the nodal frictional heat flux and the nodal conductional heat flux);

θ is the current nodal temperature;

θ^b is the basic nodal temperature;

i is the nodal label;

j is the time point number;

k is the gap conductance.

In addition, in order to improve the convergence rate during the solution of non-linear equations in an increment, the rate of change of the current nodal total heat flux with respect to the temperature, $dq_i^c / d\theta_i$ is given the value –k.

The gap conductance in the heat transfer analysis is 10000 when the tool face node is in contact with the chip and the workpiece. It is similar to the value used in the chip formation analysis. When the tool face node has no contact with the chip and the workpiece, the gap conductance is set to zero. The contact status of the tool face node at a time point is derived from the value of normal pressure at the corresponding time point in chip formation analysis of the first milling cycle. Considering the movement of the tool, a high reference film coefficient is defined in the model.

4.4.2.2 Results & Discussion

Fig. 4.9 shows the temperature distribution of the cutting tool when it cuts out of the workpiece 0.3ms in the first, forth and eighth milling cycle. The high temperature region is widening as the milling process continues.
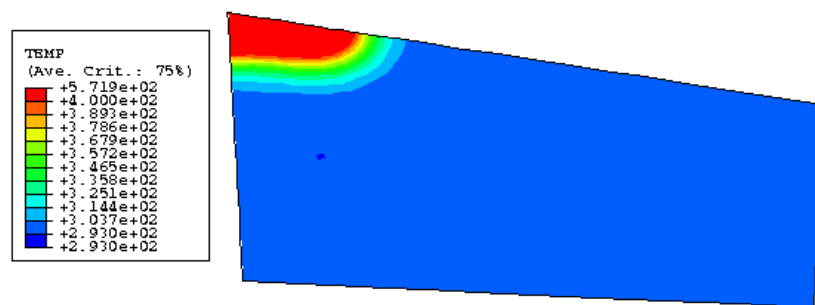
(a) At the end of chip formation analysis
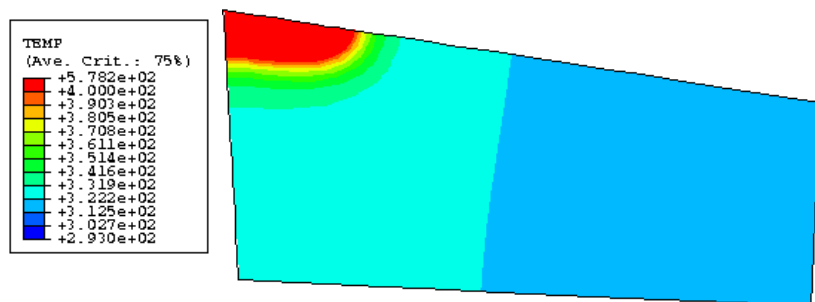
(b) After 4 milling cycles
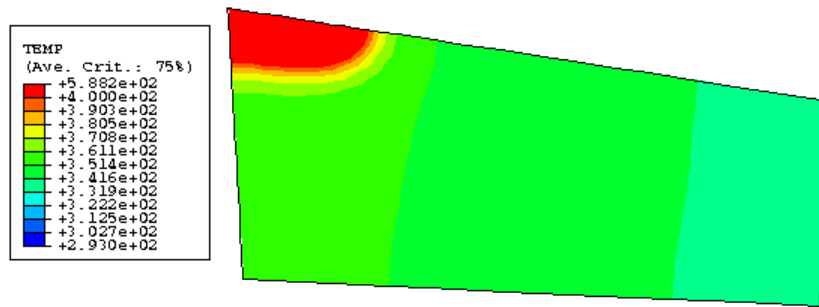
(c) After 8 milling cycles

Fig. 4.9 Temperature field (in Kelvin) progress of the tool in heat transfer analysis

Fig. 4.10 and Fig. 4.11 show the variation of nodal temperature in the cutting tool in more than 8 milling cycles, including both chip formation analysis step and heat transfer analysis step.
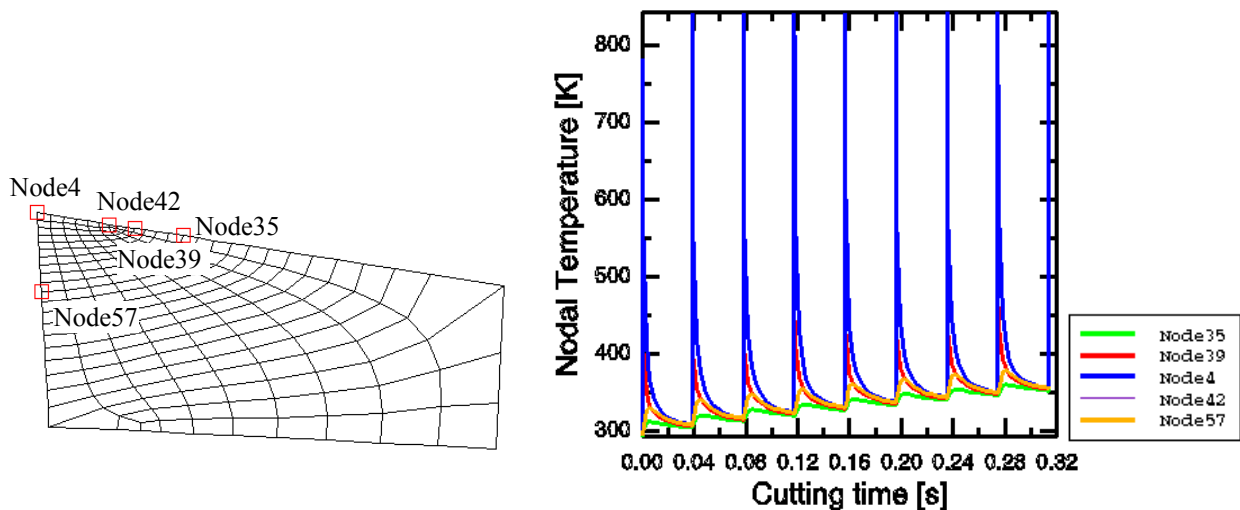
(a) Position of the selected nodes   *(b) The temperature history of the nodes*

Fig. 4.10 Progress of nodal temperature on the tool face

In Fig. 4.10 the nodal temperature at the tool face nodes on the too-chip and tool-workpiece contact interface increases in cutting phase and decreases in cooling phase. The peak value of temperature in every milling cycle appears when the cutting tool is cutting out of the workpiece. The valley value appears when the cutting tool is going to enter into the workpiece. Both the peak and valley value are increasing with the cutting process continuing, but the increments are decreasing and the increment of the peak value is smaller than 1K after every milling cycle while the increment of

the valley value is much great. In the last milling cycle, the peak value can be assumed to become steady because the increment is smaller than 0.5K, whereas the increment of the valley value is still greater than 5K.

Inside the cutting tool a different progress tendency of nodal temperature is observed. At the nodes close to the cutting area, nodal temperature increases in cutting phase and decreases in cooling phase. At the nodes far from the cutting area, nodal temperature is always increasing during the entire milling cycles, for examples N210 and N3 in Fig. 4.11.
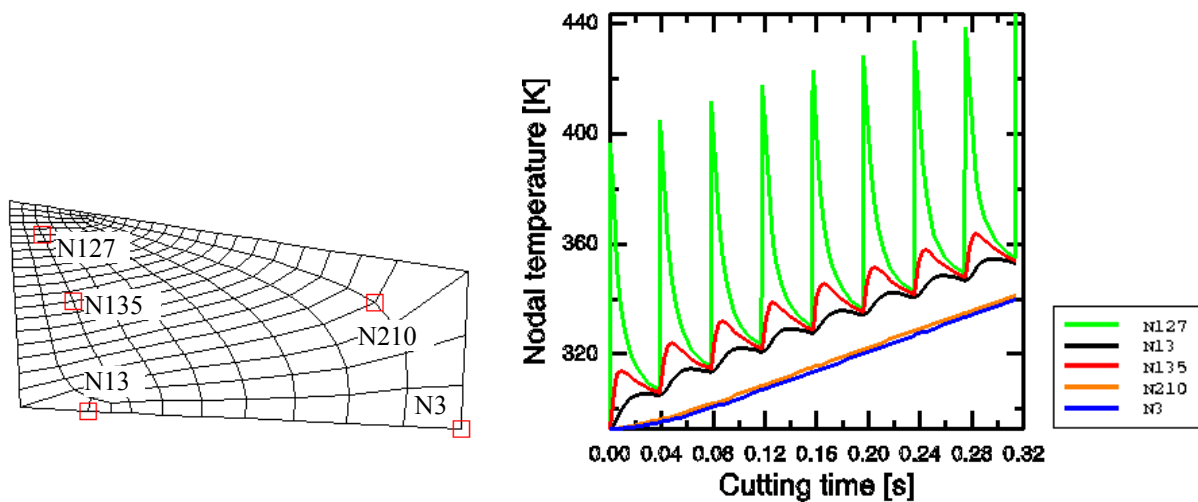
(a) Position of the selected nodes   *(b) The temperature history of the nodes*

Fig. 4.11 Progress of nodal temperature inside the tool

Both the nodal temperature of nodes inside the tool and on the tool face shows that cyclical thermal balance state is not attained in the first 9 milling cycle and heat gain is greater than heat loss in every milling cycle. Higher temperature is expected in the further milling cycles. It is very difficult to analyse the cyclical thermal balance by only manually adding more milling cycles in heat transfer model file because the number of milling cycles to reach cyclical thermal balance state is unknown.

4.4.2.3 Application Of Preheated Cutting Tool

According to the analysis above, tool temperature increases due to accumulation of remaining heat. Heat loss increases with the tool temperature. When heat loss becomes equal to heat gain, cyclical thermal balance state is attained. In order to reduce the number of milling cycles to reach cyclical thermal balance state and speed up the calculation process, the whole cutting tool is preheated beforehand by

defining a high initial temperature, then it is used in the milling process. Because at present only tool temperature is concerned, milling process is analysed by performing only heat transfer analysis. Only 8 milling cycles are included in the heat transfer analysis.

Analysis 1: Preheated to 600K

In this analysis, the cutting tool is preheated to 600K. Nodal temperature at the same tool nodes as in the former heat transfer analysis is observed. In Fig. 4.12, nodal temperature on the tool face and inside the tool is increasing after every milling cycle, but the increment is smaller than that in the former analysis.

(a)   (b)
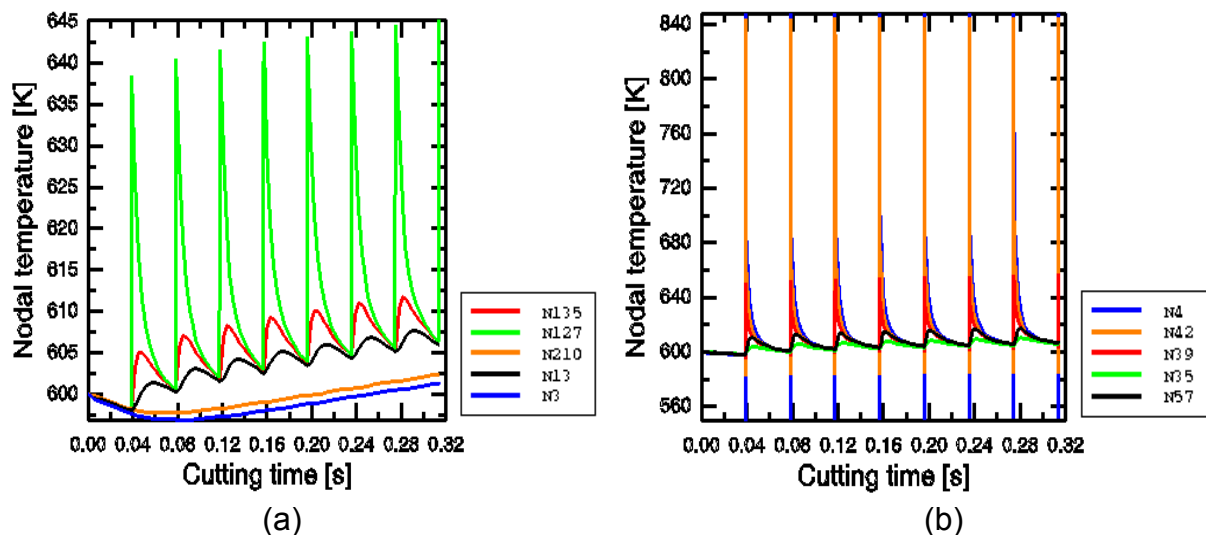
Fig. 4.12 Preheated to 600K (a) The temperature history of the nodes inside the tool
(b) The temperature history of the nodes on the tool face

At the nodes on tool-chip interface, for example N4 and N42, valley value of nodal temperature appears at the time when the tool comes into contact with the workpiece instead of before the contact takes place. This is explained by the heat conduction between the tool with higher temperature and the workpiece with room temperature. At the farthest nodes away from the cutting area, for example, node 3 and node 210, temperature decreases first and then increases again. The explanation is that at the beginning of the analysis the entire workpiece has a same temperature value, no heat conduction takes place in the vicinity of these nodes, these nodes are located at the boundary, heat convection to the environment makes the temperature decrease. After a time of cutting, the workpiece material in the vicinity is heated by the heat

generated in the cutting process and these nodes are heated because of heat conduction.

Analysis 2: Preheated to 700K

According to analysis 1, when the tool preheated to 600K is used in milling operation, tool temperature increases still and no cyclical thermal balance state is attained. Higher tool temperature is expected in cyclical thermal balance state. Therefore, in this analysis, the cutting tool is preheated to 700K.

Nodal temperature at the same tool nodes is observed. In Fig. 4.13, nodal temperature on the tool face and inside the tool is decreasing after every milling cycle and the decreasing rate is comparable to the increasing rate in analysis 1. At node 3 and node 210, temperature decreases in the entire 8 milling cycles.

The analysis shows that cyclical thermal balance state is not attained in the 8 milling cycles because the workpiece is heated too high and heat loss is greater than heat gain in every milling cycle.

(a)   (b)
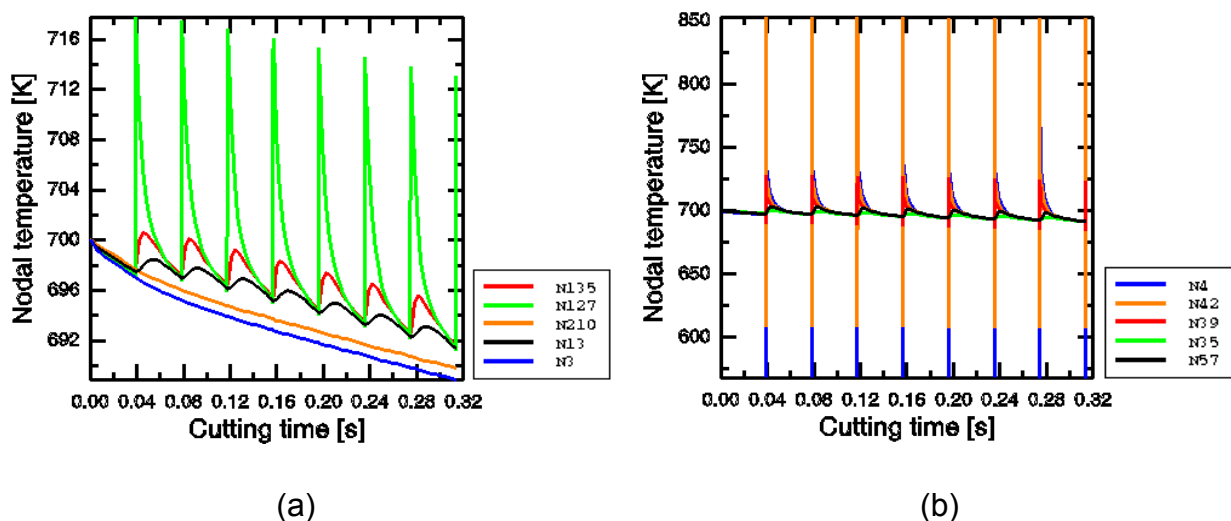
Fig. 4.13 Preheated to 700K (a) The temperature history of the nodes inside the tool
(b) The temperature history of the nodes on the tool face

Analysis 3: Preheated to 650K

According to analysis 1 and analysis 2, when the cutting tool is heated to a temperature between 700k and 600K, cyclical thermal balance state is expected to

realize in the first 8 milling cycle. Therefore, in this analysis, the cutting tool is preheated to 650K.

(a)   (b)
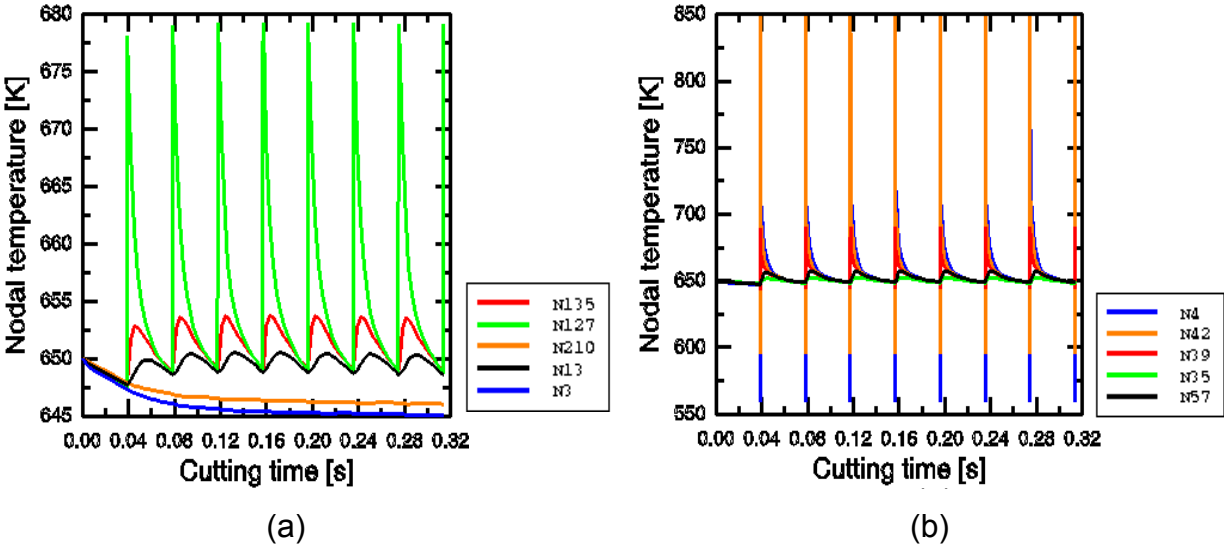
Fig. 4.14 Preheated to 650K (a) The temperature history of the nodes inside the tool

(b) The temperature history of the nodes on the tool face

Nodal temperature is monitored at the same tool nodes. In Fig. 4.14, nodal temperature on the tool face and inside the tool is approaching cyclical thermal balance state. When the cutting tool move to the same position in the 7th and the 8th milling cycle, the maximum difference in temperature at the same node is smaller than 0.1K. Therefore, it can be assumed that cyclical thermal balance state is realized in the 8th milling cycle.

4.5 Summaries & Conclusion

ABAQUS/Standard is effective in heat transfer analysis. By introducing the heat flux and temperature distribution from the chip formation analysis output file and using user-developed heat flux subroutines, thermal steady state in the turning operation and cyclical thermal balance state are analysed.

In turning operation, the heat transfer analysis is performed for the cutting tool until the thermal steady state is reached.

In milling operation, the heat transfer analysis is performed for the cutting tool for several milling cycle. By using preheated cutting tool in the heat transfer analysis, the cyclical thermal balance state is analysed.

Chapter 5 Estimation Of Tool Wear In Turning Operation

5.1 Introduction

The following two chapters will describe the modelling of progressive tool wear in turning and milling operation by developing user program with programming language Python and integrating it with commercial FEM code ABAQUS/Explicit and ABAQUS/Standard. In this chapter, the study will focus on the modelling of tool wear in turning operation. Base on the obtained experience, the more complex modelling problem, tool wear in milling operation, will be studied in the next chapter. All the tool wear simulation models will be developed for two-dimension. Solution to the problems met in 2D modelling will be helpful for the implementation of 3D modelling in the future.

Tuning operation is characterized by continuous cutting process; the entrance and exit of cutting tool takes place infrequently and takes only a short time. In continuous cutting process, if the effects of tool wear and uneven distributions of workpiece material are neglected, cutting thickness, chip shape, and various cutting process variables will have no great change and steady state can be assumed. Tool wear calculation can be simplified by assuming that tool wear is created completely by the steady state cutting process and neglecting the effect of entrance and exit phase.

By integrating tool wear mathematical model with the finite element steady-state cutting analysis, tool wear estimation is implemented. It is performed with a tool wear estimation program. The program controls the submission of chip formation and heat transfer analysis jobs, monitors their analysis process, accesses the created result and output database files once the analysis jobs are finished, performs tool wear calculation and modifies the related model files according to the calculated tool wear.

5.2 Tool Wear Calculation Program Design

Fig. 5.1 shows the flow chart of the tool wear calculation program. The program is designed to perform tool wear calculation automatically cycle by cycle until a tool reshape criterion is reached. In every calculation cycle, chip formation and heat transfer analysis jobs are submitted to analyse the steady-state cutting process and obtain the cutting process variable values necessary for the calculation of wear rate

at steady state. Nodal wear rate is calculated by using the tool wear mathematical model. Based on the calculated nodal wear rate, a suitable cutting time increment is searched by program according to a user-specified VB increment value. Then the nodal displacement due to wear in the cutting time increment is calculated at every tool face node, and the tool geometry is updated according to the calculated nodal displacement. If the produced flank wear VB is smaller than the user-defined tool reshape criterion VB_{max}, a second tool wear calculation cycle starts with the updated tool geometry.
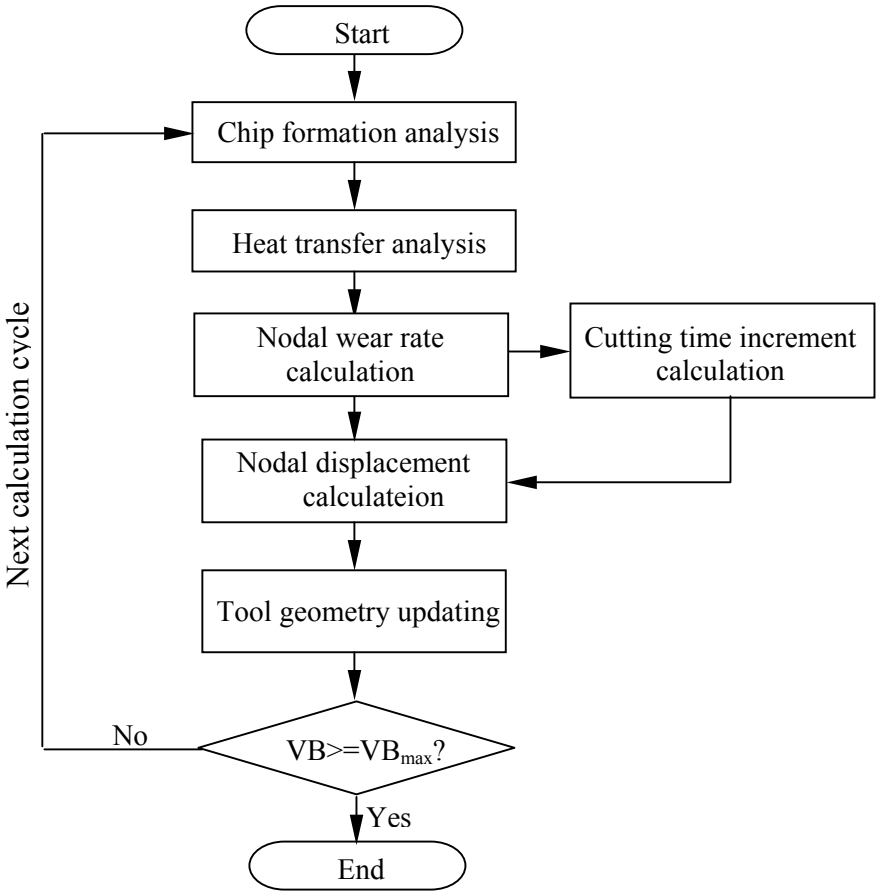
Fig.5.1 Flow chart of tool wear calculation program

5.3 Modeling Procedure

During the explanation of the entire modelling procedure, the tool wear under the same cutting condition as in the chip formation simulation of turning operation is estimated.

5.3.1 Chip Formation And Heat Transfer Analysis

Chip formation analysis provides the mechanical variables at steady state and the thermal variables at steady state are predicted by heat transfer analysis.

5.3.1.1 Normal Pressure

Fig. 5.2 shows the variation of normal pressure at the tool face nodes along the tool-chip interface at the end of chip formation analysis.

At the tool tip area, the normal pressure has the maximum value. Then the distribution exhibits a plateau of high stress near the tool. Beyond the feed distance, the normal pressure drop off sharply, as observed by Childs and Mahdi [Chil-89] when turning mild steel. At the distance of about 0.35, the chip loses contact with the tool face, therefore the normal pressure drops to zero.
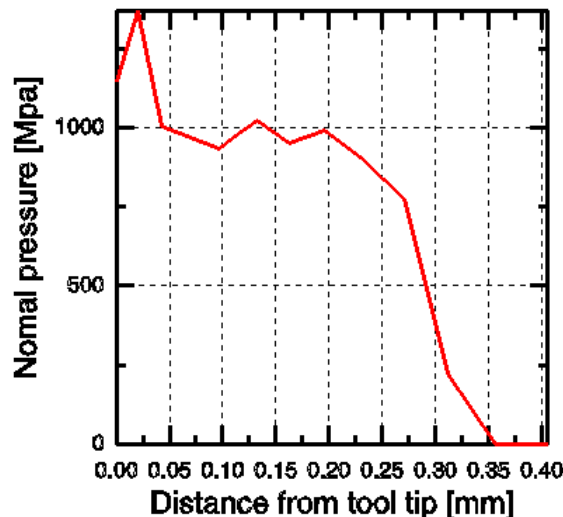
Fig.5.2 Normal pressure of the tool face nodes at tool-chip interface at steady state

5.3.1.2 Sliding Velocity

In Fig. 5.3(a) workpiece nodes in the tool tip area have negative relative sliding velocities. This means that they are flowing into machined surface. The nodes that are more than 0.02mm away from the tool tip are moving out of cutting area with the chip. There is no contact between the chip and the tool face in the area beyond the distance of 0.35mm. Therefore the sliding velocity becomes zero, as designed by ABAQUS [ABA-01a].
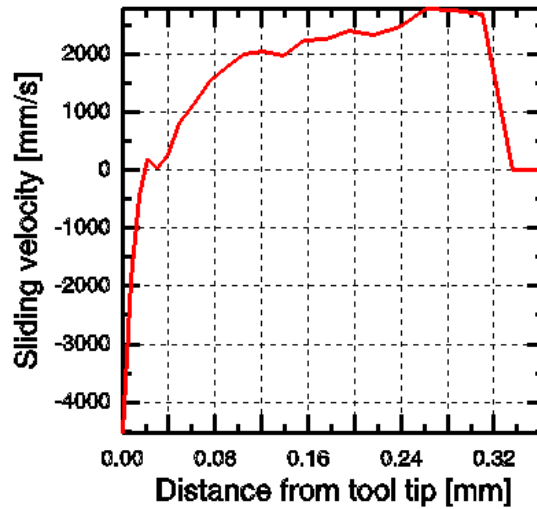
(a) Sliding velocity at the workpiece nodes at steady state
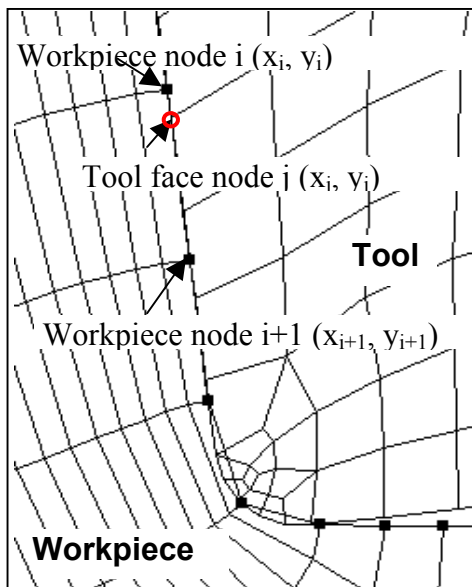
If $|y_i - y_{i+1}| \geq |x_i - x_{i+1}|$:

$$v_j^s = v_i^s + \frac{(y_j - y_i)}{y_{i+1} - y_i}(v_{i+1}^s - v_i^s)$$

Else:

$$v_j^s = v_i^s + \frac{(x_j - x_i)}{x_{i+1} - x_i}(v_{i+1}^s - v_i^s)$$

(b) Calculation of sliding velocity at the position of tool face nodes

Fig. 5.3 Calculation of sliding velocity at the position of tool face nodes

Only sliding velocities at the position of workpiece nodes can be obtained directly from the simulation. But when calculating nodal wear rate, it is necessary to know the sliding velocity value of workpiece material at the position of tool face nodes. Not all the tool face nodes and workpiece nodes are in contact. First all the tool face nodes and workpiece nodes in contact are found out depending on whether the absolute values of their normal pressure are greater than a critical value, for example, 1e-6Mpa. Then they are arranged in counter-clockwise order. Every tool face nodes in contact has two neighbouring workpiece nodes before and after it. The calculation is performed based on their position relationship, as shown in Fig. 5.3(b).

5.3.1.3 Tool Temperature

Temperature of the tool face nodes at thermal steady state is obtained from heat transfer analysis, as shown in Fig. 5.4. High temperature forms at the tool tip and a distance from the tool tip on rake face.
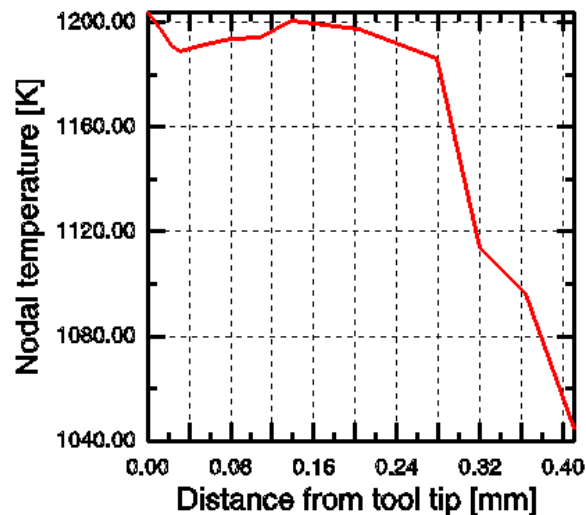
Fig. 5.4 Temperature of tool face node at steady state

5.3.2 Wear Rate Calculation

After the cutting process variables, sliding velocity of the workpiece material, tool temperature and normal pressure at every tool face node are obtained, wear rate at the position of every tool face node is calculated by using wear mathematical model. Because at low cutting speed, the flank wear and crater wear are assumed to be created mainly by abrasive wear and adhesive wear, Usui's model, described in Chapter 1, is employed in the calculation. The constants in Usui's equation for the combination of carbide cutting tool and mild steel are shown in Table 1.2.

5.3.3 Nodal Move Direction

Tool wear expression in geometry can be realized with two approaches: element deletion and nodal movement. The latter one is adopted in this paper. The nodal move direction is calculated at every tool face node.

5.3.3.1 Dividing Node

Before calculating the nodal move direction, a dividing node, the circled node in Fig. 5.5 is searched by the program. It divides the entire tool face into flank face and rake face. It has the minimum y-coordinate.

Before searching, all the tool face nodes are found out and arranged in counter clock-wise order in a list. The first tool face node in the list is given to the dividing node. Then the current dividing node is compared with all the tool face nodes. Any node, whose y coordinate is smaller than the current dividing node by 2e-4mm, will become the new dividing node. After one searching cycle, the real dividing node is found out. It is saved as the tool edge position for the latter calculation of flank wear land width.

On flank face and rake face nodal move direction is calculated with different methods.

5.3.3.2 On Rake Face

In the rake face part nodal move direction is assumed to be perpendicular to the relative sliding velocity of the workpiece material and pointed into the tool body. Every tool face node is attached with two tool face segments. On every tool face segment the sliding velocity is along the tangential direction. Points on the face segment should move along the negative normal direction. Tool face node belongs to two face segments. It moves along the negative direction of the average unit normal vector of the two face segments or the negative direction of their resultant vector, as shown in Fig. 5.5.
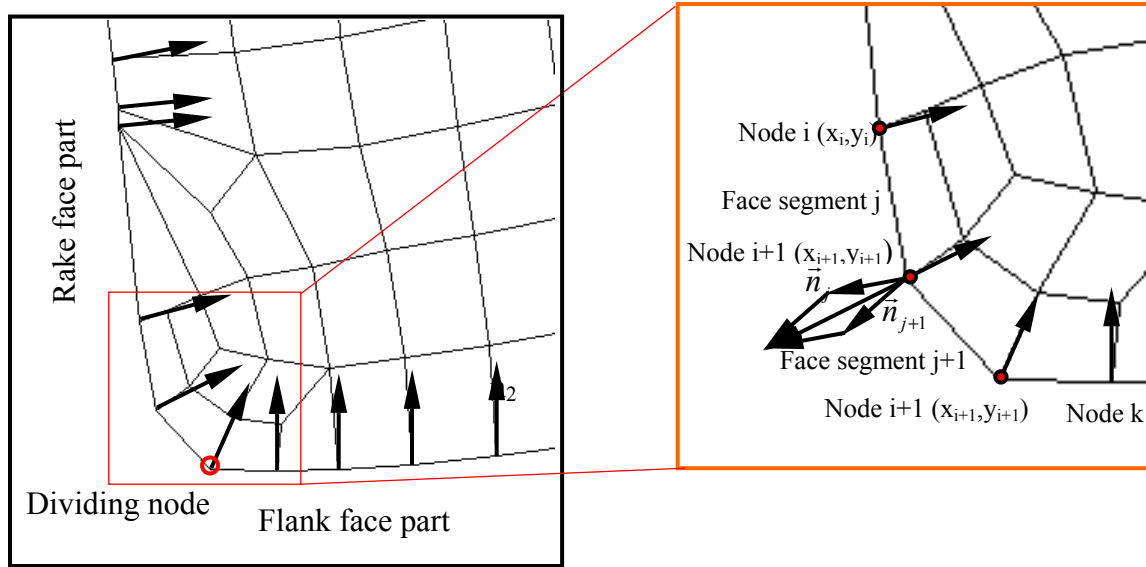
On rake face, nodal move direction $\vec{D}_i$ is calculated by

$$\vec{n}_j = \left(\frac{y_{i+1} - y_i}{\left((x_{i+1} - x_i)^2 + (y_{i+1} - y_i)^2 \right)^{1/2}} , \frac{x_i - x_{i+1}}{\left((x_{i+1} - x_i)^2 + (y_{i+1} - y_i)^2 \right)^{1/2}} \right)$$

$$\vec{n}_{j+1} = \left(\frac{y_{i+2} - y_{i+1}}{\left((x_{i+2} - x_{i+1})^2 + (y_{i+2} - y_{i+1})^2 \right)^{1/2}} , \frac{x_{i+1} - x_{i+2}}{\left((x_{i+2} - x_{i+1})^2 + (y_{i+2} - y_{i+1})^2 \right)^{1/2}} \right)$$

$$\vec{n}_i^r = \vec{n}_j + \vec{n}_{j+1}$$

$$\vec{D}_i = -\vec{n}_i^r / \left| \vec{n}_i^r \right|$$

On flank face, nodal move direction $\vec{D}_k = (0,1)$

Fig. 5.5   Nodal move directions (thick arrows) of tool face nodes

5.3.3.3 On Flank Face

In the flank face part the relative sliding velocity can be assumed to be in the cutting speed direction when the elastic recovery of workpiece material is neglected. Therefore all the nodes in this part have the same nodal move direction. It is in y-direction and pointed upwards.

Every nodal move direction is normalized to unit vector $\vec{D}_{(i,j)}$, where subscript i is nodal label, j is the calculation cycle number.

5.3.4 Cutting Time Increment Calculation

In metal cutting experiment cutting time increment means the duration of cutting time between two successive measurements of tool wear. In the simulation the calculation of tool wear and the tool geometry updating are based on a certain cutting time increment. Within the cutting time increment an unchanged nodal wear rate value is used to calculate the tool wear. Therefore, if a big cutting time increment is specified, a big error will be created during the calculation of tool wear. But if the cutting time increment is too small, only small tool wear increment is produced in every calculation cycle. In order to reach tool reshape criterion, many calculation cycles have to be performed. The chip formation analysis is carried out in every calculation cycle; it is very time-consuming. Therefore a suitable cutting time increment should be given. But when there is no knowledge about the tool wear in the simulated cutting conditions, for example, when novel workpiece material is machined, it is difficult to define a suitable value. But it is easier for the user to specify a tool wear increment. Since the nodal wear rate is already known, the cutting time increment, in which the specified tool wear increment is produced, can be searched by program. Therefore a searching module is designed to carry out the searching work. While the suitable cutting time increment is being searched, a flank wear calculation subroutine, $Flankwear(\Delta t, wearrate)$, is called frequently.

(a) Flank wear calculation   (b) Cutting time increment searching process
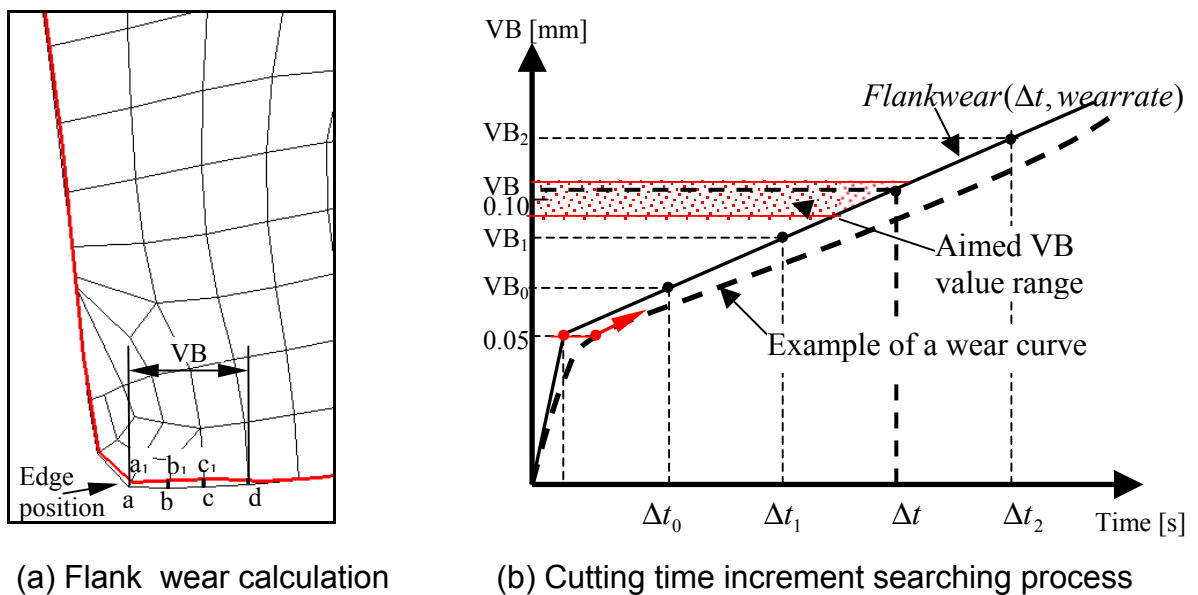
Fig. 5.6 Flank wear calculation and cutting time increment searching process

5.3.4.1 Flank Wear Calculation Subroutine

The flank wear calculation subroutine $Flankwear(\Delta t, wearrate)$ calculates flank wear land width VB. VB is the distance from the cutting edge position (which has been saved) to the last moved tool face node. For example, in Fig. 5.6(a), node a is the last tool face node with non-zero wear rate. In cutting time increment Δt, it should move to point a_1, then node b and c will have smaller y-values than point a_1, and a bulge will be formed on the flank face. But in practice the wear process is continuous. Once node b or c comes into contact with workpiece material due to wear of the cutting edge, they are also worn away and no bulge is formed. Therefore node b and c should move to point b_1 and c_1 in order to have the same y-value with point a_1. VB is calculated from the cutting edge position to node c, because it is the last moved tool face node.

5.3.4.2 Cutting Time Increment Searching Procedure

The cutting time increment searching procedure can be described by Fig. 5.7.
At the beginning the aimed VB median value VB_m is calculated according to the user-specified VB increment value. For example, in Fig. 5.6(b), the tool gets a flank wear land width of 0.05mm from the previous tool wear calculation cycle. $\Delta VB = 0.05mm$ is specified by the user. Therefore in this tool wear calculation cycle, VB_m is 0.1mm. In order to save the searching time, the aimed VB value should be given a permitted error range, e.g. the dotted range in Fig. 5.6(b). In addition, a positive initial cutting time increment value Δt_0 is given arbitrarily. Then the searching process starts.

During the searching process, the searching lower limit Δt_1 and the searching upper limit Δt_2 are changing until the calculated tool wear VB value under the cutting time increment Δt falls into the aimed VB value range.

```
                                    ┌──────────┐
                                    │  Start   │
                                    └──────────┘
                                         │
                                         ▼
                          ┌───────────────────────────┐
                          │ VB_m,  initial  value      │
                          │ Δt_0,  permitted  error    │
                          │ δ                          │
                          └───────────────────────────┘
                                         │
                                         ▼
                          ┌───────────────────────────┐
                          │ Cutting  time  increment Δt│
                          │ the searching lower limit Δt_1│
                          │ and  the  searching upper  │
                          │ limit Δt_2 are set to Δt_0  │
                          └───────────────────────────┘
```

Fig. 5.7 Flow chart of cutting time increment searching procedure

The flowchart contains the following decision and process boxes:

- Call subroutine Flankwear(Δt,wearrate) to calculated the current flank wear VB, calculate the current error, error=VB- VB$_m$
- $|error|<=\delta$? — Yes → Current cutting time increment Δt is output
- error$<-\delta$? — Yes → Δt$_1$=Δt ; No → Δt$_2$=Δt
- Δt$_2$>Δt$_1$? — Yes → Δt=(Δt$_1$+Δt$_2$)/2 ; No → Δt=2Δt
- Current cutting time increment Δt is output → End

Fig. 5.7 Flow chart of cutting time increment searching procedure

5.3.5 Nodal Displacement

Nodal displacement due to wear is calculated at every tool face node by

$$\vec{w}_{(i,j)} = \dot{w}_{(i,j)} \cdot \Delta t_j \cdot \vec{D}_{(i,j)} \tag{5.1}$$

where

$\vec{w}$ is the nodal displacement vector;

i is nodal label;

j is tool wear calculation cycle number.

In addition, some nodes on flank face must be moved in order to avoid forming bulge on flank face, as mentioned above.

5.3.6 Tool Geometry Updating

In order to visualize the tool wear profile and prepare tool geometry model for the next tool wear calculation cycle, tool geometry updating is performed. It is accomplished with two steps. In these two steps nodes on the tool bottom surface, marked with small triangles in Fig. 5.8, are fixed spatial.

5.3.6.1 Step 1: Initial Tool Wear Profile

In the first step the tool face nodes, including the nodes on rake face and flank face, the circled nodes in Fig. 5.8, are moved according to the calculated nodal displacement. The entire movement is accomplished several times. Every time the tool face node is moved a very small distance. Then the mesh inside the tool is remeshed with one of the smoothing methods: volume smoothing, Laplacian smoothing and equipotential smoothing, or their combination. In the following part, volume smoothing is employed because of the robustness. Remeshing improves mesh distortion and enables additional nodal movement of the tool face nodes in the next times. After the first step, an initial tool wear profile appears on the cutting tool, as shown in Fig. 5.9(b).
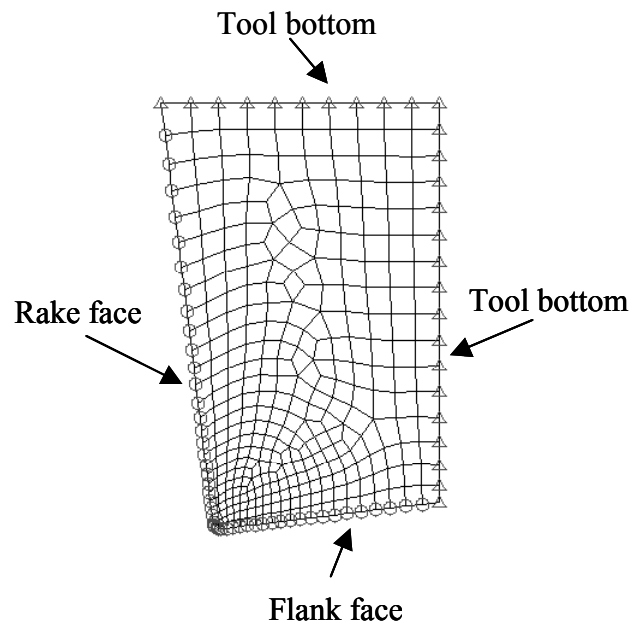
Fig. 5.8 Boundary conditions in step 1 of tool geometry updating model

5.3.6.2 Step 2: Adjustment

Because of the contact problem on the tool-chip and tool-workpiece interface caused by the coarsened workpiece mesh in chip formation analysis, the predicted distributions of cutting process variables along the tool face often contain 'vibration'. These results in zigzags of the initial tool wear profile, e.g, zone A in Fig. 5.9(b).

In addition, the mesh inside the cutting tool has been remeshed many times in step 1. But the tool face nodes are moved according to the calculated nodal displacement without any additional adjustment of nodal position. Sometime very fine mesh is formed in the cutting edge area, for example, zone B in Fig. 5.9(b); they make tool geometry updating in the next calculation cycle difficult because negative element areas may be created by the nodal displacement due to additional produced tool wear.

Fig. 5.9(c) shows that in the second step, zigzags of the crater wear profile are smoothened and the mesh near the cutting edge is coarsened. The final tool wear profile and tool geometry is produced by step 2. The tool geometry model file is updated according to the produced result in step 2.

(a)   (b)   (c)
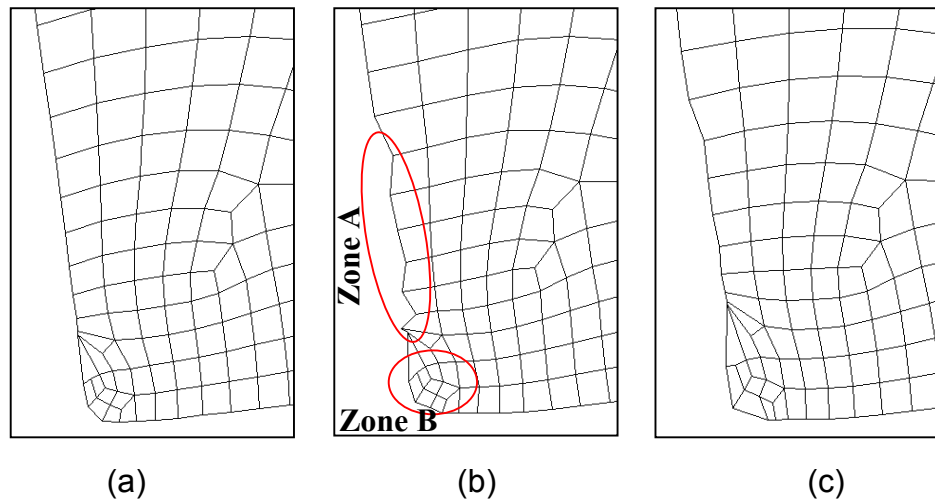
Fig. 5.9 Changes of the mesh during tool updating steps (a) The tool geometry and mesh at the beginning of step 1 (b) At the end of step 1, nodes on the tool face are moved according to the calculated nodal displacement, crater wear and flank wear are formed (c) At the end of step 2, zigzags of the crater wear are smoothened.

5.4 Results & Discussion

5.4.1 Tool Wear

With this tool wear estimation program, tool wear progress under the same turning cutting conditions as described in Table 3.1 is calculated. Tool reshape criterion is set to 0.15mm, and tool wear increment $\Delta VB = 0.05mm$ is specified by user, permitted error δ in the cutting time increment searching process is set to 0.02mm. The tool wear estimation process is accomplished with three tool wear calculation cycles. After the first calculation cycle, the new tool in Fig. 5.10(b) is updated to the worn tool in Fig. 5.10(c). After the second calculation cycle, increased crater wear and flank wear can be found on the updated tool in Fig. 5.10(d).

(a)   (b) t=0s   (c) t=5s

(d) t=46s   (e) t=187s

Fig. 5.10 Tool wear profile progress

(a) Flank wear   (b) Crater wear
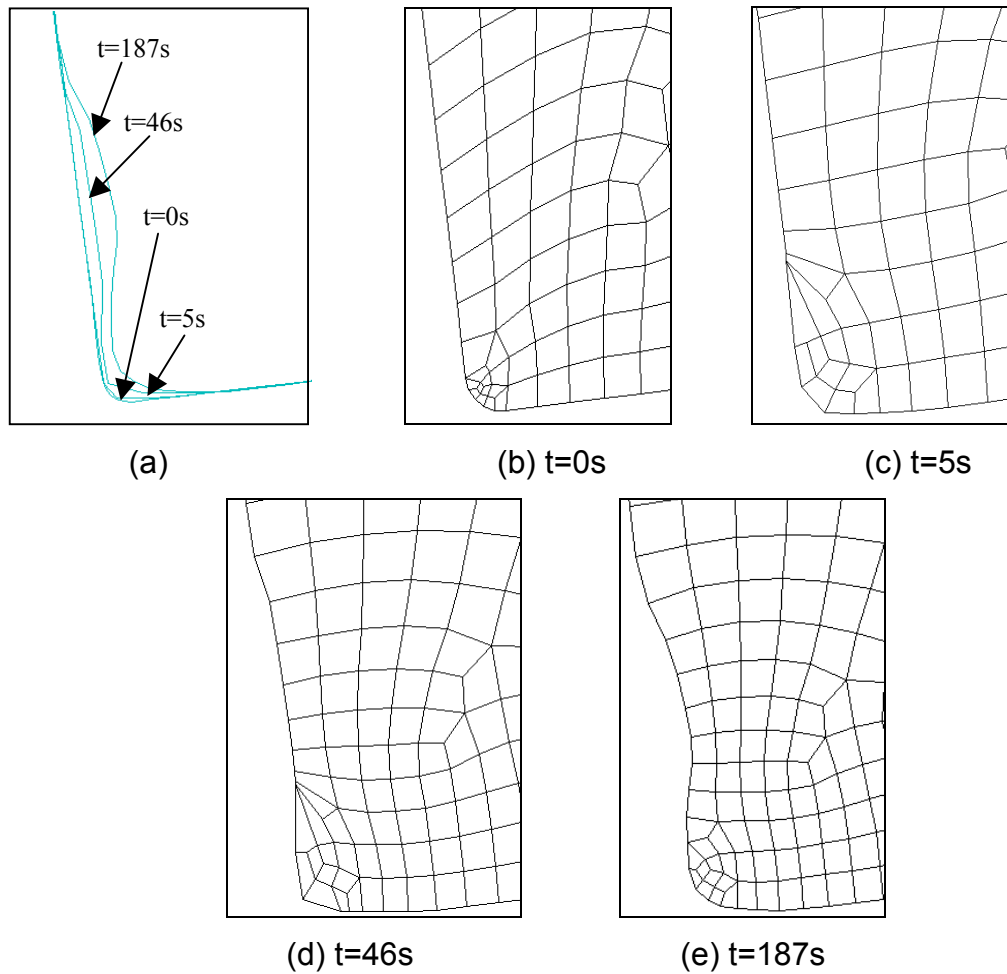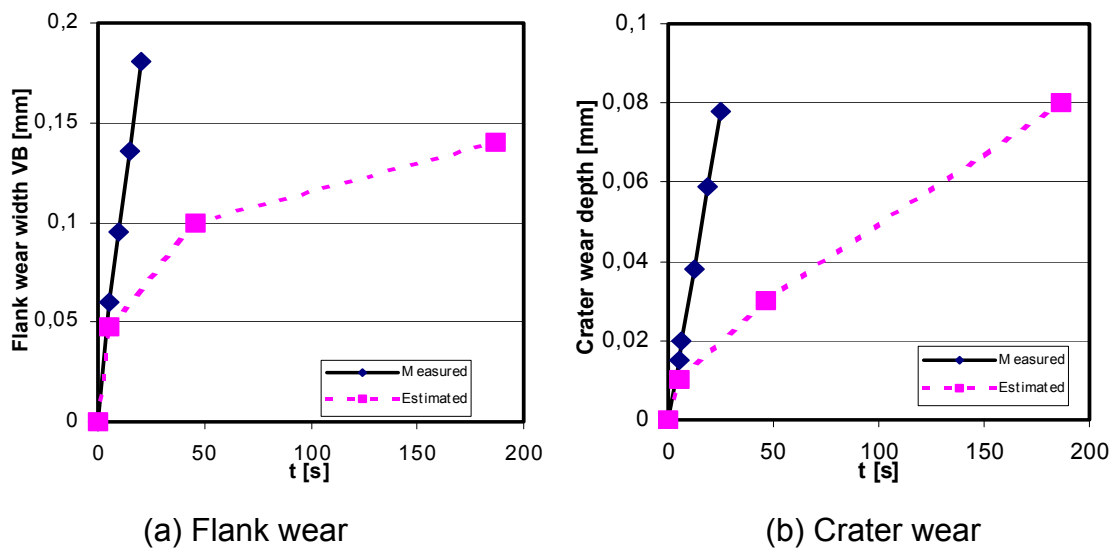
Fig. 5.11 Comparison between estimated and experimental progress curves for tool
wear (under cutting condition: v_c=300m/min, a_p=2mm, f=0.145mm/r)

The solid line in Fig. 5.11 shows the wear progress curves of flank wear and crater wear obtained from experiment [Schm-02] under the same cutting condition. The dot

lines are predicted tool wear curves. It is found that the estimated flank wear and crater wear are smaller than experimental ones. In experiment, after 20s of cutting, the flank wear has exceeded 0.15mm and crater wear 0.06mm, while after 187s, the estimated flank wear just arrives at 0.14mm and crater wear 0.08mm.

The discrepancy may be caused by:

- the simplified and low coefficient of friction. In the chip formation analysis, Coulomb's friction model is adopted and a constant coefficient of friction 0.3 is used in the whole tool wear estimation process. According to the verification of chip formation analysis in continuous chip formation, the predicted cutting force and thrust force are smaller than the experimental data by about 15% and 35% when the coefficient of friction is set to 0.3. This maybe means that the predicted variables for the calculation of tool wear have error as well. Therefore chip formation modeling is very important for the accuracy of tool wear estimation. In order to improve the prediction, it is expected that in the later tool wear estimation, the coefficient of friction should be calculated according to the cutting force and tool geometry or with a more reliable method.

- inconsistentness of material combination. Because the characteristic equation of tool wear and the tool wear data come from different literatures and researchers, it is unavoidable that difference exist in these tool and workpiece material's chemical composition and structure. It was tested by Kitagawa et al that the content and size of abrasive particle dispersed in workpiece material and chemical composition of tool material could be correlated with change in the constants of the wear characteristic equation both in higher and lower temperature ranges [Kita-88].

- contact problem between flank wear and the workpiece. From Fig. 5.11, after a certain tool wear is formed, both wear rate on flank face and on rake face are decreasing, the wear rate on flank face decreases more than that on rake face. It is observed that the temperature on flank wear drops off to a low value. This may be caused by the poor contact between flank wear and the workpiece. In order to improve the contact, maybe on the flank wear face, some nodes should be adjusted to form a small negative flank angle.

5.5 Summaries & Conclusion

In this chapter 2-D tool wear estimation in orthogonal cutting of turning operation is implemented by integrating ABAQUS/Explicit and ABAQUS/Standard with Python user-program. The main findings of this study are as follows:

(1) Python user program launches chip formation and heat transfer analysis job automatically every time the new value about cutting process variables at steady state are needed. Then displacement of every tool face node due to wear is calculated by calculating nodal wear rate at steady state, searching a suitable cutting time increment by program and nodal displacement calculation. Finally tool geometry is updated according to the calculated nodal displacements and one calculation cycle is finished.

(2) The Python user program runs automatically until a tool reshape criterion is reached. The number of calculation cycles carried on before Python user program stop is defined by dividing tool reshape criterion by the specified wear increment. Because of the huge calculation time and cost of chip formation analysis, a bigger wear increment is preferred in order to reduce the calculation cycle number, which certainly will bring bigger errors in estimated result. A trade-off value should be found.

(3) In order to improve the estimate result and realize tool wear estimation in quantity, more efforts should be made in several aspects: more reasonable frictional modelling, further mesh control, regenerate workpiece model when chip shape has a great change due to tool geometry change caused by serious tool wear and some modification of the flank wear shape in order to improve the contact between flank wear and workpiece material.

Chapter 6 Estimation Of Tool Wear In Milling Operation

6.1 Introduction

Cutting action in milling operation is different from turning operation. With the cutting tool rotating, workpiece moves in feed direction. In every rotation/milling cycle, the cutting insert cuts away a layer of workpiece material and then cools down in the environment. Therefore every milling cycle comprises cutting phase and cooling phase. In the cutting phase, cutting thickness varies with tool engage angle. For example, in the down milling operation in Fig. 6.1, cutting thickness has the maximum value when the cutting insert advances into the workpiece. Then the cutting thickness decreases continuously. At the exit the cutting thickness becomes zero. According to metal cutting theory, nearly all the cutting process variables or solutions, stress, strain, temperature, etc are related with the cutting thickness. Therefore they change with the tool engage angle and so does nodal wear rate.
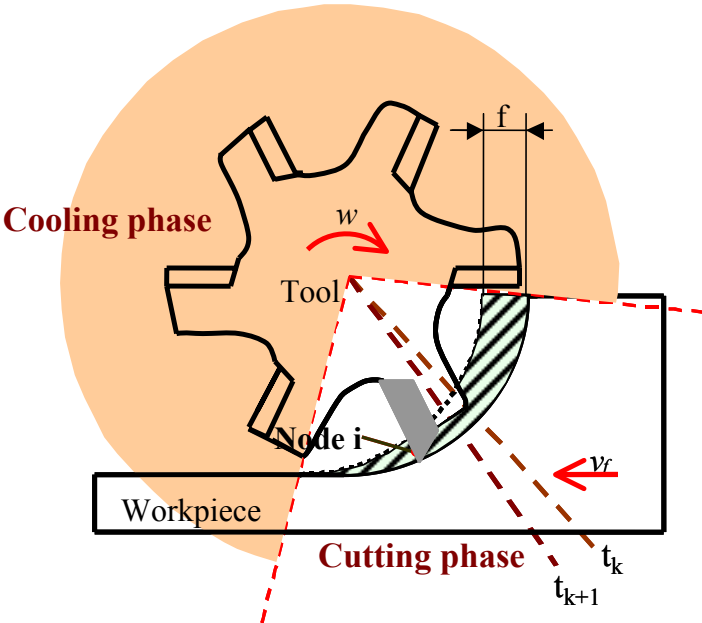
Fig. 6.1 Feature of milling operation

Although milling operation has no steady state, the cutting process possesses periodicity. If the effect of tool wear, uneven distribution of the workpiece material, etc are neglected, mechanical variables in one milling cycle can be assumed to be repeated in other milling cycles because of the same cutting path of the cutting insert

and the same change of undeformed chip thickness. Mechanical cutting process variables, normal pressure on tool face and relative sliding velocity of workpiece material on the tool face, obtained from the first milling cycle can stand for those from all other milling cycles. As tool temperature is concerned, the tool temperature obtained in one milling cycle can stand for that in other milling cycle only when the cyclical thermal balance state (heat loss is equal to heat gain per cycle) is attained. Before the cyclical thermal balance state is reached, heat loss is smaller than heat gain per milling cycle and the tool temperature increased after each milling cycle. The tool temperature obtained in one of these milling cycles is always lower than that in the milling cycle of the cyclical thermal balance state. In the milling operation with a long continuous milling path, the cyclical thermal balance state dominates the entire cutting process. The tool wear is mainly decided by the cyclical thermal balance state. If the tool wear is calculated according to the tool temperature in a milling cycle before the thermal balance state is reached, a lower estimated value of the tool wear is expected.

Periodicity of cutting action and the existence of the cyclical thermal balance state enable the implementation of tool wear estimation in milling operation. Once cyclical thermal balance state is attained, tool wear and nodal average wear rate per cycle do not change from cycle to cycle. Therefore the implementation of tool wear estimation in milling operation can be simplified by calculating nodal average wear rate per cycle in one milling cycle of cyclical thermal balance state and then using it in other milling cycles.

6.2 Tool Wear Calculation Program Design

Fig. 6.2 shows the flow chart of the tool wear calculation program.

```
                        ┌─────────────┐
                        │    Start    │
                        └─────────────┘
                               │
                               ▼
                  ┌────────────────────────┐
          ┌──────▶│  Chip formation analysis │
          │       └────────────────────────┘
          │                    │
          │                    ▼
          │       ┌────────────────────────┐
          │       │   Heat transfer analysis │
          │       └────────────────────────┘
          │                    │
          │                    ▼
          │       ┌─────────────────┐      ┌──────────────────────┐
          │       │ Nodal average wear │────▶│ Cutting time increment │
          │       │  rate per cycle    │     │     calculation        │
          │       └─────────────────┘      └──────────────────────┘
          │                    │                      │
          │                    ▼                      │
          │       ┌─────────────────┐                 │
          │       │Nodal displacement │◀───────────────┘
          │       │   calculation     │
          │       └─────────────────┘
          │                    │
          │                    ▼
          │       ┌─────────────────┐
          │       │Tool geometry updating│
          │       └─────────────────┘
          │                    │
          │        No          ▼
          └──────────────◀  ◇ VB>=VBmax? ◇
                                │ Yes
                                ▼
                        ┌─────────────┐
                        │     End     │
                        └─────────────┘
```

Next calculation cycle

VB>=VB$_{max}$?
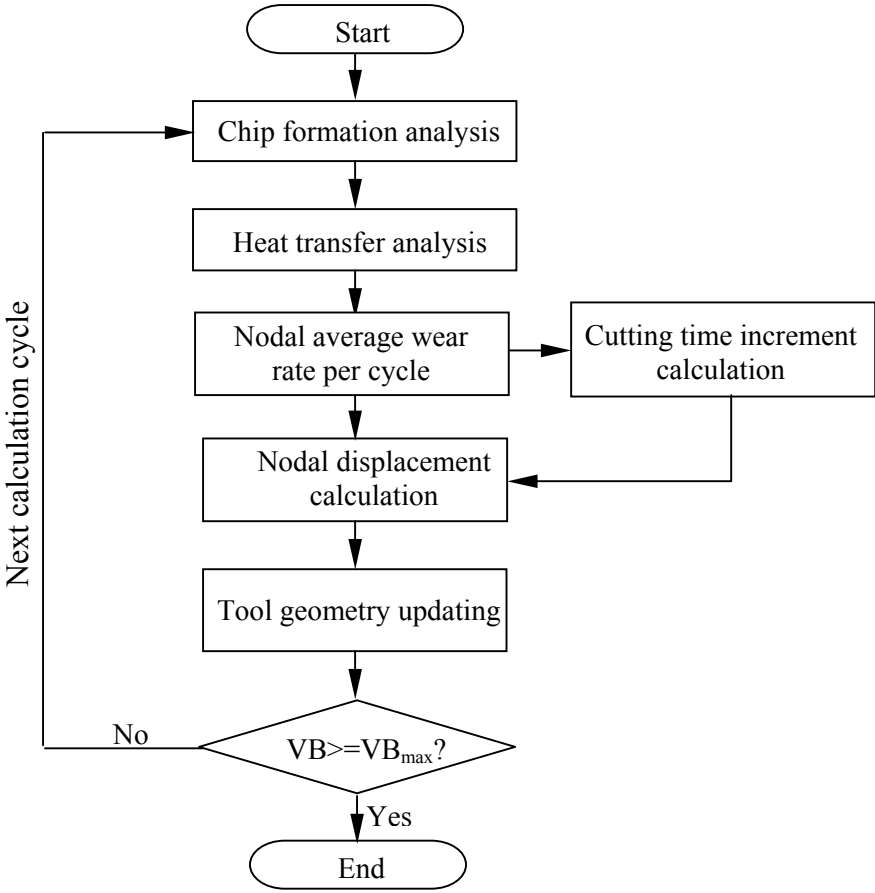
Fig. 6.2 Flow chart of the tool wear calculation program

The tool wear calculation program is designed to perform tool wear calculation automatically cycle by cycle until a tool reshape criterion is reached. In every calculation cycle, chip formation and heat transfer analysis are performed to predict the cutting process variables, which are necessary for the wear rate calculation. According to the above discussion on milling features, mechanical variables can be obtained from the first milling cycle and the heat transfer analysis helps to decide from which milling cycle tool temperature is read for the calculation of nodal wear rate. The nodal wear rate is time-dependent and calculated at some selected time points of one milling cycle, then the nodal average wear rate is calculated according to these nodal wear rate at the selected time points. Based on the calculated nodal average wear rate, a suitable cutting time increment value is searched according to a user-specified VB increment value. Then nodal displacement due to wear produced in the cutting time increment is calculated and the tool geometry updating aims at forming the tool wear profile on the tool face. If the produced flank wear VB is smaller

than the user-defined tool reshape criterion VB_{max}, a second calculation cycle will start with the updated tool geometry.

6.3 Modeling Procedure

During the explanation of the entire modelling procedure, the tool wear under the same cutting condition as described in Table 3.2 is estimated.

6.3.1 Chip Formation Analysis

Chip formation analysis aims at obtaining the mechanical variables for the calculation of nodal wear rate. Because tool wear takes place only in cutting phase and there is no tool wear created in cooling phase, chip formation analysis covering the entire cutting phase is necessary and enough for the calculation of wear rate.

During the cutting phase, mechanical variables are varying from time to time. But with explicit method, finite element analysis of chip formation process is performed by advancing the time with small time increments. Hence the time for outputting the variables is discontinuous. Furthermore, high frequency of variables outputting will result in a large output database file and increase the amount of calculation in the tool wear estimation. Therefore the frequency of mechanical variables output should be decided by making a compromise between calculation accuracy and calculation cost.

The mechanical variables, sliding velocity of workpiece material and normal pressure on tool face, are required during the calculation of wear rate. Sliding velocity is available at the workpiece node. For example, Fig. 6.3(b) shows the sliding velocity at the time when the cutting tool engaging into the workpiece 0.1ms. At the tool tip sliding velocity is very small, even some nodes flow towards the machined surface before material failure takes place. Other nodes are flowing out with the chip at increasing sliding velocity.

According to the sliding velocity at the position of workpiece nodes, sliding velocity at the position of tool face nodes are calculated at the time point when the calculation of nodal wear rate is required.

(a) The cutting at 0.100ms   (b) At t=0.100ms
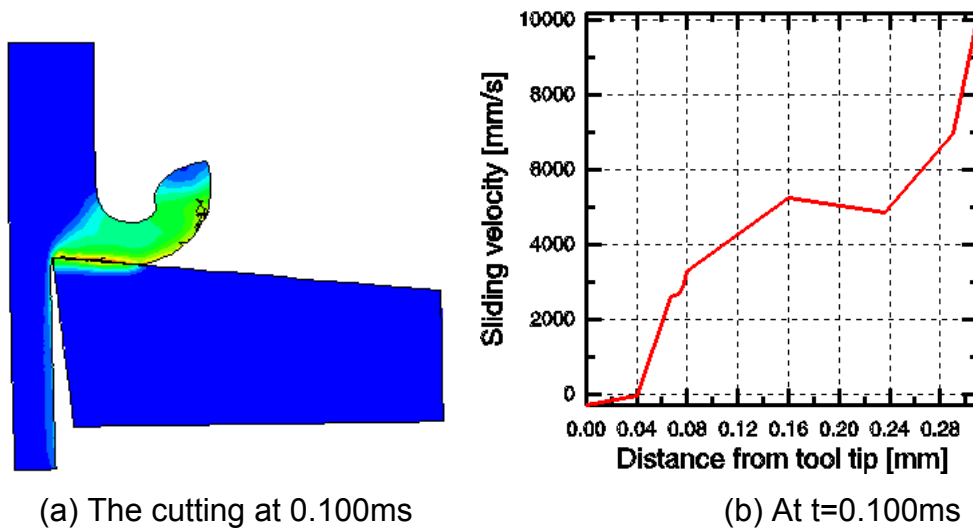
Fig. 6.3 Relative sliding velocity of workpiece material on the tool face at the time of 0.100ms

Normal pressure at the position of tool face node can be obtained directly. For example, Fig. 6.4 shows the normal pressure at the time of 0.1ms. From tool tip to the separation point of the chip and tool normal pressure is decreasing. No plateau is observed in the entire tool-chip contact area as in turning operation.
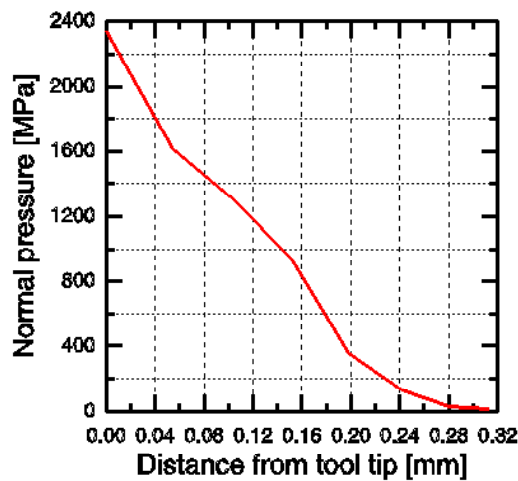
Fig. 6.4 Normal pressure on the tool face at the time of 0.100ms

6.3.2 Heat Transfer Analysis

According to the heat transfer analysis, the tool temperature at the tool face nodes increase after every milling cycle until cyclical thermal balance state is reached. Fig. 6.5 shows the nodal temperature on the tool-chip interface at the time when the tool is engaging into the workpiece 0.1ms in three selected milling cycles. The selected milling cycle are the first, the ninth and cyclical thermal balance cycle, which is obtained from the last milling cycle of heat transfer analysis of the tool preheated to 650K. It is found that from the first to the ninth milling cycle, nodal temperature at tool face has a jump, while from the ninth to cyclical thermal balance cycle; the temperature has a relative small increment.

The tool temperature in the cyclical thermal balance state is read for the calculation of tool wear.
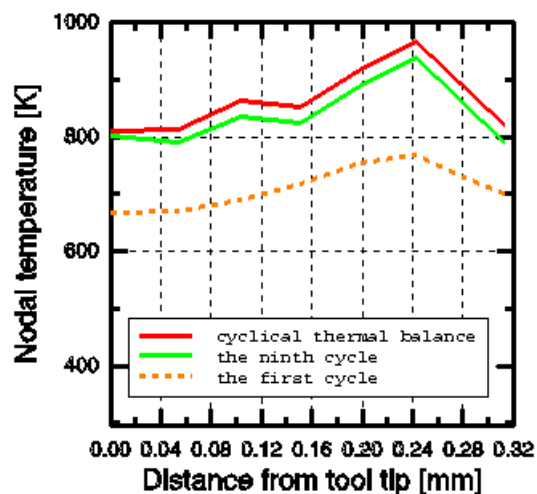
Fig. 6.5 Tool temperature at the tool face nodes after the cutting insert advancing into the workpiece 0.1ms

6.3.3 Nodal Average Wear Rate Calculation

Usui's model is employed in the calculation of nodal wear rate at a certain time. The wear characteristic constants in Usui's equation for the combination of carbide cutting tool and mild steel are shown in Table 1.2.

6.3.3.1 Discussion About The Calculation Method Of Nodal Average Wear Rate

Nodal wear rate varies with the cutting time. In the cutting phase, tool wear takes place under the contact of the tool with the workpiece. In cooling phase, nodal wear rate is equal to zero and no wear produced. Nodal average wear rate is calculated by

$$\overline{w}_{(i,j)} = \frac{\int_{t_0}^{t_0+Z} \dot{w}_{(i,j)}(t)dt}{Z} \, , \qquad\qquad (6.1)$$

where

$\overline{w}$ is the nodal average wear rate;

$\dot{w}(t)$ is nodal wear rate;

Z is the time span of one milling cycle;

i is the nodal label;

j is the milling cycle number.

At present it is very difficult to get the function of nodal wear rate $\dot{w}_{(i,j)}(t)$. But nodal wear rate values at some discrete time points can be obtained by sampling cutting process variables during chip formation and heat transfer analysis and then calculating the individual nodal wear rate values, as shown in Fig. 6.6. Based on these nodal wear rate values, an approximate nodal average wear rate can be calculated by the following equation.

$$\overline{w}_{(i,j)} = \frac{\sum_{1}^{n}\left(\dot{w}_{(i,j,k)} + \dot{w}_{(i,j,k+1)}\right)\cdot\left(t_{k+1} - t_k\right)\cdot\frac{1}{2}}{Z} \qquad\qquad (6.2)$$

where

n means that the entire milling cycle is divided into n-1 small portions by n evenly spaced time points;

k is the time point number; nodal wear rate is calculated at every time point.

In the real calculation, sampling of cutting process variables and the calculation of nodal wear rate are not performed in the entire milling cycle because no wear takes place in cooling phase. For example, the whole milling cycle may take about 39.27ms, but the cutting phase only takes place in the first 0.2ms of every milling

cycle. According to Chapter 4, the chip formation analysis includes the whole cutting phase and 0.3ms of cooling phase in the first milling cycle. During the calculation of nodal average wear rate, the mechanical variables sliding velocity and normal pressure are read only at sampling time points 0.025, 0.05, … and 0.5ms in the chip formation analysis. Tool temperature values are read at the corresponding time points 0.025, 0.05, … 0.5ms of the selected milling cycle of heat transfer analysis. Average nodal wear rate calculation is performed only at these time points. The part of cooling phase from 0.5ms to 39.27ms is not considered.
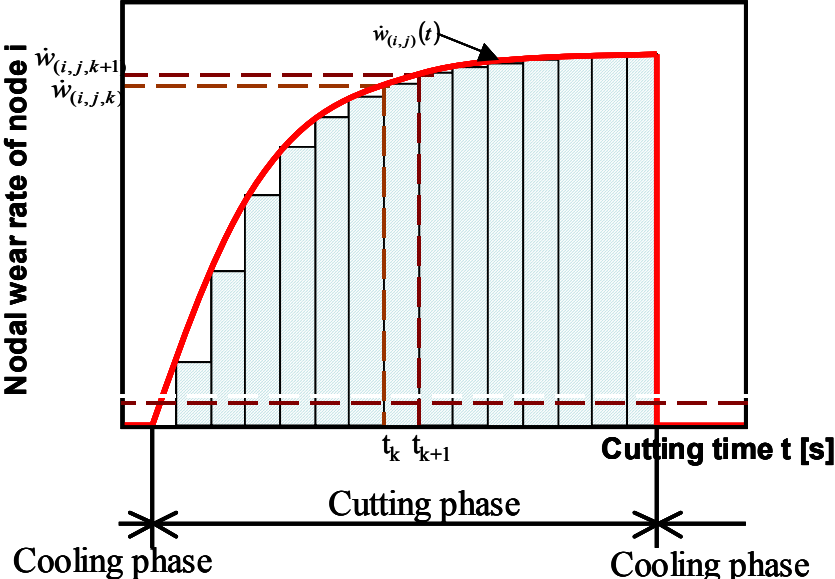
Fig. 6.6 Calculation of nodal average wear rate

Then in Eq. 6.2, the meaning of n becomes the number of time points dividing the period of chip formation analysis.

6.3.3.2 Classification Of Workpiece Node

The sliding velocity of workpiece material at the position of tool face nodes are calculated using the same method explained in Chapter 5.

Chip formation modelling in turning operation is different from milling operation. In turning operation, workpiece nodes, which have possibility of getting contact with the tool face, are fixed on several nodes on the chip underside. Only these nodes are considered during the calculation.

Since in milling operation shear failure criterion is defined in the whole workpiece, some nodes not on the moving path of the cutting edge may be exposed due to

element removal and get contact with the tool face. Therefore a large number of workpiece nodes have to be considered.

In order to calculate the sliding velocity correctly and efficiently, workpiece nodes considered are classified into three types. The first type, called inner node, includes the nodes still inside the workpiece, for example, Node 411 in Fig. 6.7. Node 343 belongs to the second type, surface node, including the nodes exposed on the surface. Node 893 is included in the third type, free node, which consists of the nodes lose connection with the workpiece body because all the attached elements are removal. Because inner nodes have no contact with the tool face, they only increase the calculation time. When free nodes get contact with the tool face, they will introduce calculation error. Hence only surface nodes join in the calculation of relative sliding velocity.
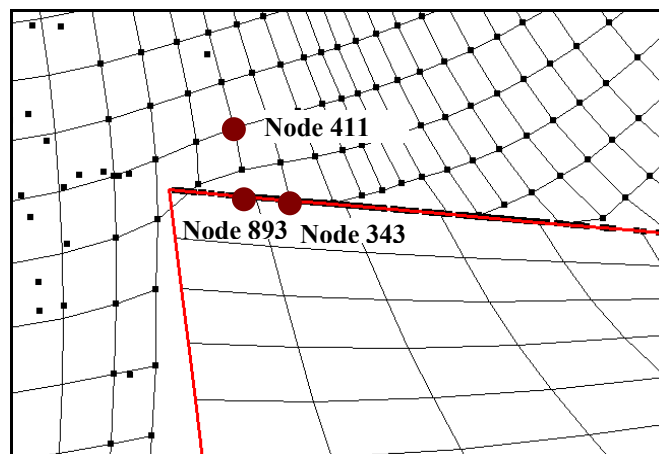
Fig. 6.7 Classification of workpiece node

Node type is judged by considering the number of the attached elements and the deleted elements of a node. Every node is attached to several elements. The number of the attached elements is denoted as $N_{attached}$. The attached element is deleted or removed as it reaches the shear failure criterion. The number of the deleted elements is denoted as N_{delete}. The type of a node is decided by:

$$\begin{cases} N_{deleted} = 0 & \text{Inner node} \\ N_{attached} > N_{deleted}, \quad N_{deleted} \neq 0 & \text{Surface node} \\ N_{attached} = N_{deleted}, \quad N_{deleted} \neq 0 & \text{Free node} \end{cases} , \qquad (6.3)$$

6.3.4 Nodal Move Direction

In milling operation, position of every tool face segment and its normal direction are varying with the rotation of the cutting tool. The calculation of nodal move directions and tool geometry updating should be performed at the same rotation position of the cutting tool, for example at the beginning of one milling cycle.

6.3.4.1 Dividing Node

Similar to the calculation of nodal move direction in turning operation, at the beginning a dividing node that divides the entire tool face into rake face and flank face is searched.

Instead of comparing the y-coordinate of every tool face node, the dividing node is defined according to the distance between tool face nodes and the rotation centre. At the beginning of the search, the first tool face node (the tool face nodes are arranged in counter-clockwise order in advance) is given to the dividing node. Then every tool face node is compared with the current dividing node one by one in counter-clockwise order. Any tool face node whose distance to the rotation center is greater than that of the current dividing node by 2e-4mm will update the record of dividing node.

Nodal move direction is calculated with different methods on the rake face and flank face, as shown in Fig. 6.8.
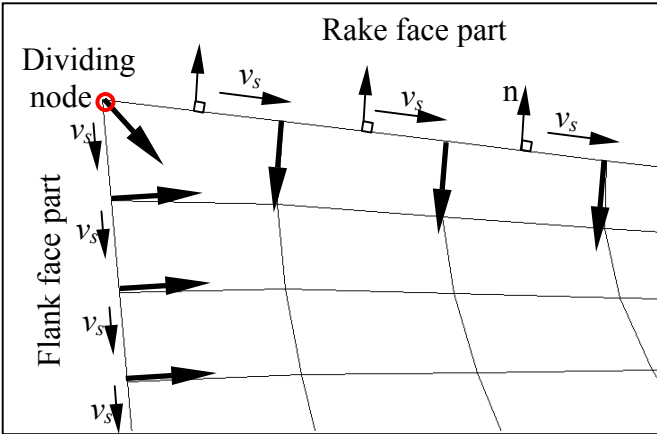
Fig. 6.8 Calculation of nodal move direction

6.3.4.2 On Rake Face

The calculation method of nodal move direction on rake face used in turning operation, explained in Chapter 5, is applied here as well.

6.3.4.3 On Flank Face

In the flank face part, relative sliding velocity of the workpiece material at each flank face node is assumed along the tangential direction of the moving path of the flank face node, when the elastic recovery of workpiece material is neglected. Nodal move direction at the flank face node is perpendicular to the relative sliding velocity, i.e. pointed from the flank face node to the rotation centre.

Every nodal move direction is normalized to unit vector $\vec{D}_{(i,j)}$, where subscript i is nodal label, j is the calculation cycle number.

6.3.5 Cutting Time Increment Calculation

Cutting time increment is searched by the program according to a user-specified flank wear increment value ΔVB and a permitted error δ. Because of the particularity of milling operation, the searching procedure and the flank wear calculation subroutine have some difference compared with those in turning operation.
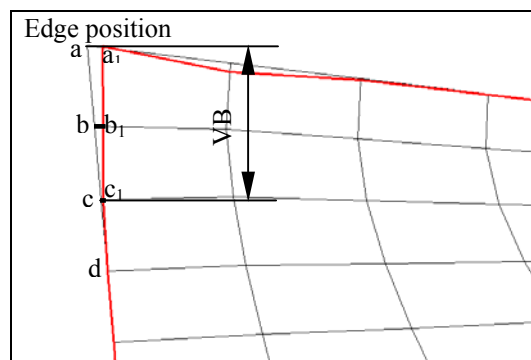
Fig. 6.9 Flank wear calculation

6.3.5.1 Flank Wear Calculation Subroutine

Flank wear land width VB is calculated by a flank wear calculation subroutine $Flankwear(\Delta t, wearrate)$.

VB is the distance from the edge position to the last moved tool face node. The last moved tool face node is searched by considering the movement of the cutting insert. In milling operation the cutting insert rotates around a rotation centre. Any tool material point which becomes the farthest point to the rotation centre will get contact with the workpiece and then be worn away. For example, in Fig. 6.9 node a is the last tool face node with non-zero nodal wear rate. According to the calculation, it should move to point a_1 in the cutting time increment Δt. Then node b becomes the farthest point to the rotation center. It will be worn away. Because in this calculation cycle the comprehensive information about the average wear rate of node b in the entire cutting time increment cannot be obtained, its displacement is decided according to node a. Node b will be move to point b_1 and it will have the same distance to the rotation centre as node a. In the same way, node c will be moved to point c_1. VB is calculated from edge position to node c, because it is the last moved tool face node.

6.3.5.2 Cutting Time Increment Searching Procedure

Because milling operation is intermittent cutting, the existence of cutting phase and cooling phase in milling cycles complexes the cutting time increment searching procedure. In order to simplify the problem, the cutting time increment is increased in step of whole milling cycles. The relationship between the milling cycle number N_{cycle} and the cutting time increment Δt is given by

$$\Delta t = N_{cycle} \times Z \tag{6.4}$$

where

N_{cycle} is positive integer;

Z is the time span of one milling cycle.

The cutting time increment searching procedure is described as follows:

    (1) At the beginning, the aimed VB median value VB_m is calculated according to the user-specified VB increment value and the tool wear obtained in the previous calculation cycle. According to the permitted error δ, the aimed VB value range $(VB_m - \delta, VB_m + \delta)$ is determined.

Then an initial cycle number N_{cycle0} is given a positive integer value arbitrary, the cycle number N_{cycle} and the cycle number lower limit N_{cycle1} are set to N_{cycle0}.

(2) Calculate the cutting time increment Δt corresponding to N_{cycle} with Eq. 6.4, and call the subroutine $Flankwear(\Delta t, wearrate)$ to calculate the flank wear land width, let

$error = Flankwear(\Delta t, wearrate) - VB_m$.

If $|error| \leq \delta$, then the searching procedure will end, and the present Δt value will be output as the result.

(3) Otherwise, if error $< -\delta$, then the cycle number lower limit $N_{cycle1}=N_{cycle}$, and $N_{cycle} = 2 \cdot N_{cycle}$, repeat step 2 until $error \geq -\delta$ is satisfied.

Else, if error $> \delta$, then the cycle number lower limit $N_{cycle1} = 1$.

(4) The cycle number upper limit $N_{cycle2} = N_{cycle}$

(5) N_{cycle} takes the integer part of $(N_{cycel1} + N_{cycle2})/2$. If the value of N_{cycle} is equal to N_{cycle1} or N_{cycle2}, then calculate the cutting time increment Δt. The present Δt value will be output as result and the searching procedure will end.

(6) Calculate the cutting time increment Δt corresponding to N_{cycle}, and call the subroutine $Flankwear(\Delta t, wearrate)$ to calculate the flank wear land width, let

$error = Flankwear(\Delta t, wearrate) - VB_m$.

If $|error| \leq \delta$, then the searching procedure will end, and the present Δt value will be output as the result. Otherwise, if error $< -\delta$, then the cycle number lower limit $N_{cycle1} = N_{cycle}$, else, the cycle number upper limit $N_{cycle2} = N_{cycle}$, repeat step 5 until $|error| \leq \delta$ is satisfied.

6.3.6 Nodal Displacement Calculation

Nodal displacement is calculated at every tool face node by

$$\vec{w}_{(i,j)} = \overline{w}_{(i,j)} \cdot \Delta t_j \cdot \vec{D}_{(i,j)} \qquad\qquad (6.5)$$

where

$\bar{w}$ is the nodal displacement vector;

i is nodal label;

j is tool wear calculation cycle number.

In addition, some nodes on flank face, e.g. node b and c in Fig. 6.9, are moved as well as explained above.

6.3.6 Tool Geometry Updating

Tool geometry updating is performed with the same procedure as explained in turning operation.

6.4 Results & Discussion

With this tool wear program, tool wear under the same cutting condition as described in Table 3.2 is estimated. $\Delta VB = 0.05mm$ is specified by the user, permitted error is set to 0.01mm. After the cutting time of about 603s, the new tool in Fig. 6.10(a) is updated to the worn tool in Fig. 6.10(b), which has a flank wear width of 0.06mm and crater wear on the rake face.

(a) t=0s   (b) t=603s

Fig. 6.10 Tool wear profile

A discrepancy between the estimated tool wear from the program and the expected tool wear from experiment is unavoidable mainly because of the following reasons:

  (1) Complex tool wear in milling operation. In this study, only the abrasive and adhesive wear are considered, whereas the main tool wear in high-speed-milling results from chipping, thermal crack, etc. They reduce the strength of the tool edge and accelerate tool wear.

(2) Chip formation analysis modeling. It is verified by the test that the chip thickness and tool/chip contact are sensitive to the element size and given value of shear failure criterion, when shear failure criterion is used as the chip separation method. A multi variable dependent shear failure criterion may provide a better chip formation simulation result and improve the predicted tool wear profile and tool wear value.

6.5 Summaries & Conclusion

In this chapter, a tool wear estimation model is implemented for the milling operation. The main findings of this study are as follows:

- Milling operation is an intermittent cutting process. By sampling the cutting process variables in the chip formation analysis and heat transfer analysis at the corresponding time points and calculating the nodal average wear rate per cycle, tool wear estimation modelling can be implemented.

- Because of the temperature difference in the cyclical thermal balance state and in the milling cycle before cycle thermal balance state is reached, tool temperature in the cyclical thermal balance state should be used in tool wear estimation. Otherwise, a very slow tool wear process is expected because in Usui's tool wear equation, wear rate and tool temperature has an exponent relationship.

- With the developed tool wear program, tool wear under a cutting condition with high cutting speed is calculated, both crater wear and flank wear are formed on the tool face.

Chapter 7 Summary And Prospect

7.1 Summaries

In this study the methodologies to numerical implementation of tool wear estimation in turning and milling operation are discussed. Based on the researches of tool wear mechanism, which show that wear rate of cutting tool is dependent on some cutting process variables such as tool temperature, sliding velocity of workpiece material and normal pressure on tool face, the preliminary qualitative tool wear estimation models are developed.

Tool wear estimation in turning operation is based on the study of finite element simulation of steady-state cutting process.

A new chip formation modeling method is developed to simulate the entire process from initial chip formation, chip growth to steady state. Chip separation is formed automatically by solution-dependent mesh adaptivity instead of material failure criterion. It is not necessary to get material failure parameters or chip geometry from experiment. Instead it provides an alternative method to decide material failure parameters. In addition, no separation path is preset in advance. No obvious crack is formed in front of the cutting edge. This chip formation model is verified by experimental data. When the coefficient of friction calculated according to cutting force in experiment is used, the error of two cutting force components is smaller than 5% compared to the experimental data.

Pure heat transfer analysis of only the cutting tool is carried out to save the calculation time to reach thermal steady state. Temperature dependent heat flux at tool-chip interface and heat convective and radiation of tool face are considered during modeling. After only several minutes of calculation the cutting tool gets a steady temperature distribution.

Then the problems about calculating nodal wear rate at steady state according to Usui's tool wear equation, cutting time increment searching, nodal displacement calculation and geometry updating are discussed. A tool wear estimation program is developed. It can calculate the tool wear until the tool reshape criterion is reached. The estimated tool wear is verified by experimental data. It is assumed that the error is created by the low coefficient of friction in chip formation analysis.

Because milling operation is intermittent cutting process, the chip formation, heat transfer and tool wear estimation modeling are different from turning operation.

The chip formation simulation is realized by introducing shear failure criterion. The strain at failure in shear failure criterion is defined according to the former chip formation modeling method. Shear failure criterion is applied to the entire workpiece. Pure heat transfer analysis of only the workpiece shows that the workpiece cool down to room temperature in the cooling phase of one milling cycle if the cutting speed is not tool high. Accordingly, the chip formation process in every milling cycle is assumed similar because of the negligible temperature increment in the workpiece. Pure heat transfer analysis of only the cutting tool is carried out for 8 milling cycles. Temperature is observed after every milling cycle. No cyclical thermal balance state is realized. In order to speed up the realization process of cyclical thermal balance state, different preheated cutting tool is used in the cutting process. It is found that the temperature in cyclical thermal balance state is higher than the first several milling cycle.

Tool wear estimation in milling operation is performed by calculation nodal average wear rate in one milling cycle and use it to other milling cycles. Because in milling cycle the cutting tool is rotating instead of the workpiece as in turning operation, all the problems about cutting time increment searching, nodal displacement calculation and geometry updating are different from turning operation and they are discussed. Then a tool wear estimation program for milling operation is developed. Using this program, tool wear in one milling case is calculated. Both crater wear and flank wear are formed.

During the study multi aspects of cutting process simulation modelling in turning and milling operations including chip formation analysis, heat transfer analysis, and tool wear estimation are studied. In order to fulfil the purpose of tool wear study, multi-programming tools including commercial FE code ABAQUS/Explicit, ABAQUS/Standard, Fortran, Python are employed and integrated. This lays a ground for the study on more complex problem and the extension of functionality of FEM in the future.

Tool wear estimation with the help of finite element method can predict not only tool life, but also wear profile of both crater wear and flank wear, and relate tool wear with some wear mechanisms. This tool wear estimation method will relate the geometry appearance to physical basic of tool wear and bridge the gap between macro and micro studies of tool wear. This is very meaningful for the scientific research and education. For tool designer, it is very helpful to optimise tool geometry and structure

knowing wear profile and wear mechanism; for material engineer, it is useful to improve tool material according to the determined main wear mechanism. In this tool wear estimation method, tool wear is related to wear mechanism, once tool wear mathematical model for a combination of tool-workpiece material is determined, it is possible to estimate tool wear by program without doing any experiment. In addition, this estimation method is helpful to reduce the size of various cutting database by replacing tool life equation with tool wear mathematical model, which is applicable to wider cutting range.

7.2 Prospect

The tool wear estimation models should be improved in several aspects:

After a certain tool wear is formed, the chip formation analysis of steady state sometimes produces relatively low tool temperature on flank wear. This may be caused by the contact problem between the flank wear and the workpiece. In order to produce good contact in this area a negative flank angle designed on the flank wear may be a good solution.

In tool geometry updating, the formed wear profile is not smooth even after the second updating step and some nodes have to be adjusted manually. A special smoothing algorithm should be designed to solve this problem.

Friction has big influence on the chip formation analysis and tool wear. When using the coefficient of friction calculated according to the cutting force from experiment, the result of tool wear estimation is maybe improved.

A further improvement of tool wear estimation may be realized by introducing multi wear mechanism. The tool wear is calculated according to their combination. It will be possible to study on the contribution of every wear mechanism under different cutting conditions.

Because in the tool wear estimation modeling, flank wear is produced by moving nodes individually according to the nodal wear rate instead of according to an average value. It provides a method to produce the complex tool wear in 3D, such as wear notch.

In order to spread the application of this method in industry practices, except improving the precision of tool wear estimation, it is necessary to develop tool wear mathematical model for most common used materials, develop tool wear estimation

model for coated carbide tool, CBN cutting tool, ceramics cutting tool, etc, and research on 3D tool wear estimation model in the future.

References

[ABA-01a]   ABAQUS/Explicit User's Manual Version 6.2, HSK, Inc., U.S.A., 2001

[ABA-01b]   ABAQUS/Standard User's Manual Version 6.2, HSK, Inc., U.S.A., 2001

[ABA-01c]   ABAQUS Scripting Manual Version 6.2, HSK, Inc., U.S.A., 2001

[Ahma-89]   Ahmad, M. M., Draper, W. A., and Derricott, R. T., An application of the finite element method to the prediction of cutting tool performance, Int. J. Mach. Tools Manufact. 29 (2) (1989) 197-206.

[Amon-99]   Amontons, Historie de l'Academie Royale des Sciences avec les Memoires de Mathematique et de Physique, 1699.

[Arnd-73]   Arndt, G., Ultra-high-speed machining: a review and an analysis of cutting forces, Applied Mechanics Group, Proc. Instn. Mech. Engrs. 187 (1973) 625-634.

[Arol-02]   Arola, D., Sultan, M. B., Ramulu, M., Finite element modeling of edge trimming fiber reinforced plastics, Journal of Manufacturing Science and Engineering 124 (2) (2002) 32-41.

[Arra-02]   Arrazola, P. J., Meslin, F., Hamann, J-C. and Le Maitre, F., Numerical cutting modeling with Abaqus/Explicit 6.1, 2002 ABAQUS Users's Conference, Newport, Rbode Island, May 29-31, 2002.

[Atha-98]   Athavale, S. M., Strenkowski, J. S., Finite element modeling of machining: from proof-of-concept to engineering applications, in: Proceedings of the CIRP International Workpshop on Modeling of Machining Operations, Atlanta, USA, 1998, pp. 203-216.

[Baca-00]   Bacaria, J. L., Dalverny, O., Pantale, O., Rakotomalala, R., and Caperaa, S., 2D and 3D numerical models of metal cutting with damage effects, European Congress on Computational Methods in Applied and Engineering, Barcelona, Sep. 11-14, 2000.

[Bäke-00]   Bäker, M., Rösler, J., Siemers, C., High speed chip formation of Ti6Al4V, Proceedings of Materials Week, Munich, 2000

[Bäke-02]   Bäker, M., Rösler, J., Siemers, C., Finite element simulation of segmented chip formation of Ti6Al4V, Journal of Manufacturing Science and Engineering 124 (2002) 485-488.

[Batz-02]   Batzer, S. A., Subhash, G., Olson, W., and Sutherland, J. W., Large

strain constitutive model development for application to orthogonal machining, in: Proc. 5th CIRP International Workshop on Modeling of Machining Operations, West Lafayette, USA, 2002, pp. 31-40.

[Behr-98a]   Behrens, A., Westhoff, B., Anwendung von MARC auf Zerspanprozesse, MARC Benutzertreffen 1998, München, 1998.

[Behr-98b]   Behrens, A., Westhoff, B., Probleme und Herausforderungen bei der Simulation von Zerspanprozessen, XXV. FEM-Kongress, Baden-Baden, 1998.

[Behr-99]   Behrens, A., Westhoff, B., Finite element modeling of high speed machining processes, 2nd International German and French Conference on High Speed Machining, Darmstadt, 1999, pp. 185-190.

[Boot-89]   Boothroyo, G., Knight, W. A., Fundamentals of machining and machine tools, Marcel Dekker, Inc. USA, 1989

[Chil-89]   Childs, T., Mahdi, M., On the stress distribution between the chip and tool during metal turning, Ann. CIRP 38 (1) (1989) 55-58.

[Cere-96]   Ceretti, E., Fallböhmer, p., Wu, W.-T., Altan, T., Application of 2D FEM to chip formation in orthogonal utting, Journal of Materials Processing Technology 59 (1996) 169-180.

[Cere-99]   Ceretti, E., Lucchi, M., Altan, T., FEM simulation of orthogonal cutting: serrated chip formation, Journal of Materials Processing Technology 95 (1999) 17-26.

[Cere-00]   Ceretti, E., Lazzaroni, C., Menegardo, L., Altan, T., Turning simulations using a three-dimensional FEM code, Journal of Materials Processing Technology 98 (2000) 99-103.

[Chil-98]   Childs, T. H. C., Dirikolu, M. H., and Maekawa, K., Modelling of friction in the simulation of metal machining, in: 24th Leeds-Lyon Symposium on Tribology. Amsterdam: Elsevier Tribology Series No. 34, 1998, pp.337-46.

[Chuz-03a]   Chuzhoy, L., Devor, R. E., and Kapoor, S. G., Machining simulation of ductile iron and its constituents, part 1: estimation of material model parameters and their validation, Journal of Manufacturing Science and Engineering 125 (5) (2003) 181-191.

[Chuz-03b]   Chuzhoy, L., Devor, R. E., and Kapoor, S. G., Machining simulation of ductile iron and its constituents, part 2: numerical simulation and

experimental validation of machining, Journal of Manufacturing Science and Engineering 125 (5) (2003) 192-201.

[Coul-85]   Coulomb, C. A., Memoires de Mathematique et de Physique de l'Academie Royale des Sciences, Paris, 1785.

[Didj-97]   Didjanin, L. and Kovac, P., Fracture mechanisms in chip formation processes, Materials Science and Technology 13 (1997) 439-444.

[Dill-00]   Dillon, O. W., Zhang, H., An analysis of cutting using a grooved tool, International Journal of Forming Processes 3 (1-2) (2000) 115-130.

[Feve-01]   Feve, S., Yen, Y-C., Altan, T., Tool wear in orthogonal turning of AISI 1045 steel with uncoated tungsten carbide tool, ERC/NSM Report No. HPM/ERC/NSM-01-R-13, The Ohio State University, 2001.

[Finn-56]   Finnie, I., Shaw, M. C., The friction process in metal cutting, Transactions of the ASME 78 (1956) 1649-57.

[Fran-02]   Frank, P., Improvement of the FEM-based Predictive Model of Tool Wear, Diplomarbeit, Universität Karlsruhe (TH), 2002.

[Gu-02]   Gu, L. Z., Wang, d., Xing, L., Chang, J., Chen, G. J., Computer simulation and optimization of metal cutting process for mild carbon steels, Journal of Materials Processing Technology 129 (2002) 60-65.

[Guo-00]   Guo, Y. B., Dornfeld, D. A., Finite element modeling of burr formation process in drilling 304 stainless steel, Journal of Manufacturing Science and Engineering 122 (2000) 612-619.

[Guo-02]   Guo, Y. B., Liu, C. R., 3D FEA modeling of hard turning, Journal of Manufacturing Science and Engineering 124 (2002) 189-199.

[Hast-79]   Hastings, W.F., Mathew, P., Oxley, L.B., Taylor, J., *Proc. 20th Int. M.T.D.R. Conf.*, 1979, pp.313

[Huan-96]   Huang, J. M., Black, J. T., An evalution of chip separation criteria for the FEM simulation of machining, Journal of Manufacturing Science and Engineering 118 (1996) 545-554.

[Iwat-84]   Iwata, K., Osakada, K., Terasaka, Y., Process modeling of orthogonal cutting by the rigid-plastic finite element method, Journal of Engineering Materials and Technology 106 (1984) 132-138.

[John-01]   Johnson, D., Why cutting tools fail, CNC Machining Magazine 5 (18) (2001).

[Kalh-01]   Kalhori, V., Modelling and Simulation of Mechanical Cutting, Doctoral

thesis, Institutionen för Maskinteknik, Avdelningen för Datorstödd maskinkonstruktion, Lulea Tekniska Universitet, 2001.

[Kato-72]   Kato, S., Yamaguchi, K., Yamada, M., Stress distribution at the interface between tool and chip in machining, Journal of Engineering for Industry 94 (1972) 683-689.

[Kim-99]   Kim, K. W., Lee, W. Y., Sin, H. C., A finite-element analysis of machining with the tool edge considered, Journal of Materials Processing Technology 86 (1999) 45-55.

[Kita-88]   Kitagawa, T., Maekawa, K., Shirakashi, T. and Usui, E., Analytical prediction of flank wear of carbide tools in turning plain carbon steels, part 1: characteristic equation of flank wear, Bull. Japan Soc. of Prec. Engg. 22 (4) (1988) 263-269.

[Kita-89]   Kitagawa, T., Maekawa, M., Shirakashi, T. and Usui, E., Analytical prediction of flank wear of carbide tools in turning plain carbon steels, part 2: prediction of flank wear, Bull. Japan Soc. of Prec. Engg. 23 (2) (1989) 126-133.

[Klam-73]   Klamecki, B. E., Incipient chip formation in metal cutting - a three dimension finite element analysis, Ph. D. dissertation, University of Illinois, 1973.

[Kopp-01]   Koppka, F., Sartkulvanich, P. and Altan, T., Experimental Determination of Flow Stress Data for FEM Simulation of Machining Operations, ERC/NSM Report No. HPM/ERC/NSM-01-R-63, The Ohio State University, 2001.

[Köni-84]   König, W., Fertigungsverfaren / Manufacturing Methods, VDI-Verlag, Dusserdolf, Germany, 1984.

[Kwon-00]   Kwon, P., Predictive models for flank wear on coated inserts, Journal of Tribology 122 (1) (2000) 340-347.

[Leop-98]   Leopold Jürgen, FEM modeling and simulation of 3-D chip formation, in: Proceedings of the CIRP International Workpshop on Modeling of Machining Operations, Atlanta, USA, 1998, pp. 235-245.

[Li-02]   Li, K., Gao, X.-L., Sutherland, J. W., Finite element simulation of the orthogonal metal cutting process for qualitative understanding of the effects of crater wear on the chip formation process, Journal of Materials Processing Technology 127 (2002) 309-324.

[Lim-01]   Lim, C. Y. H., Lau, P. P. T., Lim, S. C., The effects of work material on tool wear, Wear 250 (2001) 344-348.

[Lin-99]   Lin, L.-C., Lin, Y.-Y., A study of an oblique cutting model, Journal of Materials Processing Technology 86 (1999) 119-130.

[Lin-00]   Lin, Z.-C., Zheng, Y.-L., Three-dimensional thermo-elastic-plastic finite element analysis with different cutting speeds, International Journal of Computer Applications in Technology 13 (2000) 210-220.

[Lin-01b]   Lin, Z.-C., Lin, Y.-Y., A study of oblique cutting for different low cutting speeds, Journal of Materials Processing Technology 115 (2001) 313-325.

[Liu-00]   Liu, C. R., Guo, Y. B., Finite element analysis of the effect of sequential cuts and tool-chip friction on residual stress in a machined layer, International Journal of Mechanical Science 42 (2000) 1069-1086.

[Lutt-98]   van Luttervelt, C. A., Childs, T. H. C., Jawahir, I. S., Klocke, F., Venuvinod, P. K., Keynote papers: present situation and future trends in modeling of machining operations progress report of the CIRP Working Group 'Modelling of Machining Operations', Annals CIRP 47 (2) (1998) 587-626.

[Maru-95]   Marusich, T. D., Oritz, M., Modelling and simulation of High-Speed Machining, International Journal for Numerical Methods in Engineering 38 (1995) 3675-3694.

[Maru-02]   Marusich, T. D., Brand, C. J., and Thiele, J. D., A methodology for simulation of chip breakage in turning processes using an orthogonal finite element model, in: Proc. 5th CIRP International Workshop on Modeling of Machining Operations, West Lafayette, USA, 2002, pp. 139-148.

[McCl-02]   McClain, B., Batzer, S. A., Maldonado, G. I., A numeric investigation of the rake face stress distribution in orthogonal machining, Journal of Materials Processing Technology 123 (2002) 114-119.

[Merc-98]   Merchant, E., in Proceedings of the CIRP International Workshop on Modeling of Machining Operations, Atalantic, USA, 1998

[Moli-00]   Molinari, J. F., Ortiz, M., Radovitzky, R., and Repetto, E. A., Finite-element modeling of dry sliding wear in metals, Engineering

Computations 18 (3/4) (2001) 592-609.

[Mona-99] Monaghan, J. and MacGinley, T., Modelling the orthogonal machining process using coated carbide cutting tools, Computational Materials Science 16 (1999) 275-284.

[Mova-02] Movahhedy, M. R., Altintas, Y., Gadala, M. S., Numerical analysis of metal cutting with chamfered and blunt tools, Journal of Manufacturing Science and Engineering 124 (2002) 178-187.

[Ng-99] Ng, E.-G., Aspinwall, D. K., Brazil, D., and Monaghan, J., Modelling of temperature and forces when orthogonally machining hardened steel., International Journal of Machine Tools & Manufacture 39 (1999) 885-903

[Ng-02a] Ng, E.-G. and Aspinwall, D. K., Modelling of hard part machining, Journal of Materials Processing Technology 127(2002) 222-229.

[Ng-02b] Ng, E.-G., EI-Wardany, T., Dumitrescu, M., and Elbestawi, M. A., Proc. 5th CIRP International Workshop on Modeling of Machining Operations, West Lafayette, IN, USA, May 20-21, 2002, pp. 1-19.

[Ohbu-03] Ohbuchi, Y., Obikawa, T., Finite element modeling of chip formation in the domain of negative rake anlge cutting, Journal of Engineering Materials and Technology 125 (2003) 324-332.

[Okus-71] Okushima, K., Kakino, Y., The residual stress produced by metal cutting, Ann. CIRP 20 (1) (1971) 13-14.

[Owen-99] Owen, D. R. J., M. Vaz Jr., Computational techniques applied to high-speed machining under adiabatic strain localizetion conditions, Computer methods in applied mechanics and engineering 171 (1999) 445-446.

[Özel-00a] Özel, T., Altan, T., Process simulation using finite element method – prediction of cutting force, tool stress and temperatures in high-speed flat end milling, International Journal of Machine Tools & Manufacture 40 (2000) 713-738.

[Özel-00b] Özel, T., Altan, T., Determination of workpiece flow stress and friction at the chip.tool contact for high-speed cutting, International Journal of Machine Tools & Manufacture 40 (2000) 133-152.

[Özel-02] Özel, T., Modeling of hard part machining: effect of insert edge preparation in CBN cutting tools, Journal of Materials Processing

Technology (2002).

[Rice-60]   Rice, W. B., Salmon, R., Syniuta, W. D., Photoelastic determination of cutting tool stress, Transactions of the E. I. C. 4 (1) (1960) 20-23.

[Sand-98]   Sandstrom, D. R., Modeling the physics of metal cutting in High-Speed machining, in: Proceedings of the CIRP International Workpshop on Modeling of Machining Operations, Atlanta, USA, 1998, pp. 217-224.

[Schm-02]   Schmidt, C., Development of a FEM-based Tool Wear Model to Estimate Tool Wear and Tool Life in Metal Cutting, Diplomarbeit, Universität Karlsruhe (TH), 2002.

[Schu-00]   Schulze, V. and Vöhringer, O., Influence of alloying elements on the strain rate and temperature dependence of the flow stress of steels, Metallurgical and Materials Transactions A 31A (2000).

[Shat-00]   Shatla, M., Yen, Y.-C., Altan, T., Tool-workpiece interface in orthogonal cutting-application of FEM modeling, Transactions of NAMRI/SME 2000, XXVIII, 177-178.

[Shat-01a] Shatla, M., Kerk, C., Altan, T., Process modeling in machining. part I: determination of flow stress data, International Journal of Machine Tools & Manufacture 41 (2001) 1511-1534a.

[Shat-01b] Shatla, M., Kerk, C., Altan, T., Process modeling in machining. part II: validation and applications of the determined flow stress data, International Journal of Machine Tools & Manufacture 41 (2001) 1659-1680.

[Shet-00]   Shet, C., Deng, X., Finite element analysis of the orthogonal metal cutting process, Journal of Material Processing technology 105 (2000) 95-109.

[Shet-03]   Shet, C., Deng, X., Residual stress and strains in orthogonal metal cutting, International Journal of Machine Tools & Manufacture 43 (2003) 573-587.

[Shi-02]   Shi, G. Q., Deng, X. M., Shet, C., A finite element study of the effect of friction in orthogonal metal cutting, Finite Elements in Analysis and Design 38 (2002) 863-883.

[Shih-91]   Shih, A., Yang, H. T. Y., Experimental and finite element simulation methods for rate-dependent metal forming processes, International Journal for Numerical Methods in Engineering 31 (1991) 345-367.

[Shih-93]   Shih, A. J., Yang, H. T. Y., Experimental and finite element predictions of residual stresses due to orthogonal metal cutting, International Journal for Numerical Methods in Engineering 36 (1993) 1487-1507.

[Shih-95]   Shih, A. J., Finite element simulation of orthogonal metal cutting, Journal of Engineering for Industry 117 (1995) 84-93.

[Shih-96]   Shih, A. J., Finite element analysis of the rake angle effects in orthogonal metal cutting, International Journal of Mechanical Sciences 38 (1) (1996) 1-17.

[Shir-93]   Shirakashi, T., New trend on machining theory-way to computational machining, Int. J. Jpn. Soc. Prec. Eng. 27 (1993) 299-302.

[Söhn-01a]   Söhner, J. and Altan, T., Material Database for Manufacturing Simulation (MADAMS): Summary of the Activities and Flow Stress Database, ERC/NSM Report No. HPM/ERC/NSM-01-R-76, ERC for Net Shape Manufacturing, Ohio State University, 2001

[Söhn-01b]   Söhner, J. and Yen, Y.-C., Estimation of tool wear in metal cutting with the finite element method –a progress report-, ERC/NSM Report No. HPM/ERC/NSM–01–R-67, ERC for Net Shape Manufacturing, Ohio State University, 2001

[Söhn-03]   Söhner, J., Beitrag zur Simulation zerspanungstechnologischer Vorgäng mit Hilfe der Finite-Element-Methode, Dissertation, Universität Karlsruhe (TH), 2003

[Stre-93]   Strenkowski, J. S., Carroll III, J. T., A finite element model of orthogonal metal cutting, Journal of Engineering for Industry 107 (1985) 347-354.

[Stre-02]   Strenkowski, J. S., Shih, A. J., Lin, J.-C., An analytical finite element model for predicting three-dimensional tool faces and chip flow, International Journal of Machine Tools & Manufacture 42 (2002) 723-731.

[Tay-74]   Tay, A. O., Stevenson, M. G., David, G. V., Using the finite element method to determine temperature distributions in orthogonal machining, Proc. Inst. Mech. Eng. 188 (1974) 627-638.

[Tayl-07]   Taylor, F.W., Trans. Am. Soc. Mech. Engrs 28,31 (1907)

[Tren-77]   Trent, E.M., Metal Cutting, Butterworths, England, 1977

[Usui-78a]   Usui, E., Hirota, A., Analytical prediction of three dimensional cutting

process, part 2: chip formation and cutting force with conventional single-point tool, Journal of Engineering for Industry 100 (5) (1978) 229-235.

[Usui-78b]   Usui, E., Hirota, A., Masuko, M., Analytical prediction of three dimensional cutting process, part 1: basic cutting model and energy approach, Journal of Engineering for Industry 100 (5) (1978) 222-228.

[Usui-78c]   Usui, E., Shirakashi, T. and Kitagawa, T., Analytical prediction of three dimensional cutting process, part 3: cutting temperature and crater wear of carbide tool, Journal of Engineering for Industry 100 (5) (1978) 236-243.

[Usui-84]   Usui, E., Obikawa, T., Shirakashi, T., Study on chip segmentation in machining Titanium alloy, in: Proceedings of the 5th International Conference on Production Engineering, Tokyo, Japan, 1984, pp. 233-239.

[Walt-98]   Walter, U., Einfluss des Kühlschmierstoffes beim Fräsen, Dissertation Universität Karlsruhe (TH), Karlsruhe, Germany, 1998

[West-01]   Westhoff, B., Modellierungsgrundlagen zur FE-Analyse von HSC-Prozessen, Dissertation, Institut für Konstrucktions- und Fertigungstechnik, Laboratorium Fertigungstechnik, Universität der Bundeswehr, 2001.

[Wu-96]   Wu, J. S., Dillon, O. W., Lu, W.-Y., Thermo-viscoplastic modeling of machining process using a mixed finite element method, Journal of Manufacturing Science and Engineering 118 (1996) 470-482.

[Yang-02]   Yang, X.-P., Liu, C. R., A new stress-based model of friction behavior in machining and its significant impact on residual stresses computed by finite element method, International Journal of Mechanical Sciences 44 (2002) 703-723.

[Yen-02]   Yen, Y. C., Söhner, J., Weule, H., Schmidt, J. and Altan, T., Estimation of tool wear of carbide tool in orthogonal cutting using FEM simulation, in: Proceedings of the 5th CIRP International Workshop on Modeling of Machining Operations, West Lafayette, USA, 2002, pp.149-160

[Zhan-94]   Zhang, B., Bagchi, A., Finite element simulation of chip formation and comparison with machining experiment, Journal of Engineering for Industry 116 (8) (1994) 289-297.

[Zore-63]   Zorev, N.N., Inter-Relationship between Shear Processes occurring along Tool Face and Shear Plane in Metal Cutting, International Research in Production Engineering (1963) 42-49.

Resume

Name:	Lijing Xie
Nationality:	China
Date and place of birth:	June. 17, 1971 in China
Family Status:	Married with Dan Zheng since May. 18, 1998

Education:

1978-1983	Tangshan Nanxindao Elementary School, Hebei, China
1983-1986	The Eighth Junior High School, Tangshan, China
1986-1989:	The First Senior High School, Tangshan, China
1989-1993	B.S., Department of Mechanical Engineering, Tangshan Institute of Technology, Hebei, China
1993-1996	M.S., Department of Mechanical Engineering, Beijing Institute of Technology, Beijing, China

Employment History:

1996-2000	Lecturer at Beijing Institute of Technology, Beijing, China
Since Nov. 2000	Scientist at Werkzeugmaschinen und Betriebstechnik (WBK), Uni-Karlsruhe (TH), Germany